

ENSEMBLE FLUORESCENCE RESONANCE ENERGY TRANSFER
ANALYSIS OF RNA POLYMERASE CLAMP CONFORMATION

by

DONGYE WANG

A Dissertation submitted to the
Graduate School-New Brunswick
Rutgers, The State University of New Jersey
in partial fulfillment of the requirements

for the degree of

Doctor of Philosophy

Graduate Program in Chemistry and Chemical Biology

Written under the direction of

Dr. Richard H. Ebright

and approved by

New Brunswick, New Jersey

October, 2008

ABSTRACT OF THE DISSERTATION

ENSEMBLE FLUORESCENCE RESONANCE ENERGY TRANSFER ANALYSIS OF RNA POLYMERASE CLAMP CONFORMATION

By DONGYE WANG

Dissertation Director:

Dr. Richard H Ebright

Crystal structures of RNA Polymerase (RNAP) and RNAP complexes indicate that the RNAP β' pincer (“clamp”) can exist in a range of conformational states, ranging from a fully open conformation that permits entry and exit of DNA, to a fully closed conformation that prevents entry and exit of DNA. Clamp closure involves a swinging motion of the β' pincer by the switch region at the base of the β' pincer.

In order to define RNAP clamp conformation in solution, we have used fluorescence resonance energy transfer (FRET) to monitor the distance between a first fluorescent probe, serving as donor, incorporated at the tip of the β' pincer and a second fluorescent probe, serving as acceptor, incorporated at the tip of the β pincer.

We have developed a procedure that permits incorporation of a fluorescent probe within a protein. The procedure involves preparation of a protein containing the azide-containing unnatural amino acid p-azidophenylalanine at the site of interest, followed by

incorporation of a fluorescent probe through azide-specific chemical modification (accomplished by Staudinger-Bertozzi ligation using a phosphine derivative of the fluorescent probe). We have used this procedure to incorporate fluorescent probes at the tips of the RNAP β' pincer and RNAP β pincer.

We have used the resulting labeled RNAP derivatives in FRET experiments addressing opening and closing of the RNAP active-center-cleft in transcription initiation and elongation and in FRET experiments addressing effects of small-molecule effectors, myxopyronin (Myx), coralopyronin (Cor), ripostatin (Rip), and lipiarmycin (Lpm), on opening and closing of the RNAP active-center cleft. Results indicate that: (1) RNAP holoenzyme in solution exists predominantly in a partly closed clamp conformational state (2) the RNAP clamp closes upon formation of the RNAP-promoter open complex, yielding a fully closed clamp conformational state (3) the RNAP clamp remains closed—and exhibits no further change in mean clamp conformation—upon formation of RNAP-promoter initial transcribing complexes and transcription elongation complexes. The results support the proposal that Myx, Cor, Rip and Lpm bind to an RNAP- switch-region conformational state and Myx, Cor, Rip and Lpm inhibit RNAP function by trapping the RNAP switch region in this conformational state, thereby interfering with conformational cycling of RNAP clamp important for RNAP function.

Abbreviations

CTD: C-terminal domain

DMF: Dimethyl formamide

EDTA: Ethylenediaminetetraacetic acid

FRET: Fluorescence resonance energy transfer

HPLC: High performance liquid chromatography

IPTG: Isopropyl-thio-beta-D-galactoside

NTD: N-terminal domain

PAGE: Polyacrylamide gel electrophoresis

PCR: Polymerase chain reaction

RNAP: RNA polymerase

RPo: RNA polymerase-promoter open complex

RPitc: initial transcribing complex

RDe: RNA polymerase-DNA elongation complex

SDS: Sodium dodecyl sulfate

Taq: *Thermus aquaticus*

TFA: Trifluoroacetic acid

Acknowledgements

I would like to thank my mentor, Dr. Richard H. Ebright for his support, patient guidance, and encouragement all these years. Without his valuable advice and insightful ideas, I would not have been able to finish this thesis. It is always exciting and intriguing to discuss with him. The experience in Richard's lab will be beneficial to my future career in many ways.

I am also grateful to my dissertation committee members: Dr. Eddy Arnold, Dr. Wilma Olsen, Dr. Richard Ludescher and Dr. Bryce Nickels for their critical and helpful comments on the thesis.

I wish to thank Dr. Olve Peersen, my master's advisor at Colorado State University, for his guidance and encouragement. Olve not only taught me a great deal of biochemistry and molecular biology techniques but also shared with me his views on science and life. My gratitude is also extended to Dr. A-Young Moon Woody, Dr. Robert Woody at Colorado State University for their guidance, encouragement, and help.

I thank all the former and current members of Ebright's laboratory, especially Dr. Jayanta Mukhopadhyay, Dr. Ekaterine Kortkhonjia, Dr. Yon Ebright, and Dr. Vladimir Mekler for their help to this thesis. I extend my appreciation to Dr. Aashish Srivastava, Dr. Sergei Druzhinin, Dr. Rui Rong Niedfeldt, Dr. Candida Perera, Dr. Yi Jiang, Dr. Tatyana

Naryshkina, Dr. Sukhendu Mandal, Mr. Chuck Obrien, Mr. David Degen, Ms. Qiaorong Jiang, and Ms. Qumiao Xu for their collaboration and support.

I would like to thank Dr. Anup Singh, Dr. Patricia Gao and Dr. Pochien Greg Hsu at Saint Peter's University Hospital for their help to my family.

I would like to express my thanks to my family members for their unconditional love and support, to my parents who are doing everything they can to provide the care to us so that I can focus on my study, to my two lovely daughters Katherine and Grace for their love, and to my dear husband Qiang Zhu for his patience and giving his support in every possible way to help me.

Finally, I would like to thank God for everything. All are attributed to the glory of God.

Dedication

To my dearest husband Qiang Zhu

Table of contents

Abstract	ii
Abbreviations	iv
Acknowledgements	v
Dedication	vii
Table of contents	viii
List of tables	xi
List of figures	xiii
1. General introduction	1
1.1. Multi-subunit RNA polymerases.....	1
1.2. Bacterial promoter elements.....	4
1.3. Transcription initiation and elongation.....	6
1.4. Structures of RNAP and RNAP complexes.....	9
1.4.1. Structure of RNAP core enzyme.....	9
1.4.2. Structure of RNAP holoenzyme.....	13
1.4.3. Structure of RNAP-promoter open complex.....	16
1.4.4. Structure of RNAP transcription elongation complex.....	19
1.5. RNAP clamp and switch region.....	22
1.6. Switch-region-target inhibitors.....	25
2. Objectives	29
3. Rationale	31
3.1. Incorporation of fluorescent probes into RNAP.....	31

3.2. Choice of donor/acceptor pair.....	41
3.3. Rationale of labeling positions.....	43
3.4. Determination of mean clamp conformational states.....	46
4. Incorporation of fluorescent probes into RNAP.....	55
4.1. Materials and methods.....	55
4.1.1. Plasmids.....	55
4.1.2. Synthesis of Alexa488 phosphine and Cy3B phosphine.....	58
4.1.3. Preparation of RNAP subunits and derivatives.....	61
4.1.4. Analysis of labeled RNAP activity.....	68
4.2. Results and discussion.....	71
4.2.1. Preparation of <i>E. coli</i> RNAP β' and β derivatives with azido-phenylalanine residue at desired positions.....	71
4.2.2. Labeling of RNA polymerase β and β' derivatives through Staudinger ligation.....	84
4.2.3. In vitro reconstitution of RNAP with the fluorescent donor Alexa 488 at the distal tip of the β' pincer and the fluorescent acceptor Cy3B at the distal tip of the β pincer.....	91
4. RNAP clamp conformational states.....	102
5.1. Objectives.....	102
5.2. Materials and methods.....	103
5.2.1. Fluorescent labeled RNAP derivatives.....	103
5.2.2. Fluorescence resonance energy transfer.....	103
5.2.3. Fluorescence anisotropy.....	105

5.2.4. Fluorescence spectroscopy.....	106
5.3. Results and discussion.....	111
5.3.1. Anisotropy results.....	111
5.3.2 R_0 calculation.....	112
5.3.3. Ensemble FRET measurements of mean clamp conformational states....	114
5.3.4. Detection of effects on RNAP clamp conformation of switch-region-target inhibitors.....	120
6. Conclusion and perspectives.....	131
References.....	133
Curriculum vita.....	143

List of tables

Table 3.1. NTP subsets and the corresponding RNA products and complexes.....	49
Table 3.2. In-gel FRET results for holoenzyme, RP_o , $RP_{itc, \leq 2}$, $RP_{itc, \leq 4}$, $RP_{itc, \leq 7}$ $RD_{e,11}$, and $RD_{e,15}$ formed by [Alexa488-Phe284] β ' ; [Cy3B-Phe106] β -RNAP with <i>lac</i> CONS-11 and <i>lac</i> CONS-15.....	51
Table 3.3. In-gel FRET results for holoenzyme, RP_o , $RP_{itc, \leq 2}$, $RP_{itc, \leq 4}$, $RP_{itc, \leq 7}$ $RD_{e,11}$, and $RD_{e,15}$ formed by [Alexa488-Phe284] β ' ; [Cy3B-Phe222] β -RNAP with <i>lac</i> CONS-11 and <i>lac</i> CONS-15.....	52
Table 3.4. Effects of Myx, Cor, Rip and Lpm on RNAP holoenzyme [Alexa488- Phe284] β ' [Cy3B-Phe106] β -RNAP clamp conformation.....	53
Table 3.5. Effects of Myx, Cor, Rip and Lpm on RNAP holoenzyme [Alexa488- Phe284] β ' [Cy3B-Phe222] β -RNAP clamp conformation.....	54
Table 4.1. Plasmids.....	57
Table 4.2. Parallel expression series for each protein studied.....	76
Table 4.3. Increase of activity using α^I NTD- α^{II} NTD instead of α	95
Table 4.4. The effect of σ on reconstitution of active RNAP.....	97
Table 5.1. In-solution FRET results for holoenzyme, RP_o , $RP_{itc, \leq 2}$, $RP_{itc, \leq 4}$, $RP_{itc, \leq 7}$ $RD_{e,11}$, and $RD_{e,15}$ formed by [Alexa488-Phe284] β ' ; [Cy3B-Phe106] β -RNAP with <i>lac</i> CONS-11 and <i>lac</i> CONS-15.....	118
Table 5.2. In-solution FRET results for holoenzyme, RP_o , $RP_{itc, \leq 2}$, $RP_{itc, \leq 4}$, $RP_{itc, \leq 7}$ $RD_{e,11}$, and $RD_{e,15}$ formed by [Alexa488-Phe284] β ' ; [Cy3B-Phe222] β -RNAP with <i>lac</i> CONS-11 and <i>lac</i> CONS-15.....	119

Table 5.3. Effects of Myx, Cor, Rip and Lpm on RNAP holoenzyme [Alexa488-Phe284] β' [Cy3B-Phe106] β -RNAP clamp conformation.....124

Table 5.4. Effects of Myx, Cor, Rip and Lpm on RNAP holoenzyme [Alexa488-Phe284] β' [Cy3B-Phe222] β -RNAP clamp conformation.....125

Table 5.5. Effects of CBR703, FPET, CTC-ME and CTC-EE on RNAP holoenzyme [Alexa488-Phe284] β' [Cy3B-Phe106] β -RNAP clamp conformation.....128

Table 5.6. Effects of CBR703, FPET, CTC-ME and CTC-EE on RNAP holoenzyme [Alexa488-Phe284] β' [Cy3B-Phe222] β -RNAP clamp conformation.....129

List of figures

Figure 1.1. Transcription initiation and elongation pathways.....	8
Figure 1.2. Structure of RNAP core (Zhang et al., 1999). Subunits α I, α II, β , β' and ω are shown in light blue, dark blue, orange, green and gray. Active-center Mg^{2+} is in magenta. (A) Front view. (B) Top view.....	12
Figure 1.3. Structure of RNAP holoenzyme. Subunits α^I , α^II , β , β' , ω and σ are shown in light blue, dark blue, orange, green, gray and yellow. Active-center Mg^{2+} is in magenta. (A) Front view. (B) Top view.....	15
Figure 1.4. The RP_o model. (A) model of RP_o ; (B) Magnified view of RP_o , showing the details of the core promoter interactions, transcription bubble, and downstream DNA. The RNAP holoenzyme is shown as a molecular surface, color coded as follows: α^I , α^II , ω , gray; β , cyan; β' , pink; and σ , orange.....	18
Figure 1.5. Overall structure of the ttEC.....	21
Figure 1.6. RNAP clamp and RNAP switch region. Structure of RNAP core showing open (red), intermediate (yellow), and closed (green) clamp conformations, as observed in crystal structures (PDB 1I3Q, PDB 1HQM, PDB 1I6H)	24
Figure 1.7. Structures of switch-region-target inhibitors.....	28
Figure 3.1. Nonsense suppression method. L. Wang and P.G. Schultz <i>Angew. Chem. Int. Ed.</i> 2005 44 , 34-66.....	33
Figure 3.2. Staudinger reaction between a phosphine and azide to form an aza-ylide.....	35
Figure 3.3. Staudinger-Bertozzi ligation.....	36

Figure 3.4. A. Cu(I)-catalyzed Huisgen cycloaddition (“click chemistry”). B. Tris(1-benzyl-1 <i>H</i> -[1,2,3]triazol-4-ylmethyl)amine (TBTA) and Alkyne-fluorescein. C. Strain-promoted [3+2] cycloaddition of azides and cyclooctynes. D. Cyclooctyne-fluorescein and DIFO-488.....	38
Figure 3.5. Incorporation of Alexa488 at the tip of the clamp and cy3B at the tip of the β pincer, through a combination of unnatural amino acid mutagenesis, Staudinger-Bertozzi ligation, and RNAP reconstitution.....	40
Figure 3.6. FRET analysis of clamp opening/closing.....	45
Figure 3.7. Sequences of DNA fragments used for the formation of promoter-open complex and elongation complexes 11, 15 nt in length. Positions of promoter -10 and -35 elements are highlighted in grey. Transcription start site is indicated with an arrow. Terminating nucleotide is shown in red.....	48
Figure 4.1. The chemical structure of p-azido-L-phenylalanine.....	73
Figure 4.2. Plasmid pAmberAzide.....	74
Figure 4.3. SDS-PAGE (4-20% gradient) of purified inclusion bodies produced from expression trials indicated in Table 2. The gel was stained with Coomassie Blue. Lane M shows the molecular weight standards. Lane 1-12: expression trials 1-12 in table 2.....	77
Figure 4.4. SDS-PAGE (4-20% gradient) of fractions from Ni-affinity chromatography.....	78
Figure 4.5. SDS-PAGE (4-20% gradient) of fractions from Ni-affinity chromatography.....	79

Figure 4.6. SDS-PAGE (4-20% gradient) of fractions from Ni-affinity chromatography.....	80
Figure 4.7. SDS-PAGE (4-20% gradient) of fractions from Ni-affinity chromatography.....	81
Figure 4.8. SDS-PAGE (4-20% gradient) of fractions from Ni-affinity chromatography.....	82
Figure 4.9. SDS-PAGE (4-20% gradient) of fractions from Ni-affinity chromatography.....	83
Figure 4.10. Synthesis of 1-Methyl-2-Diphenylphosphinoterephthalate (compound 2)	85
Figure 4.11. Synthesis Alexa Fluor 488 phosphine derivative.....	86
Figure 4.12. Mass spectra (ESI) of Alexa 488 phosphine.....	87
Figure 4.13. Synthesis of Cy3B phosphine derivatives. EDC 1-(3-dimethylaminopropyl)-3-ethyl carbodiimide hydrochloride, HOBt N-hydroxy benzotriazole, TFA trifluoroacetic acid, DIPEA N,N-diisopropylethylamide.....	88
Figure 4.14. Fluorescence scan and Coomassie-stained SDS-PAGE of proteins labeled with Alexa 488 and Cy3B phosphine derivatives.....	90
Figure 4.15. Nondenaturing PAGE analysis of reconstituted RNAP holoenzyme derivatives. Lane 1, holo β' 284Alexa488; Lane 2, holo β 106Cy3B; Lane 3, holo β' 284A488 β 106 Cy3B.....	92
Figure 4.16. Nondenaturing PAGE of Alexa488-Cy3B labeled core, holo, RPo and RDe,15 (Alexa488 at β' 284, Cy3B at β 222, DNA template was labeled with Cy5)	101

Figure 5.1. Determination of donor labeling efficiency (d) in reconstituted donor-acceptor labeled RNAP derivative by use of alternating-laser excitation (ALEX)- confocal single molecule measurement.....	110
Figure 5.2. Spectral overlap between Alexa488 and Cy3B.....	113
Figure 5.3. FRET results for holoenzyme, RP_o , $RP_{itc, \leq 2}$, $RP_{itc, \leq 4}$, $RP_{itc, \leq 7}$, $RD_{e,11}$ and $RD_{e,15}$ formed by (A) [Alexa488-Phe284] β' ; [Cy3B-Phe106] β -RNAP with <i>lac</i> CONS-11 and <i>lac</i> CONS-15; (B) [Alexa488-Phe284] β' ; [Cy3B-Phe222] β -RNAP with <i>lac</i> CONS-11 and <i>lac</i> CONS-15.....	115
Figure 5.4. Effects of Myx, cor, Rip and Lpm on RNAP holoenzyme clamp conformation (A) [Alexa488-Phe284] β' ; [Cy3B-Phe106] β -RNAP; (B) [Alexa488-Phe284] β' ; [Cy3B-Phe222] β -RNAP.....	122
Figure 5.5. Changes in FRET efficiency induced by Myx, Cor, Rip and Lpm binding to RNAP holoenzyme.....	123
Figure 5.6. RNAP inhibitors: CTC-ME, CTC-EE, CBR703, and FPET.....	127

1. General introduction

1.1. Multi-subunit RNA polymerases (RNAPs)

The first step of gene expression is the synthesis of RNA from the DNA template, a process called transcription. Regulation of gene expression occurs primarily at the step of transcription. RNA polymerase (RNAP) is the enzyme responsible for transcription and is the main target for transcription regulation (Chamberlin, 1976; von Hippel, 1998). RNA polymerases are conserved in all living organisms - bacteria, archaeas, and eukaryotes - and are members of a family of “multi-subunit RNAP family” (Ebright, 2000; Minakhin et al., 2001). All members of this protein family contain five conserved subunits: (β' , β , α^I , α^{II} , and ω in bacterial RNAP; A, B, D, L, and K in archaeal RNAP; RPB1, RPB2, RPB3, RPB11, and RPB6 in eukaryotic RNAP II). Bacterial RNAP core enzymes contain only the five conserved subunits (Chamberlin, 1976). Archaeal and eukaryotic RNAP core enzymes contain the five conserved subunits and also contain additional subunits (Ebright, 2000).

Bacterial core RNAP has subunit composition $\alpha^I\alpha^{II}\beta\beta'\omega$ and a molecular mass of about 380 kDa. Two α subunits are identical in sequence but structural distinct in the context of RNA polymerase. α^I forms protein-protein contacts with subunit β and α^{II} , while α^{II} contacts β' and α^I . Each α subunit consists of two independently folded domains: the N-terminal domain (α NTD) and the C-terminal domain (α CTD), connected by a long, flexible linker (Ebright and Busby, 1995). The N-terminal domain of α is responsible for

the dimerisation, interaction with the rest of RNA polymerase and interaction with transcriptional activators. The C-terminal domain of α is also capable of dimerisation (although weaker than α NTD), is responsible for interaction with upstream DNA (weak, non-sequence specific and stronger, sequence specific interactions) and interaction with transcriptional factors (activators, repressors and elongation and termination factors). The flexible linker connecting α NTD and α CTD is about 13-36 amino acid residues long and allows α CTD to occupy different positions relative to the RNA polymerase.

The two largest subunits of RNA polymerase β and β' make up most of the RNA polymerase-DNA interface, forming an active center of the enzyme where synthesis of the RNA transcript takes place. Three highly conserved Aspartate residues of β' coordinate two Mg^{2+} ions that are essential for the function of the enzyme.

The smallest subunit of RNA polymerase, ω , forms protein-protein contacts with β' subunit and has been shown to aid in the assembly of the RNA polymerase, although it is not required for the enzyme function *in vitro* (Gentry et al., 1993; Ghosh et al., 2001; Vrentas et al., 2005).

RNAP core enzyme is competent for non-specific transcription initiation and elongation (Wheeler et al., 1987), but is unable to locate and bind promoter DNA. To carry out promoter-specific initiation, RNAP core must associate with additional initiation factors - σ factors (Gross et al., 1998) that direct the core enzyme to the promoter sequences by recognizing the specific sequences of the promoter (deHaseth et al., 1998). The complex

of RNAP core enzyme with initiation factors capable of initiating transcription in a regulated manner is referred to as RNAP holoenzyme (composition $\alpha^I\alpha^{II}\beta\beta'\omega\sigma$).

The σ factors contain determinants for sequence-specific interaction with DNA and, through these determinants, targets RNAP holoenzyme to promoters (Busby and Ebright, 1994; Roberts and Roberts, 1996; Gross et al., 1992, 1998). In addition, σ plays critical role in promoter melting, promoter escape, early elongation and response to transcriptional regulators (Helmann and Chamberlin, 1998; Ring et al., 1996; Busby and Ebright, 1994; Gross et al., 1992,1998).

Bacterial σ factors are subdivided into two major categories: the σ^{70} family of σ factors (Paget and Helmann, 2003) and the σ^{54} family of σ factors (Buck et al., 2000). Most bacterial σ factors belong to the σ^{70} family with distinct regions of highly conserved sequence (Lonetto et al., 1992). The principal σ factors of bacterial species-- σ^A in *T. thermophilus* and *T. aquaticus*, σ^{70} in *E. coli*--contain five conserved regions: $\sigma R1.1$, $\sigma R2$, $\sigma R3$, the $\sigma R3/\sigma R4$ linker, and $\sigma R4$ (Gross et al., 1998). $\sigma R2$, $\sigma R3$, and $\sigma R4$ are structured, independently folded domains that contain determinants for sequence-specific interactions with, respectively, the promoter -10 element, the promoter extended -10 element, and the promoter -35 element (Gross et al., 1998; Severinova et al., 1996; Malhotra et al., 1996; Campbell et al., 2002). $\sigma R1.1$ and the $\sigma R3/\sigma R4$ linker (also known as $\sigma R3.2$) are unstructured, highly negatively charged segments (Campbell et al., 2002). *Escherichia coli* σ^{70} , the most abundant σ factor in *E. coli*, is the best-characterized σ factor. *E. coli* σ^{70} RNAP holoenzyme is the subject of the work in this thesis.

1.2. Bacterial promoter elements

Promoters are specific DNA sequences that mark the transcriptional start site. RNA polymerases recognize promoter sequences, bind to them and start transcription. Bacterial promoters contain two crucial sequence elements: the -10 element and the -35 element (Hawley and McClure, 1983; 1986; Keilty and Rosenberg, 1987; Harley and Reynolds, 1987). The -10 element is located near position -10 relative to the transcription start site and has the consensus sequence 5'-TATAAT-3'. The -35 element is located near position -35 relative to the transcription start site and has the consensus sequence 5'-TTGACA-3' (Gross et al., 1992). The -10 element is specifically recognized by σ^{70} region 2 within RNAP holoenzyme and the -35 element is specifically recognized by σ^{70} region 4 within RNAP holoenzyme. The elements are separated by a ~17 bp spacer of a non-conserved sequence (Harley and Reynolds, 1987). Spacing has been proposed to be important for correct orientation of -10 and -35 elements relative to each other.

The -10 and -35 elements are referred to as the core promoter elements. Strength of promoters containing these regions is generally determined by their resemblance to the consensus.

Some promoters have an “extended -10 element”, located immediately upstream of the -10 element of the promoter and having the consensus sequence 5'-TGN-3' (Ponnambalam et al., 1996; Keilty and Rosenberg, 1987). Sequence-specific recognition

of the extended -10 element is mediated by σ^{70} region 3 (Barne et al., 1996; Bown et al., 1999).

Some promoters, such as *rrn* promoters, which direct ribosomal RNA synthesis, contain an additional element located immediately upstream from the -35 element, referred to as UP-element (Ross et al., 1993). The full UP element is a ~20 nt long, A/T rich sequence. The UP element is specifically recognized by determinants within the C-terminal domains (CTDs) of α^I and α^{II} subunits of RNAP (Aiyar et al., 1998). The presence of UP element can increase the binding affinity of RNAP holoenzyme to the promoter by two orders of magnitude (Rao et al., 1994).

1.3. Transcription initiation and elongation

Transcription can be divided into three distinct steps: initiation, elongation and termination. Transcription initiation is a multistep process (Record et al., 1996). Transcription initiation by RNA polymerase holoenzyme involves the following steps (Figure 1.1) (deHaseth et al., 1998; Young et al., 2002; Murakami and Darst, 2003; Record et al., 1996).

(1) RNAP holoenzyme recognizes core promoter elements and binds to the promoter DNA, interacting solely with the promoter region upstream of the transcription start site, to yield an RNAP-promoter closed complex (RP_c).

(2) RNAP then clamps tightly onto the promoter DNA, extending its interactions with the promoter downstream from the transcription start site, to yield an RNAP-promoter intermediate complex (RP_i).

(3) RNAP then unwinds and melts approximately 14 base pairs of promoter DNA surrounding the transcription start site, forming a single-stranded region (“transcription bubble”), to yield an RNAP-promoter open complex (RP_o).

(4) If nucleoside triphosphates (NTPs) are available, RNAP begins RNA synthesis as an initial transcribing complex (RP_{itc}). Typically, RNAP fails to achieve productive RNA synthesis on its first attempt and enters into abortive cycles of synthesis and release of

short RNA products—RNA products 2-9 nt in length. RNA products below a threshold length of 9-11 nt are not stably retained within the RNAP active center, and dissociate at rates comparable to nucleotide-addition rate.

(5) When by chance, RNAP succeeds in synthesizing an RNA product of the threshold length of ~9-11 nucleotides, RNAP breaks its interactions with promoter DNA, breaks at least some of its interactions with σ^{70} , and begins to translocate along DNA, processively synthesizing RNA as a RNAP-DNA elongation complex (RD_e) with stably bound nascent RNA. The transition from RP_{itc} to RD_e is referred to as “promoter clearance” or “promoter escape”.

The elongation complex is highly processive until it is terminated by signals in the termination region. During termination, the synthesis of an RNA molecule stops and the elongation complex containing the RNA, DNA and RNA polymerase dissociates. After termination, the core RNAP is recycled back to the promoter region to reform the holoenzyme and start the transcription cycle again.

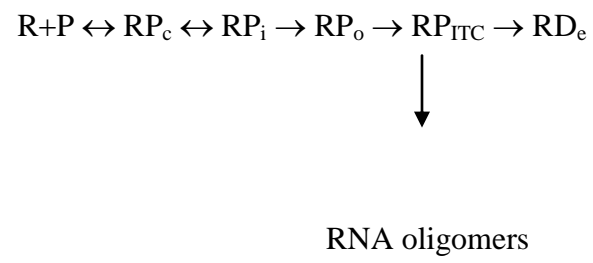


Figure 1.1. Transcription initiation and elongation pathways.

1.4. Structures of RNAP and RNAP complexes

The crystal structures of the *Thermus aquaticus* RNAP core, *Thermus aquaticus* RNAP holoenzyme, *Thermus aquaticus* RNAP holoenzyme in complex with a fork-junction DNA, *Thermus thermophilus* RNAP holoenzyme, *Thermus thermophilus* RNAP elongation complex, yeast *Saccharomyces cerevisiae* RNAP II (Pol II), yeast Pol II elongation complex, and RNAP bound with inhibitors have been determined in the past ten years. The crystal structures revealed the high degree of structural similarity between the prokaryotic and eukaryotic RNAPs.

1.4.1. Structure of the RNA polymerase core enzyme

From a function point of view, *E. coli* RNA polymerase is the best-characterized cellular RNAP. However, up until now the only structure available for *E. coli* core RNA polymerase has been determined to a resolution of 15 Å by cryo-electron microscopy (EM) and image processing of helical crystals (Darst et al. 2002). The first high resolution structure of core RNA polymerase was resolved at 3.3 Å resolution from *Thermus aquaticus* (*Taq*, Zhang et al 1999). The very high conservation of sequence, structure, and function between *E. coli* and *Taq* RNA polymerases make the structural information available for *Taq* RNAP directly applicable to *E. coli* RNAP.

The crystal structure of *Taq* RNA polymerase contains most of the β' subunit, complete β subunit, the N-terminal domains of two α subunits and ω subunit. RNA polymerase core

has dimensions of $\sim 150 \text{ \AA} \times \sim 100 \text{ \AA} \times \sim 100 \text{ \AA}$ and has a shape reminiscent of a crab claw (Figure 1.2). The two “pincers” of the “claw” define the active-center cleft, which has a diameter of 25 \AA —a diameter that can accommodate a double-stranded helix of a nucleic acid. The active site of the enzyme with Mg^{++} is located at the base of the cleft. The β' subunit of RNAP makes up one pincer and part of the base of the active-center cleft. The β subunit of RNAP makes up the other pincer and part of the base of the active-center cleft. The N-terminal domains (NTDs) of α^I and α^{II} subunits are located distal to the active-center cleft. α^I NTD is located closer to the active-center cleft and interacts with β subunit, while α^{II} NTD is located farther from the active-center cleft and interacts with β' subunit. C-terminal domains of α subunits were not resolved in this structure of RNA polymerase core. The ω subunit interacts exclusively with β' and is located distal to the active-center cleft, near the base of the β' “pincer”.

In addition to the active-center cleft, RNAP core contains two other distinct channels: the secondary channel, which mediates access of NTP substrates to the active center cleft; and the RNA-exit channel, which mediates egress of nascent RNA from the active-center cleft.

The major structural difference between the *Taq* core RNAP crystal structure and the *E. coli* core RNAP cryo-EM map resides in the position of the β' pincer relative to the rest of the enzyme. A large conformation change of the *Taq* RNAP crystal structure is required for an optimal fit to the *E. coli* cryo-EM structure (Darst et al. 2002). The conformational change involves a nearly 20° hinge-like rotation of the β' pincer, resulting

in the opening of the main RNAP channel by 25 Å in *Taq* RNAP. The difference reflects the structural flexibility of RNA polymerase and different conformations it is capable of assuming.

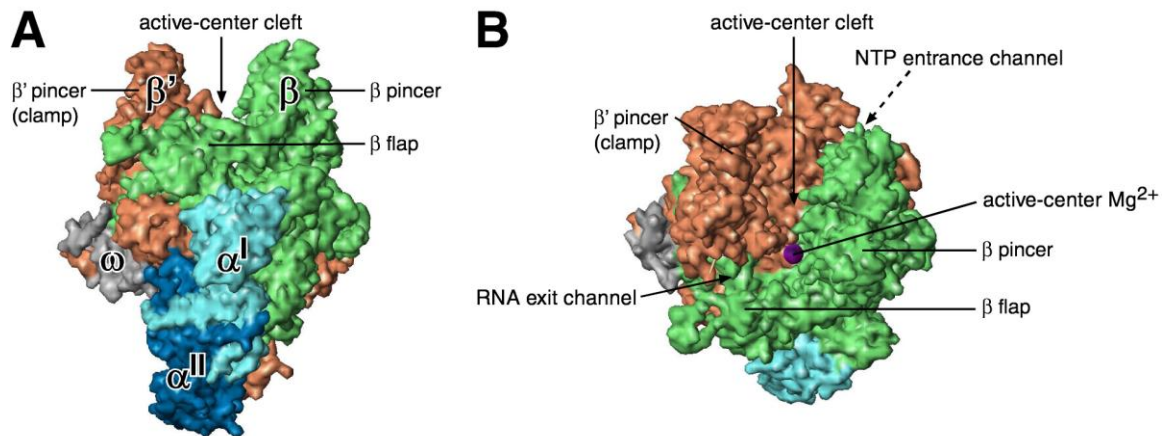


Figure 1.2. Structure of RNAP core (Zhang et al., 1999). Subunits α^I , α^{II} , β , β' and ω are shown in light blue, dark blue, orange, green and gray. Active-center Mg^{2+} is in magenta. (A) Front view. (B) Top view.

1.4.2. Structure of the RNAP holoenzyme

The structure of *Thermus thermophilus* RNAP holoenzyme was determined at 2.6 Å resolution (Vassylyev et al., 2002) and the structure of *T. aquaticus* σ^A RNAP holoenzyme was determined at 4.0 Å resolution (Murakami et al., 2002) (Figure 2.3). In addition the positions of $\sigma R1.1$, $\sigma R2$, $\sigma R3$, $\sigma R3/\sigma R4$ linker, and $\sigma R4$ relative to RNAP core in *E. coli* σ^{70} RNAP holoenzyme have been determined by systematic fluorescence resonance energy transfer (FRET) study (Mekler et al. 2002). The structure organization of core subunits is essentially identical in RNAP core and in RNAP holoenzyme, except that the β' pincer rotates, as a unit, $\sim 16^\circ$ into the active-center cleft in RNAP holoenzyme (Vassylyev et al., 2002; Murakami et al., 2002; Mekler et al. 2002). The structure of σ is comprised of three independently folded domains corresponding to the conserved regions 2, 3, and 4 of σ connected by flexible linkers (Figure 1.3). The interface between the core subunits and σ in RNAP holoenzyme is extensive (Sharp et al., 1999; Vassylyev et al., 2002; Murakami et al., 2002; Mekler et al. 2002). $\sigma R2$ interacts with the β' pincer and is positioned within and above the RNAP active-center formed by the β and β' pincers. $\sigma R3$ interacts with the base of the β flap and $\sigma R4$ interacts with the tip of the β flap. Each of the two unstructured highly negatively charged σ regions-- $\sigma R1.1$ and the $\sigma R3/\sigma R4$ linker--also interacts with core subunits. $\sigma R1.1$ and the $\sigma R3/\sigma R4$ linker serve as “molecular mimics” for DNA and RNA. i.e., $\sigma R1.1$ is located in the RNAP active-center cleft and must be displaced to permit access of promoter DNA to the active-center cleft; and the $\sigma R3/\sigma R4$ linker is located in the RNA-exit channel and must be displaced to permit

access of nascent RNA to the RNA exit channel (when nascent RNA reaches a length of ~11-13nt).

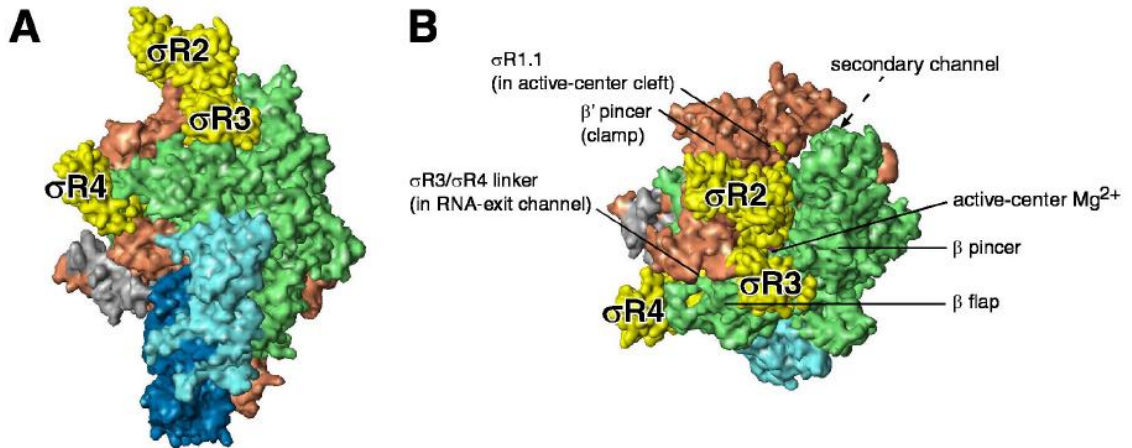


Figure 1.3. Structure of RNAP holoenzyme. Subunits α^I , α^{II} , β , β' , ω and σ are shown in light blue, dark blue, orange, green, gray and yellow. Active-center Mg^{2+} is in magenta. (A) Front view. (B) Top view.

1.4.3. Structure of the RNAP –promoter open complex

Site-specific protein-DNA photocrosslinking and a crystal structure of *T. aquaticus* RNA polymerase holoenzyme ($\alpha^I\alpha^{II}\beta\beta'\omega\sigma^A$) in complex with a fork-junction promoter DNA fragment have defined protein-DNA interactions in bacterial RNAP-promoter open complex (RP_o) (Naryshkin et al. 2000; Murakami et al., 2002). The structure explains the mechanism of specific promoter recognition and promoter melting. In the structural model of RP_o (Figure 1.4), the position and orientation of the downstream promoter DNA duplex, the positions of the template and non-template strands in the transcription bubble, and the position and orientation of the upstream promoter DNA duplex were defined. In RP_o, the downstream DNA duplex binds deep within the active-center cleft. The downstream end of the transcription bubble also binds deep within the active-center cleft, with position +1 of the template strand being located on the floor of the active-center cleft. The template strand of the transcription bubble rises up from the floor of the active-center cleft, along an axis nearly perpendicular to the downstream duplex. The nontemplate strand of the transcription bubble does not go toward the active site. It turns away from the active site immediately after the DNA strand separation occurs around position +2, continues its path along the jaws of RNAP formed by the β subunit and meets the template strand at the up edge of the active-center cleft. The structure also defines locations of segments of σ relative to promoter DNA. σ region 4 interacts with the -35 element, σ region 3 interacts with the “extended -10 element”, and σ region 2 interacts with the -10 element.

In addition, modeled structure of the RNA polymerase-DNA open complex based on FRET information (Mekler et al., 2002) has provided information for the position of the σ R1.1. This region of σ is displaced from the DNA binding channel of the enzyme to form alternative contacts with β subunit 51 Å away from its position in holoenzyme.

Overall structure of the core enzyme is mostly unchanged in the RNA polymerase-DNA open complex. The comparison of holoenzyme within the holoenzyme/ fork-junction DNA complex to holoenzyme alone reveals a conformational change of the RNAP clamp domain, which is rotated in toward the active center by 3°, closing the RNAP active-center cleft by about 3 Å relative to the holoenzyme alone (Murakami et al., 2002).

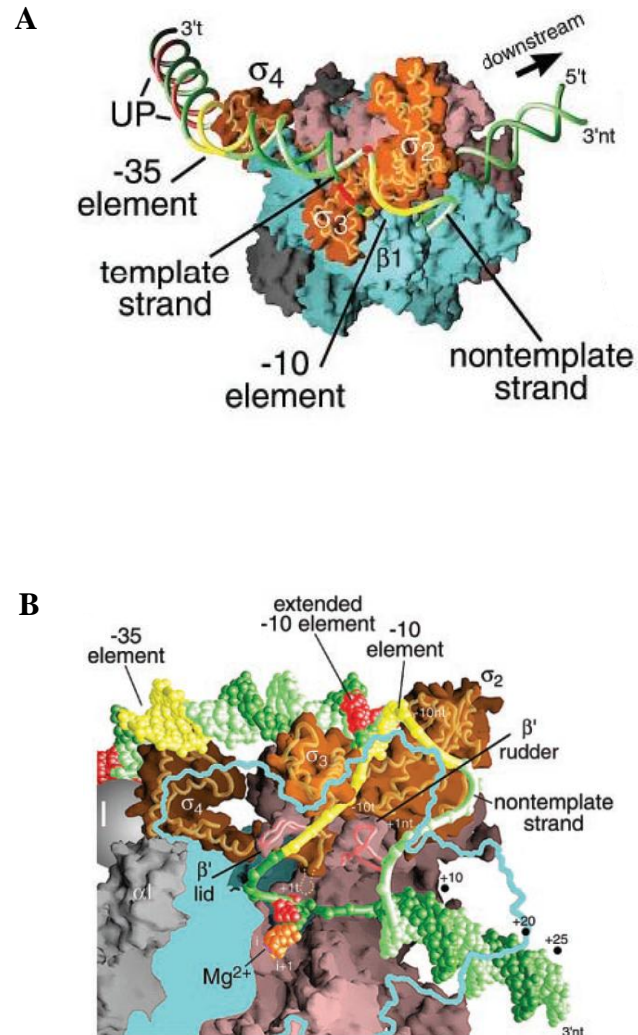


Figure 1.4. The RP_0 model. (A) model of RP_0 ; (B) Magnified view of RP_0 , showing the details of the core promoter interactions, transcription bubble, and downstream DNA. The RNAP holoenzyme is shown as a molecular surface, color coded as follows: α^I , α^{II} , ω , gray; β , cyan; β' , pink; and σ , orange.

1.4.4. Structure of the RNAP transcription elongation complex

The positions of the downstream duplex and the RNA/ DNA hybrid within RNAP in the transcription elongation complex have been defined by RNA- and DNA-protein cross-linking (Korzheva et al., 2000). Crystal structures of *Thermus thermophilus* RNAP elongation complex without bound NTP (Figure 1.5, Vassylyev et al., 2007), with bound NTP (Vassylyev et al., 2007), and yeast Pol II elongation complex (Gnatt et al., 2001) have been reported. These structures reveal detailed network of interactions between nucleic acid chains and RNAP side chains, thereby providing information for explaining the determinants of the high stability and processivity of the elongation complex. The clamp is the central feature in this interaction network. It contacts the downstream DNA, the hybrid, the exiting RNA, and the bridge helix. The core enzyme conformations in the elongation complex and the holoenzyme are not identical. In comparison with the holoenzyme, the elongation complex structure undergoes closure of the RNAP claws to reduce the size of the main channel substantially. Based on these crystal structures, it has been proposed that each nucleotide-addition cycle is coupled to an RNAP active-center conformational cycle, involving closing of the RNAP active center upon binding of the incoming nucleotide, followed by opening of the RNAP active center upon formation of the phosphodiester bond. First, the NTP binds to the open active center to form an inactive, preinsertion intermediate, working as a 'ratchet' that stabilizes the post-translocated elongation complex. Second, on folding of the active-center structural element termed the "trigger loop" into two α -helices (trigger helices), the NTP is repositioned to form the catalytically competent insertion complex, in which the active

site is closed. Upon formation of the phosphodiester bond, the loss of phosphate moieties then triggers the opening of the RNAP active center mediated by the unfolding of the “trigger loop”.

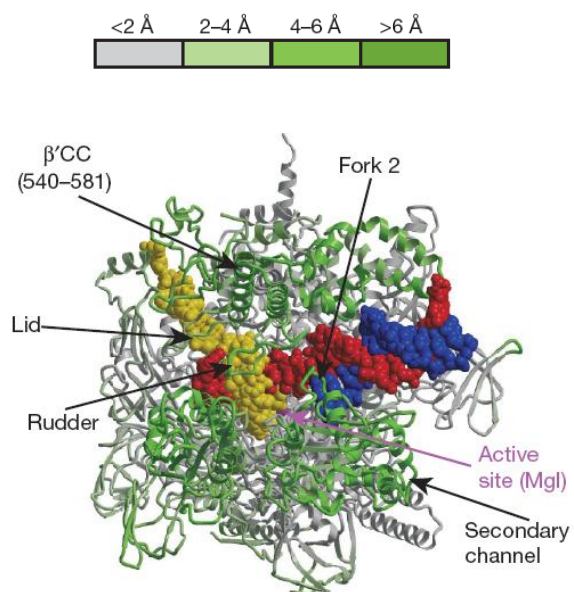


Figure 1.5. Overall structure of the ttEC. The RNAP core enzyme structure in the ttEC is coloured from grey (less than 2 Å) to green (more than 6 Å) according to the deviation in the positions of the C_{α} atoms of the corresponding core and holoenzyme (PDB ID 2A6H) residues. (grey, RNAP; red, DNA template; blue, DNA non-template; yellow, RNA.)

1.5. RNAP clamp and switch region

The comparison of the different crystallographic structures of RNAP and RNAP complexes has revealed the presence of mobile domains and conformational changes that are important for function. The most prominent mobile domain, termed the clamp (Cramer 2001), ranges in position from relatively closed in γ RNAPII and bacterial elongation complex to open in an *E. coli* RNAP EM structure (Gnatt et al., 2001; Cramer et al., 2001; Campbell et al., 2001; Darst, 2001). The clamp forms one side of the enzyme's active-center cleft, comprising the N-terminal segment of β' , the C-terminal domain of β and ω in bacterial RNAP. At the base, clamp is connected to the stationary part of RNAP through five polypeptide segments, termed switches 1, 2, 3, 4, and 5 that are flexible and enable clamp movement. The clamp and switches are structurally conserved in bacterial RNAP (except the clamp head) (Cramer 2001).

The RNAP clamp can exist in a range of distinct conformational states—from an open clamp conformation that permits entry and exit of DNA, to a closed conformation that prevents entry and exit of DNA (Gnatt et al., 2001; Cramer et al., 2001; Campbell et al., 2001; Darst, 2001) (Figure 1.6). The transition between the open and closed clamp conformations involves a swinging motion of the clamp by the switch region at the base of the clamp, and conformational changes and folding transitions in the switch region. Interestingly, the switches are disordered when the clamp is open, but folded cooperatively upon interacting with nucleic acids and the bridge helix when the clamp closes in the transcription elongation complex (Landick, 2001).

It has been proposed that the clamp opens to permit DNA to enter the active center in initiation, closes after DNA enters the active-center cleft in initiation, and further closes, or acquires further stability in the closed state, upon transition to elongation. Clamp closure is proposed to mediate the high stability of the transcription initiation complexes and exceptionally high stability and high processivity of the transcription elongation complexes.

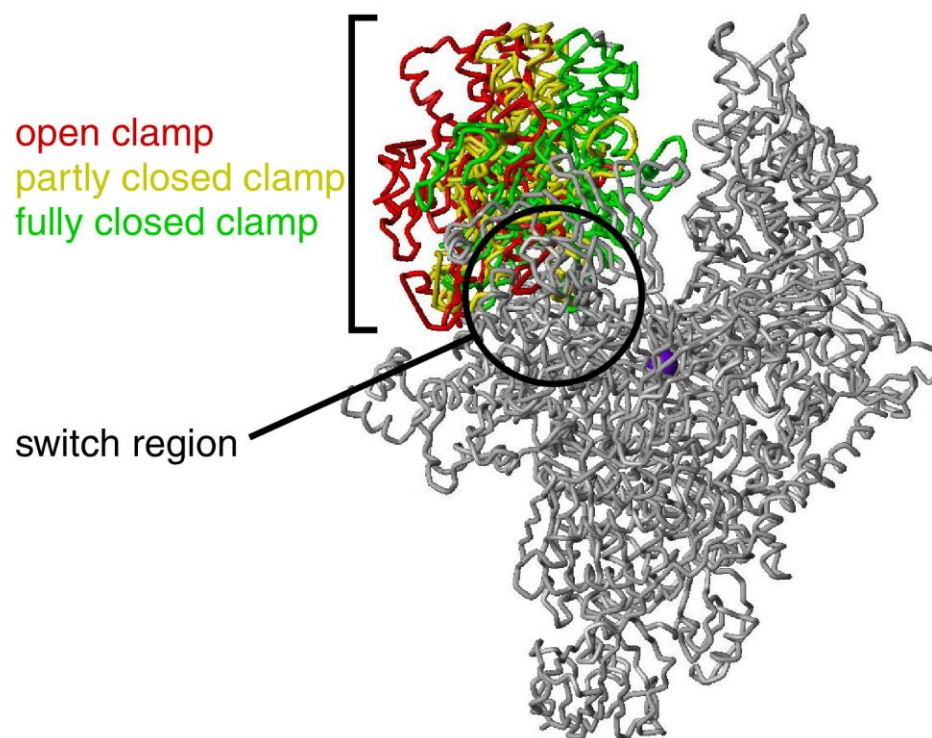


Figure 1.6. RNAP clamp and RNAP switch region. Structure of RNAP core showing open (red), intermediate (yellow), and closed (green) clamp conformations, as observed in crystal structures (PDB 1I3Q, PDB 1HQM, PDB 1I6H).

1.6. Switch-region-target inhibitors

Bacterial RNAP is the main target for many antibiotics. These compounds: myxopyronin (Myx), corallopyronin (Cor), ripostatin (Rip), lipiarmycin (Lpm) (Figure 1.7), have been identified inhibiting bacterial RNAP through interactions with the RNAP switch region and appearing to function by preventing clamp opening required for DNA binding and /or clamp closure required for DNA retention.

Myxopyronin, produced by the myxobacterium *Myxococcus fulvus* strain Mxf50, is a polyketide-derived α -pyrone antibiotic (Irschik et al., 1983; Kohl et al., 1983; Kohl et al., 1984). Myx exhibits antibacterial activity against Gram-positive and Gram-negative bacteria. Myx inhibits bacterial RNAP ($K_i = 1 \mu\text{M}$) but does not inhibit eukaryotic RNAP II. Myx exhibits no cross-resistance with rifampicin, the inhibitor of bacterial RNAP widely used to treat tuberculosis (Hu et al., 1998).

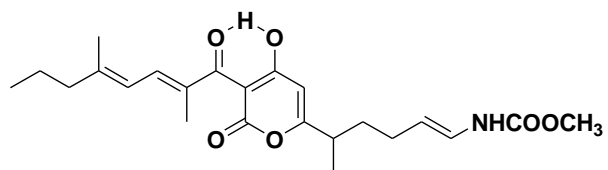
Corallopyronin, produced by the myxobacterium *Coralloccoccus coralloides* strain Cc c127, is a polyketide-derived α -pyrone antibiotic structurally related to Myx, differing only by possession of a seven-carbon side-chain extension (Irschik et al, 1985). Cor exhibits antibacterial activity against Gram-positive and Gram-negative bacteria. Cor inhibits bacterial RNAP ($K_i = 4 \mu\text{M}$) but does not inhibit eukaryotic RNAP II. Cor exhibits no cross-resistance with rifampicin, the inhibitor of bacterial RNAP widely used to treat tuberculosis (O'Neill et al 2000).

Ripostatin, produced by the myxobacterium *Sorangium cellulosum* strain So ce377, is a polyketide-derived macrocyclic-lactone carbonic acid (Irschik et al, 1995; Augustiniak et al 1996). Rip exhibits antibacterial activity against Gram-positive and Gram-negative bacteria. Rip is an inhibitor of bacterial RNAP but not eukaryotic RNAP II. It interferes with the initiation of RNA synthesis. Rip exhibits no cross-resistance with rifampicin, the inhibitor of bacterial RNAP widely used to treat tuberculosis (O'Neill et al 2000).

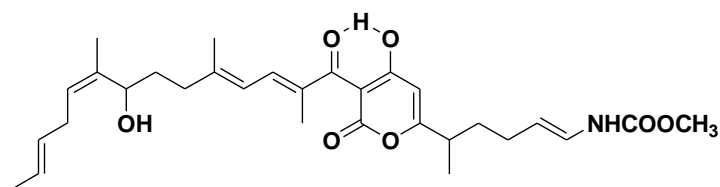
Lipiamycin, also known as tiacumicin, is a complex of an unsaturated 18-membered macrolide ring with a seven-carbon sugar at carbon 11 and a 6-carbon sugar at carbon 20 (Sergio et al 1975; Hochlowski et al 1987). Lip is produced by *Actinoplanes deccanensis*. It is active against Gram-positive bacteria but ineffective against Gram-negative bacteria. Lpm interferes with RNA synthesis specifically at initiation.

The target, mechanism, and structural basis of inhibition of bacterial RNAP by Myx, Cor, Rip, and Lpm have been defined by a combination of genetic, biochemical, and crystallographic approaches (Ebright, 2007). The results indicate that myxopyronin, coralopyronin, ripostatin and lipiamycin interact with the RNAP "switch region"--i.e., with the hinge that mediates rotation of the RNAP clamp relative to the remainder of RNAP and, correspondingly, that mediates opening and closing of the RNAP active-center cleft. Crystal structure of *T. thermophilus* RNAP holoenzyme in complex with Myx shows that Myx binds within the RNAP switch region. Myx makes direct interactions with switch 1 and, especially, switch 2, and also makes direct interactions with adjacent segments of the β' and β subunits (Ebright, 2007).

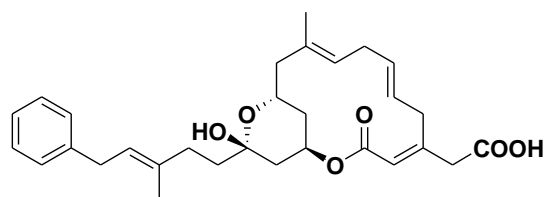
It has been proposed that Myx, Cor, Rip, and Lpm inhibit transcription by locking the RNAP switch region and clamp in one conformational state, thereby preventing switch-region conformational cycling. In the absence of switch-region conformational cycling, the RNAP clamp is unable to open to permit entry of DNA into the RNAP active-center-cleft, unable to close to permit retention of DNA within the RNAP-active-center cleft, or both.



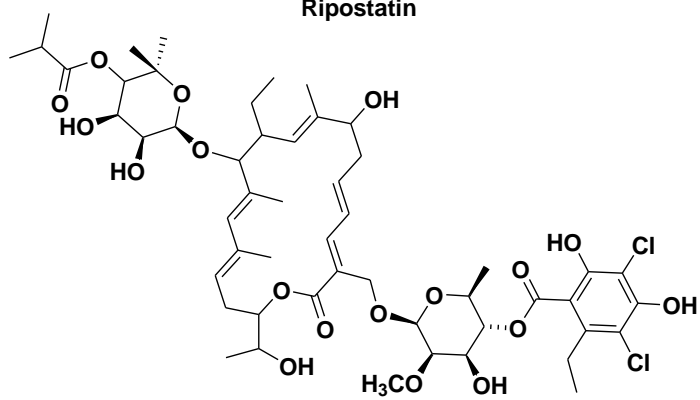
Myxopyronin



Corallopyronin



Ripostatin



Lipiarmycin

Figure 1.7. Structures of switch-region-target inhibitors.

2. Objectives

The clamp movements discussed in the introduction are so far based on static crystal structures describing essentially two different conformational states of the clamp. These movements are yet to be observed in solution or in real time; moreover, there may exist so far unobserved transient states that have escaped detection by X-ray crystallography. As discussed, clamp closure plays a significant role in transcription initiation and elongation. However, no information currently is available—for any stage of transcription—regarding the mean clamp conformation in solution, the distribution of clamp conformations in solution, or the kinetics of transitions among clamp conformations in solution. Part of the slow progress towards answering questions about clamp closure is due to the absence of assays that can accurately measure clamp closure in solution.

The overall objective of this work was to develop a fluorescence energy transfer assay to access clamp conformational states in solution. Such an assay would allow the measurement of the mean clamp conformation in RNAP holoenzyme, in transcription initiation, in transcription elongation and termination. The specific objectives of this work were:

- (1) To develop labeling procedures for incorporation of fluorescent probes into RNAP clamp (β' pincer) and β pincer.

(2) To define RNAP clamp conformation at each stage of transcription by measuring the energy transfer efficiency between fluorescent donor and fluorescent acceptor groups that are incorporated at specific sites in RNAP clamp (β' pincer) and β pincer.

(3) To define effects on RNAP clamp conformation of small-molecule inhibitors that interact with the RNAP switch region.

3. Rationale

3.1. Incorporation of fluorescent probes into RNAP

Structural and mechanistic characterization of proteins by fluorescence resonance energy transfer (FRET) requires the ability to incorporate fluorescent probes at specific defined sites. Several strategies for site-specific modification of proteins have been reported: (1) cysteine-mediated labeling, (2) oxidation-mediated labeling (Geoghegan and Stroh, 1992), (3) intein-mediated labeling ("expressed protein ligation") (Muir et al. 1998; Ayers et al. 2000; Tolbert and Wong, 2000; Mukhopadhyay et al. 2001), (4) trivalent-arsenic-mediated labeling (Griffin et al. 1998; 2000), (5) hexahistidine-tag-mediated labeling (Kapanidis et al. 2001), (6) nonsense-suppression-mediated introduction of unnatural amino acids (Wang and Schultz, 2005) followed by ketone-specific labeling or Huisgen [3+2] cycloaddition reaction, (7) Labeling of azide-containing proteins through Staudinger -Bertozzi ligation.

Cysteine-mediated labeling involves site-directed mutagenesis to introduce a cysteine residue at the site of interest, followed by cysteine-specific chemical modification to incorporate the fluorescent probe. Selective modification, however, requires a single reactive cysteine which is often not the case with large proteins (proteins with MW > 50 kDa). Oxidation-mediated labeling involves the oxidation of an N-terminal serine or threonine (Geoghegan and Stroh, 1992). This method is limited since it can only be used to modify the N-terminal position of a protein and the protein must be stable to oxidation. Intein-mediated labeling has been used to site-specifically incorporate fluorescent probes

into proteins (Muir et al. 1998; Ayers et al. 2000; Tolbert and Wong, 2000) including *E. coli* RNAP (Mukhopadhyay et al. 2001). Unfortunately, the modification is limited to the C-terminus of a protein. Trivalent-arsenic-mediated labeling and hexahistidine-tag-mediated labeling have not been successfully used to incorporate probes into two largest subunits of *E. coli* RNAP.

Nonsense suppression

The nonsense suppression method allows site-specific incorporation of unnatural amino acids into proteins with high fidelity and efficiency (Wang and Schultz, 2005). In this method, an engineered tRNA-synthetase pair can site-specifically insert the unnatural amino acid of interest into proteins in response to the amber codon (Figure 3.1). To date, more than 30 unnatural amino acids have been genetically incorporated into proteins in response to nonsense and frameshift codons in both prokaryotes and eukaryotes, including photoreactive and redox active amino acids, glycosylated amino acids, and amino acids containing keto, azido, alkynyl, and iodo groups (Wang et al. 2001, 2003, 2005; Deiters et al. 2003). Introduction of these reactive groups allows site-specific modification of proteins. It has been demonstrated that the unnatural amino acid, p-azido-L-phenylalanine (pAzPhe), can be selectively incorporated into proteins in *E. coli* by using a suppressor tRNA-aminoacyl tRNA synthetase pair (Wang et al. 2001, 2003). The azide-containing protein have been modified by Huisgen [3+2] cycloaddition reaction (Wang et al. 2001, 2003) and Staudinger-Bertozzi ligation (Tsao et al. 2005; Saxon and Bertozzi, 2000).

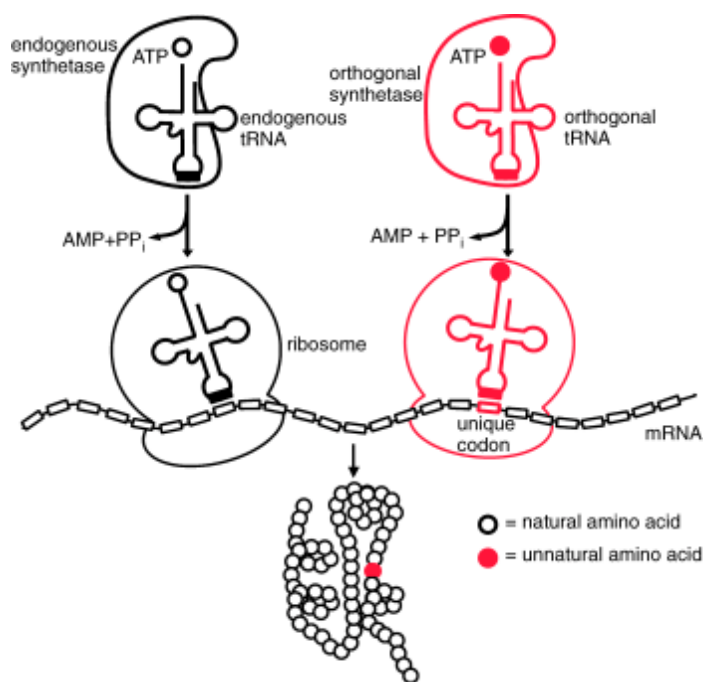


Figure 3.1. Nonsense suppression method. L. Wang and P.G. Schultz *Angew. Chem. Int.*

Ed. 2005 **44**, 34-66.

Staudinger- Bertozzi ligation

The classic Staudinger reaction (Staudinger and Meyer, 1919) (Figure 3.2) between a phosphine and an azide produces an unstable intermediate, aza-ylide, which hydrolyzes spontaneously to yield a primary amine and the corresponding phosphine oxide. To produce a stable amide-linked product, Bertozzi et al (Saxon and Bertozzi, 2000) designed a specifically engineered triarylphosphine that allows rearrangement of the unstable aza-ylid to a stable covalent adduct by intramolecular cyclization (Figure 3.3). This chemical reaction proceeds with excellent yields at room temperature under physiological conditions and is highly selective for azides. The Staudinger-Bertozzi ligation reaction has been employed in a wide range of applications, including modification of cell surfaces, protein engineering, specific labeling of nucleic acids, and as a general tool for bioconjugation (Kiick et al. 2002; Wang et al. 2003).

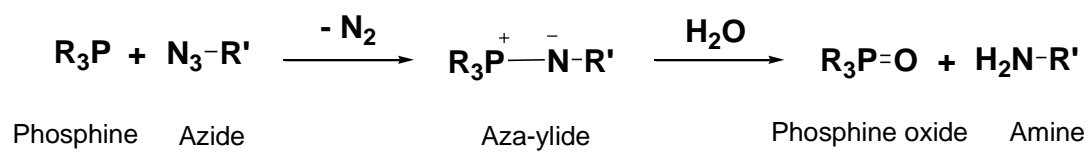


Figure 3.2. Staudinger reaction between a phosphine and azide to form an aza-ylide.

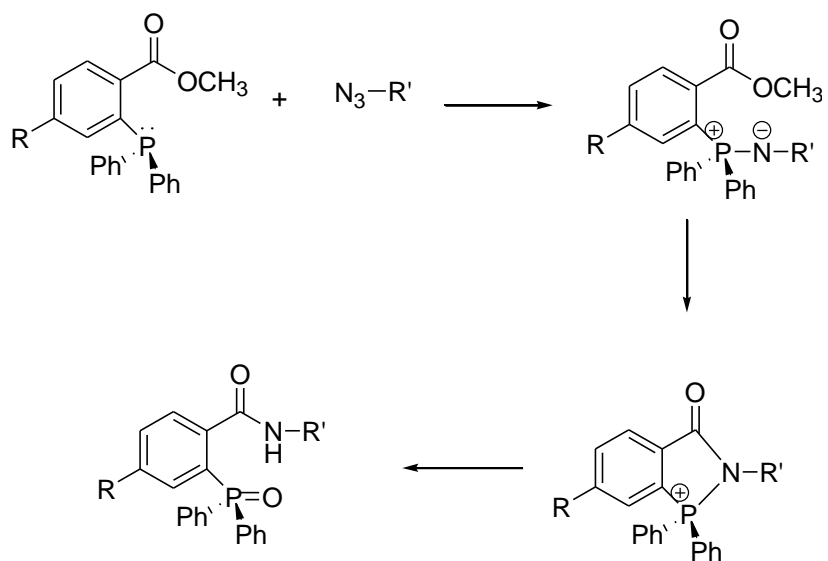


Figure 3.3. Staudinger-Bertozzi ligation.

In the development of procedures for labeling of RNAP, first, we have incorporated the azide-containing unnatural amino acid p-azido-L-phenylalanine at the site of interest into RNAP β' and β subunits by the nonsense suppression method. We explored the labeling of the azide-containing proteins with alkyne-fluorescein (Figure 3.4B) through Cu(I)-catalyzed Huisgen [3+2] cycloaddition (“click chemistry”) (Figure 3.4A, Deiters et al 2003; Rostovtsev et al 2002) under conditions: (1) Cu wire, CuSO₄; (2) Cu wire, CuSO₄, ligand (tris(1-benzyl-1*H*-[1,2,3]triazol-4-ylmethyl)amine, TBTA); (3) CuSO₄, sodium ascorbate. Under condition (1), with the absence of ligand, the proteins were labeled by alkyne-fluorescein with low efficiency. Under condition (2), upon the addition of TBTA to the reaction mixture the proteins were precipitated. Under condition (3), the proteins were completely degraded when sodium ascorbate was used in the reaction. We also explored the labeling of the azide-containing β' and β derivatives with cyclooctyne-fluorescein and difluorinated cyclooctyne-Alexa488 (DIFO-488) (Figure 3.4D) through a strain-promoted [3+2] azide-alkyne cycloaddition (Figure 3.4C, Agard et al 2004; Baskin et al 2007). When wild-type β' and β subunits were subjected to the same reaction as a control, significant labeling of wild-type proteins were observed. Thus, this reaction yielded very low selectivity between the azide-containing proteins and the wild-type protein.

We also explored the labeling of the azide-containing β' and β derivatives with phosphine-derived dyes through Straudinger-Bertozzi ligation. This reaction proceeded with high selectivity and efficiency. Therefore we used Staudinger-Bertozzi reaction as a modification method.

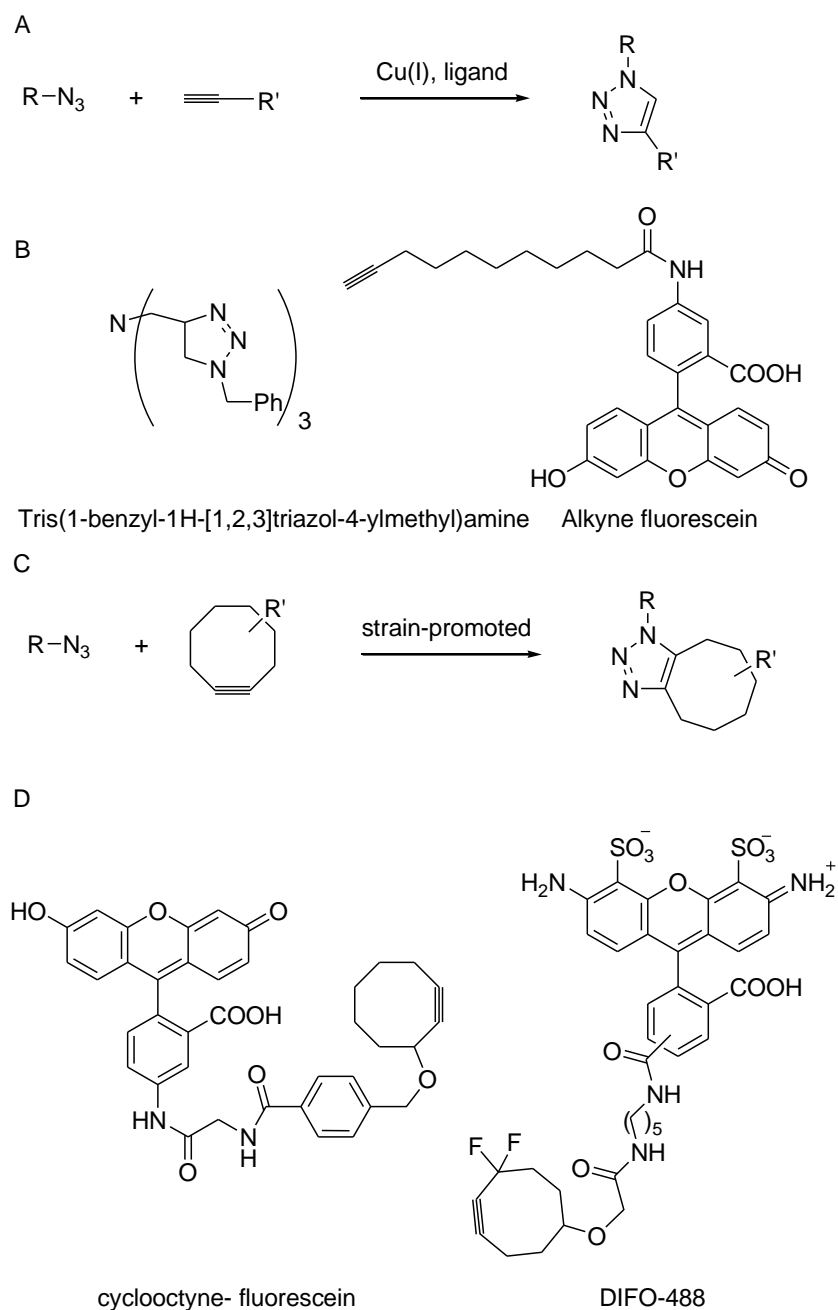


Figure 3.4. A. Cu(I)-catalyzed Huisgen cycloaddition (“click chemistry”). B. Tris(1-benzyl-1H-[1,2,3]triazol-4-ylmethyl)amine (TBTA) and Alkyne-fluorescein. C. Strain-promoted [3+2] cycloaddition of azides and cyclooctynes. D. Cyclooctyne-fluorescein and DIFO-488.

In this work, we have extended these two approaches of nonsense suppression and Staudinger-Bertozzi ligation to the incorporation of fluorescent probes into RNAP. To attach fluorescent donor into RNAP β' pincer and fluorescent acceptor into RNAP β pincer, we have employed the strategy summarized in Figure 3.5. First, we have incorporated the azide-containing unnatural amino acid p-azido-L-phenylalanine at the site of interest into RNAP β' and β subunits by the nonsense suppression method. Then, we labeled the azide-containing subunits through Staudinger-Bertozzi ligation using phosphine-derived fluorescent probes. The finally reconstitution of labeled β' and β subunits and other recombinant subunits provided RNAP with fluorescent donor incorporated at β' pincer and fluorescent acceptor incorporated at β pincer.

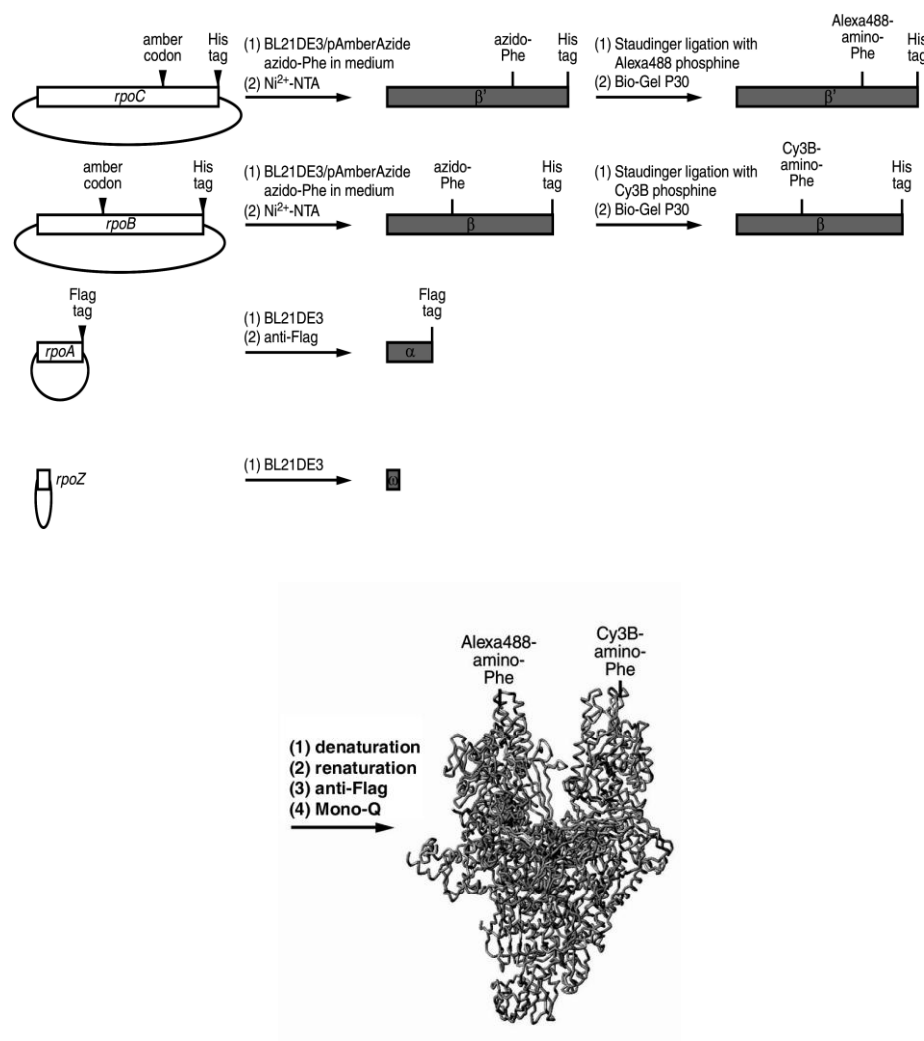


Figure 3.5. Incorporation of Alexa488 at the tip of the clamp and cy3B at the tip of the β pincer, through a combination of unnatural amino acid mutagenesis, Staudinger-Bertozzi ligation, and RNAP reconstitution.

3.2. Choice of donor/acceptor pair

The energy transfer donor-acceptor pair of Alexa 488 and Cy3B was used (Panchuk-Voloshina et al. 1999; Cooper et al. 2004). Alexa488 has similar absorbance and emission spectra as fluorescein, but it is more fluorescent in its conjugates and significantly more photostable than fluorescein. The Alexa Fluor 488 dye is by far the best fluorescein substitute available for most applications. Alexa488 carries several advantages as a donor:

- long life time (fluorescence lifetime of ~4.1 nanoseconds)
- Strong absorption, with an extinction coefficient greater than $65,000 \text{ cm}^{-1}\text{M}^{-1}$
- Much greater photostability than fluorescein, allowing more time for observation
- pH-insensitive fluorescence between pH 4 and 10
- Water solubility, with no organic co-solvents required in labeling reactions,
- Superior fluorescence output per protein conjugate, surpassing that of any other spectrally similar fluorophore-labeled protein
- good quantum yields

The energy acceptor Cy3B is characterized by an excellent spectral overlap with Alexa488 and high extinction coefficients ($130,000 \text{ M}^{-1}\text{cm}^{-1}$) leading to high R_0 values of ~ 60 Å for the Alexa488/Cy3B pair. Cy3B has the same common chromophore as Cy3. But open chain trimethine cyanine dyes e.g. Cy3 can exist in many conformations and are capable of undergoing numerous rotational and translational modes of vibration which result in the loss of energy by non-radiative processes. In Cy3B, a rigid backbone has

therefore been introduced to provide a trimethine dye with a fixed conformation in both the relaxed and excited states. This increases the efficiency of the fluorescent output and quantum yield upon excitation.

3.3. Rationale of labeling positions

The fluorescent donor Alexa 488 was attached to *E. coli* RNAP β' residue 150 and 284 located at the distal tip of the clamp (β' pincer). The fluorescent acceptor Cy3B was attached to *E. coli* RNAP β residue 106 located at the tip of the β pincer and β residue 222 located at the tip of the β lobe (Figure 3.6). The β pincer is immobile in the crystal structures of RNAP therefore it serves as a reference to measure the clamp conformation. The distance between probes on β' residue 284 and β residue 106 provides information for clamp conformation. The β lobe is a mobile module in the crystal structures of RNAP. The distance between probes on β' residue 284 and β residue 222 includes contributions from the clamp conformation and superimpose of the β lobe. The labeling positions in RNAP have to satisfy the two conditions: (1) should not affect RNAP function; (2) should be within the distance range where FRET is very sensitive to any changes in distance ($\sim 40\text{-}80$ Å). The RNAP derivatives with fluorescent groups attached to position β' residue 284 and β residue 106 and 222 were verified to be functional in transcription but RNAP derivatives with the fluorescent donor was attached to β' residue 150 are not functional in transcription.

As observed in crystal structures (PDB 1I3Q, PDB 1HQM, PDB 1L9Z), the donor-acceptor distances for probes at β' residue 284 and β residue 106 are ~ 80 Å in an open clamp conformational state, ~ 65 Å in partly closed clamp conformational state, and ~ 50 Å in a fully closed clamp conformational state. The donor-acceptor distances for probes at β' residue 284 and β residue 222 are ~ 95 Å in an open clamp conformational

state, $\sim 85\text{\AA}$ in partly closed clamp conformational state, and $\sim 70\text{\AA}$ in a fully closed clamp conformational state. The donor-acceptor distances are within the distance range where FRET is very sensitive to any changes in distance and are sensitive reporters of clamp conformation (Figure 3.6).

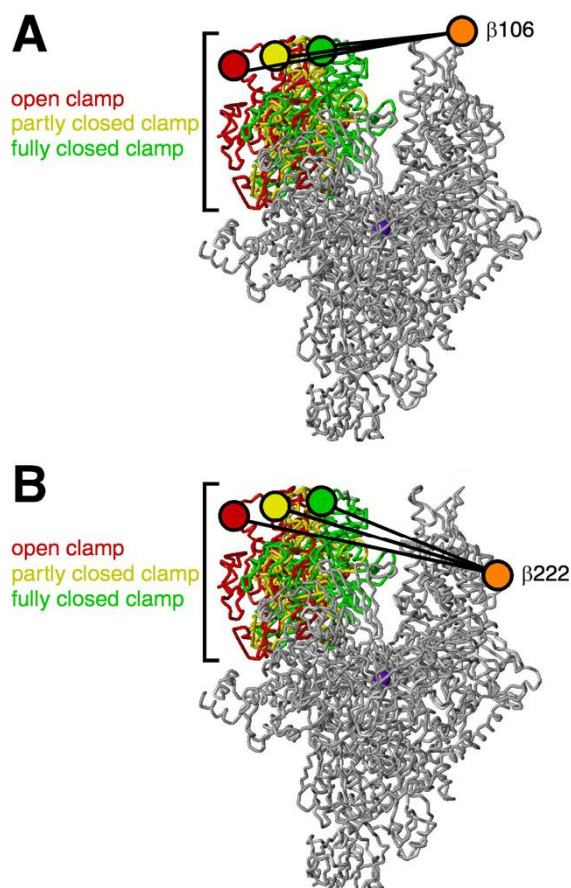


Figure 3.6. FRET analysis of clamp opening/closing. Structure of RNAP showing open (red), partly closed (yellow), and fully closed (green) clamp conformations, as observed in crystal structures (PDB 1I3Q, PDB 1HQM, PDB 1L9Z) ($\sigma 70$ omitted for clarity). Red, yellow, and green circles, positions of probe sites at the tip of the clamp (β' residue 284); orange circle, position of reference probe site at the tip of the β pincer (β residue 106 or residue 222); violet sphere, active-center Mg^{2+} . (A) Probes at β' residue 284 and β residue 106 (distances = ~ 80 , ~ 65 , and ~ 50 Å in open, partly closed, and fully closed states). (B) Probes at β' residue 284 and β residue 222 (distances = ~ 95 , ~ 85 , and ~ 70 Å in open, partly closed, and fully closed states).

3.4. Determination of mean clamp conformational states

To define mean clamp conformational states during transcription, we have used FRET to monitor the distance between a first fluorescent probe, serving as donor, incorporated at the tip of the β' pincer (residue 284) and a second fluorescent probe, serving as acceptor, incorporated at the tip of the β pincer (residue 106 and 222). We have measured the distances in RNAP holoenzyme, in promoter open complex, in initial transcribing complexes, and in elongation complexes.

The DNA fragments carrying the *lac* CONS (Figure 3.7) promoters that are derivatives of *lac* promoter were used for the formation of RNAP-promoter open complex (RP_o), initial transcribing complexes carrying out iterative abortive initiation and containing RNA products up to 2, up to 4, up to 7 ($RP_{itc, \leq 2}$, $RP_{itc, \leq 4}$, and $RP_{itc, \leq 7}$) and elongation complexes ($RD_{e,11}$ and $RD_{e,15}$). The sequence of *lac* CONS promoters differs from the sequence of wild type *lac* promoter by a consensus “-35” element, a consensus “-10” element, and a consensus spacer of 17 base pairs between the two core elements. *Lac* CONS promoter is expected to be one of the strongest promoters in terms of stability of the open complex (Mukhopadhyay et al. 2001). Using promoters *lac* CONS-11 and *lac* CONS-15, with limited set of nucleotide triphosphates (NTPs), initiating dinucleotide ApA and a terminating nucleotide (3'-OMe CTP), we were able to form promoter open complex, complexes engaged in abortive synthesis and containing RNA products up to 2, up to 4, and up to 7 in length ($RP_{itc, \leq 2}$, $RP_{itc, \leq 4}$, and $RP_{itc, \leq 7}$), and defined elongation

complexes containing RNA product of 11nt or 15nt in length ($RD_{e,11}$ and $RD_{e,15}$; Table 3.1).

lac CONS-11 (161bp)

TCCCGACTGGAAAGCGGGCAGTGAGCGCAACGCAATAAATGTGATCTAGATCACATTTTAGGCACCCAGGCTTGACAC
 AGGGCTGACCTTTCGCCCGTCACTCGCGTTGCGTTATTTACACTAGATCTAGTGTAAAATCCGTGGGGTCCGAACTGTG

-35

TTTATGCTTCGGCTCGTATAATGTGTGGAAATTGTGAGACCGGATAACAATTTACACAGGAAACAGCTATGACCATGATT
 AAATACGAAGCCGAGCATATTTACACACCTTTAACACTCTCCCTATTGTTAAAGTGTGTCCTTTGTCGATACTGGTACTAA

17 bp spacer **-10** **+1**

ACG
 TGC

*lac*UV5 CONS-15 (164bp)

TCCCGACTGGAAAGCGGGCAGTGAGCGCAACGCAATAAATGTGATCTAGATCACATTTTAGGCACCCAGGCTTGACAC
 AGGGCTGACCTTTCGCCCGTCACTCGCGTTGCGTTATTTACACTAGATCTAGTGTAAAATCCGTGGGGTCCGAACTGTG

-35

TTTATGCTTCGGCTCGTATAATGTGTGGAAATTGTGAGGAGGACGGATAACAATTTACACAGGAAACAGCTATGACCAT
 AAATACGAAGCCGAGCATATTTACACACCTTTAACACTCCTCCTCCCTATTGTTAAAGTGTGTCCTTTGTCGATACTGGTA

17 bp spacer **-10** **+1**

GATTACG
 CTAATGC

Figure 3.7. Sequences of DNA fragments used for the formation of promoter-open complex and elongation complexes 11, 15 nt in length. Positions of promoter -10 and -35 elements are highlighted in grey. Transcription start site is indicated with an arrow.

Terminating nucleotide is shown in red.

Table 3.1. NTP subsets and the corresponding RNA products and complexes

promoter	NTP subset	RNA product	complex
<i>lac</i> CONS-11	none	none	RP _o
	ApA	AA	RP _{itc, ∅}
	ApA+UTP	AAUU	RP _{itc, ≤4}
	ApA+UTP+GTP	AAUUGUG	RP _{itc, ∇}
	ApA+UTP+GTP+ATP	AAUUGUGAGAC	RD _{e,11}
	+3'-OMe CTP		
<i>lac</i> CONS-15	none	none	RP _o
	ApA	AA	RP _{itc, ∅}
	ApA+UTP	AAUU	RP _{itc, ≤4}
	ApA+UTP+GTP	AAUUGUG	RP _{itc, ∇}
	ApA+UTP+GTP+ATP	AAUUGUGAGGA	RD _{e,15}
	+3'-OMe CTP	GGAC	

Initially, the fluorescent labeled RNAP derivatives prepared contain large fraction of aggregates, therefore the ensemble FRET experiment were performed in the gel matrix (“in-gel” FRET, Mukhopadhyay et al 2001) to minimize complications due to fluorescence arising from RNAP aggregates. The RNAP holoenzyme and RP_o were isolated by nondenaturing PAGE and analyzed in situ in gel slices. To obtain data for RP_{itc} and RD_e , ApA, ATP, GTP, UTP and 3'OMe-CTP were added directly to the cuvette containing the gel slice of RP_o . To obtain data for the effects of switch-region-target inhibitors (Myx, Cor, Rip, and Lpm), the inhibitors were added directly to the cuvette containing the gel slice of holoenzyme. An increase in FRET efficiency upon formation of RP_o from holoenzyme and upon the binding of Myx, Cor, Rip to RNAP was observed in the in-gel measurements (Table 3.2-3.5). However, the experimental error in in-gel FRET was high due to the gel scattering and low signal to noise ratio. Later, the *in vitro* reconstitution conditions were optimized to yield fluorescent RNAP derivatives with low aggregates and high activity and are suitable for measurements in solution. The ensemble FRET in solution which provided higher signal to noise ratio and low experimental error were performed to define the clamp conformational changes and the effects of small molecule effectors.

Table 3.2. In-gel FRET results for holoenzyme, RP_o , $RP_{itc, \leq 2}$, $RP_{itc, \leq 4}$, $RP_{itc, \leq 7}$, $RD_{e,11}$, and $RD_{e,15}$ formed by [Alexa488-Phe284] β^3 ; [Cy3B-Phe106] β -RNAP with *lac* CONS-11 and *lac* CONS-15.

complex	E (%)
holoenzyme	30 \pm 0.5
RP_o	35 \pm 1.4
$RP_{itc, \leq 2}$	35 \pm 1.6
$RP_{itc, \leq 4}$	35 \pm 1.7
$RP_{itc, \leq 7}$	33 \pm 1.4
$RD_{e,11}$	30 \pm 3.6
$RD_{e,15}$	35 \pm 2.0

Table 3.3. In-gel FRET results for holoenzyme, RP_o , $RP_{itc, \leq 2}$, $RP_{itc, \leq 4}$, $RP_{itc, \leq 7}$, $RD_{e,11}$, and $RD_{e,15}$ formed by [Alexa488-Phe284] β^3 ; [Cy3B-Phe222] β -RNAP with *lac* CONS-11 and *lac* CONS-15.

complex	E (%)
holoenzyme	33 \pm 0.6
RP_o	35 \pm 1.7
$RP_{itc, \leq 2}$	34 \pm 1.5
$RP_{itc, \leq 4}$	35 \pm 1.4
$RP_{itc, \leq 7}$	34 \pm 1.6
$RD_{e,11}$	33 \pm 1.7
$RD_{e,15}$	32 \pm 3.8

Table 3.4. Effects of Myx, Cor, Rip and Lpm on RNAP holoenzyme [Alexa488-Phe284] β' [Cy3B-Phe106] β -RNAP clamp conformation.

complex	E	ΔE
holo	0.30 ± 0.005	
holo + Myx	0.34 ± 0.01	0.04
holo + Rip	0.35 ± 0.008	0.05
holo + Cor	0.39 ± 0.008	0.09
holo + Lpm	0.30 ± 0.01	0

Table 3.5. Effects of Myx, Cor, Rip and Lpm on RNAP holoenzyme [Alexa488-Phe284] β' [Cy3B-Phe222] β -RNAP clamp conformation.

complex	E	ΔE
holo	0.33 ± 0.006	
holo + Myx	0.40 ± 0.009	0.07
holo + Rip	0.38 ± 0.01	0.05
holo + Cor	0.40 ± 0.01	0.07
holo + Lpm	0.30 ± 0.01	-0.03

4. Incorporation of fluorescent probes into RNAP

4.1. Materials and Methods

4.1.1. Plasmids

A list of plasmids used in this chapter is presented in Table 4.1. Plasmid pRL663 encodes C-terminal hexahistidine-tagged *E. coli* RNAP β' subunit under control of the *tac* promoter (Wang et al., 1995). Plasmid pRL706 encodes C-terminal hexahistidine-tagged *E. coli* RNAP β subunit under control of the *trc* promoter (Severinov et al., 1997). Plasmids pMKSe2, pT7 β' and pT7 ω coding for the subunits β' , β , and ω were previously described (Naryshkin et al., 2001; Mekler et al., 2002;)

Plasmid pET21a rpoC-H6 encoding C-terminal hexahistidine-tagged β' subunit were constructed by replacement of BsmI – HindIII segment of pET21a rpoC with the correspondent BsmI – HindIII rpoC DNA fragment of pRL663. Amber stop codon (TAG) substitutions at residues 150 and 284 were introduced by site-directed mutagenesis.

Plasmid pET21d rpoB-H6 encoding C-terminal hexahistidine-tagged β subunit were constructed by inserting the NcoI – HindIII fragment of plasmid pRL706 into pET21d vector (Novagen) and deletion of 44bp between NcoI site and rpoB start codon. Amber

stop codon (TAG) substitutions at residues 106 and 222 were introduced by site-directed mutagenesis.

Plasmid pAmberAzide encoding a *Methanococcus jannaschii* mutant amber suppressor tRNA^{Tyr}_{CUA} (mutRNA^{Tyr}_{CUA}) and a mutant *Methanococcus jannaschii* tyrosyl-tRNA synthetase (*MjTyrRS*) which specifically charges tRNA^{Tyr}_{CUA} with pAzPhe was requested from Peter Schultz.

Plasmid pET21aNF α encoding N-terminal FLAG tagged α subunit were constructed by inserting the XbaI-BamHI fragment of plasmid pWNNF α into pET21a vector (Novagen).

Plasmid pET21d NF α^I NTD- α^II NTD encodes N-terminal FLAG tagged fusion protein of two α NTDs. This plasmid was constructed using pET21aNF α by add-on PCR to generate DNA fragment coding for FLAG- α NTD (residues 1-235) with NcoI and BamHI digestion sites at the ends using 5'- GGAATTCCATGGACTACAAGGACG ACGATGACAAGG-3' and 5'- TCGCGGATCCACGTAAGTCAACGAAAGCTTCCA GTTGTTTCAGC-3' primers. The PCR product was digested with NcoI and BamHI. Add-on PCR was performed using pREIINH α to generate DNA fragment coding for the short linker GSGGSG and α NTD (residues 1-235) with BamHI and NotI digestion sites at the ends using 5'- TCGCGGATCCGGTGGCAGCGGGATGCAGGGTTCTGTGACAGAG TTTCTA AAACCG-3' and 5'-TGC GGCGGCCGCTTAACGTAAGTCAACGAAAGC TTCCAGTTG TTCAGC-3' primers. The PCR product was digested with BamHI and NotI. The two PCR products were inserted into pET28a (Novagen) vector between NcoI and NotI sites by three way ligation.

Table 4.1. Plasmids

Plasmids	Characteristics	Source
pRL663	Ap ^R ; ori-pBR322; P _{lpp} -P _{lacUV5} -rpoC (CH6)	Wang et al., 1996
pET21a rpoC	Ap ^R ; ori-pBR322; P _{φ10} -rpoC	Novagen
pET21a rpoC-H6	Ap ^R ; ori-pBR322; P _{φ10} -rpoC(CH6)	This work
pET21a rpoC-H6 150TAG	Ap ^R ; ori-pBR322; P _{φ10} -rpoC150amber (CH6)	This work
pET21a rpoC-H6 284TAG	Ap ^R ; ori-pBR322; P _{φ10} -rpoC284amber (CH6)	This work
pRL706	Ap ^R ; ori-pBR322; P _{lpp} -P _{lacUV5} -rpoB (CH6)	Severinov et al., 1997
pET21d rpoB-H6	Ap ^R ; ori-pBR322; P _{φ10} -rpoB (CH6)	This work
pET21d rpoB-H6 106TAG	Ap ^R ; ori-pBR322; P _{φ10} -rpoB106amber (CH6)	This work
pET21d rpoB-H6 222TAG	Ap ^R ; ori-pBR322; P _{φ10} -rpoB106amber (CH6)	This work
pWNNFα	Km ^R ; ori-pSC101; P _{lpp} -P _{lacUV5} -rpoA(NFLAG)	Niu et al., 1996
pET21a NFα	Ap ^R ; ori-pBR322; P _{φ10} -rpoA(NFLAG)	This work
pET21d NF αINTD-αIINTD	Ap ^R ; ori-pBR322; P _{φ10} -rpoA(1-235)-rpoA(1-235)(NFLAG)	This work
pREIINHα	Ap ^R ; ori-pBR322; P _{lpp} -P _{lacUV5} -rpoA(NH)	Niu et al., 1996
pMKSe2	Ap ^R ; ori-pBR322; P _{lacUV5} -rpoB	Lee et al, 1991
pT7β'	Ap ^R ; ori-pBR322; P _{φ10} -rpoC	Naryshkin et al., 2001
pT7ω	Ap ^R ; ori-pBR322; P _{φ10} -rpoZ	Naryshkin et al., 2001

4.1.2. Synthesis of Alexa488 and Cy3B phosphine derivatives

Reaction progress was monitored by thin-layer chromatography and visualized by illuminating with UV light. Preparative HPLC was performed with a SUPELCO Discovery BIO C-18 reversed-phase column (25cm x 10mm, 10 μ m) using a linear gradient of H₂O and CH₃CN. Mass spectra were obtained using electrospray ionization (ESI) or matrix-assisted laser desorption ionization (MALDI) techniques.

Synthesis of 1-Methyl-2-Diphenylphosphinoterephthalate

1-Methyl-2-Diphenylphosphinoterephthalate (Figure 4.9, compound **2**) was synthesized according to published procedures.

Methyl-2-Iodoterephthalate (1). 1-Methyl-2-aminoterephthalate (Aldrich) (1g, 5.12mmol) was added to 10ml of ice-cold concentrated HCl (Fisher) in a round-bottom flask. A solution of NaNO₂ (Fisher) (360mg, 5.18mmol) in 2ml of H₂O was added dropwise, resulting in evolution of a small amount of orange gas. The mixture was stirred for 30min at room temperature and then centrifuged to remove insoluble solid. The supernatant was added into a solution of KI (Fisher) (8.6g, 50mmol) in 14ml of H₂O. The dark red solution was stirred for 1h at room temperature and then diluted with CH₂Cl₂ (200ml) and washed with saturated Na₂SO₃ (2 x 20ml). The organic layer was washed with water (2x40ml) and saturated NaCl (2 x 20ml) and dried over Na₂SO₄ and concentrated. The crude product was dissolved in a minimal amount of MeOH (5ml), and H₂O was added until the solution appeared cloudy. Cooling to 4 °C and filtration afforded

380mg (24% yield) a bright yellow solid. ^1H NMR (500MHz, CDCl_3): δ 3.98 (s, 3H), 7.84 (d, 1H, $J = 7.5$), 8.12 (d, 1H, $J = 8.0$), 8.69 (s, 1H).

1-Methyl-2-Diphenylphosphinoterephthalate (2). Anhydrous MeOH (Aldrich) (3ml), triethylamine (Aldrich) (0.3ml, 2mmol), compound **1** (306mg, 1.0mmol), and palladium acetate (Aldrich) (2.2 mg, 0.010mmol) were added to a flame-dried flask. The mixture was degassed in vacuo. While stirring under an atmosphere of Ar, diphenylphosphine (Aldrich) (0.17ml, 1.0 mmol) was added. The resulting solution was heated at reflux overnight, and then allowed to cool to room temperature and concentrated. The residue was dissolved in 250 ml of a 1:1 mixture of $\text{CH}_2\text{Cl}_2/\text{H}_2\text{O}$ and layers were separated. The organic layer was washed with 1M HCl (1x10ml) and concentrated. The crude product was recrystallized in $\text{CH}_2\text{Cl}_2/\text{Hexane}$. The resulting yellow solid 216mg (60% yield) was collected and dried. MS (ESI) m/z 364.9 (MH^+).

Synthesis of Alexa 488 phosphine derivative

1-ethyl-3-(3-dimethylaminopropyl)-carbodiimide, hydrochloride (EDAC, 9.8mg, 51.2 μmol) (Invitrogen) and N-hydroxysulfosuccinimide, sodium salt (NHSS, 8.2mg, 37.8 μmol) (Invitrogen) were dissolved in 0.1ml H_2O and added to compound **2** (11.4mg, 31.2 μmol) in 0.25ml DMF. The mixture was added to Alexa Fluor 488 cadaverine, sodium salt (2.0mg, 3.1 μmol) (Invitrogen) dissolved in 0.1ml H_2O and N,N-diisopropylethylamide (DIPEA, 11.2 μl 62.4 μmol) (Aldrich) was added. After 3h at room temperature, the product was purified by reversed-phase HPLC (30% to 100% B from 0-

30min. Solvent A: water + 0.1% trifluoroacetic acid; solvent B: 90% acetonitrile, 10% water + 0.1% trifluoroacetic acid.) and lyophilized. MS (ESI) m/z 964.9 (MH⁺)

Synthesis of Cy3B phosphine derivative

Cy3B Mono NHS ester (5mg, 6.5 μ mol) (Amersham Biosciences) was dissolved in 50 μ l of anhydrous DMF (Aldrich). Triethyl amine (TEA, 60 μ l, 430 μ mol) and (tritylamino) methanaminium acetate (23.5mg, 65 μ mol) (Novabiochem) were added. After 2h at room temperature, the reaction was checked by thin-layer chromatography (CHCl₃/CH₃OH = 1:1). The product compound **3** was purified by reversed-phase HPLC (30% to 100% B from 0-30min. Solvent A: water; solvent B: 90% acetonitrile, 10% water.) and lyophilized. MS (MALDI) m/z 845.6 (MH⁺).

Cy3B NH₂ (4). Compound **3** was dissolved in 100 μ l of CHCl₃ and 20 μ l TFA was added. After 30min at room temperature, the reaction was checked by thin-layer chromatography (CHCl₃/CH₃OH = 1:1). The product Cy3B NH₂ was purified by reversed-phase HPLC (30% to 80% B from 0-30min. Solvent A: water + 0.1% trifluoroacetic acid; solvent B: 90% acetonitrile, 10% water + 0.1% trifluoroacetic acid.) and lyophilized. MS (MALDI) m/z 603.3 (MH⁺).

Cy3B phosphine. 1-ethyl-3-(3-dimethylaminopropyl)-carbodiimide, hydrochloride (EDAC, 2.3mg, 12 μ mol) (Invitrogen), N-hydroxy benzotriazole (HOBt, 1.6mg, 12 μ mol) (Aldrich) and compound **2** (4.4mg, 12 μ mol) were dissolved in 50 μ l DMF. The mixture

was added to Cy3B NH₂ (1.0mg, 1.2μmol) dissolved in 50μl DMF and N,N-diisopropylethylamide (DIPEA, 4.3μl 24μmol) (Aldrich) was added. After 2h at room temperature, the reaction was checked by thin-layer chromatography (CHCl₃/CH₃OH = 2:1) and the product was purified by reversed-phase HPLC (20% to 100% B from 0-30min. Solvent A: water + 0.1% trifluoroacetic acid; solvent B: 90% acetonitrile, 10% water + 0.1% trifluoroacetic acid.) and lyophilized. MS (MALDI) *m/z* 948.5 (MH⁺)

4.1.3. Preparation of RNAP subunits and derivatives

Expression of C-terminal Hexahistidine-tagged RNA polymerase β' and β and derivatives with p-azidophenylalanine

Escherichia coli BL21(DE3) cells (Stratagene) were transformed with plasmid pAmber-Azide, plated onto LB plates containing 20ug/ml tetracycline and grown overnight at 37 °C. A single colony was inoculated into 5ml of LB with 20ug/ml tetracycline and grown overnight at 37 °C. 0.5ml of the overnight culture was inoculated into 50ml of LB medium with 20ug/ml tetracycline and grown to OD₆₀₀ = 0.37. The cells were recovered by centrifugation to make competent cells (BL21(DE3) pAzide) using 0.1 M CaCl₂. Competent BL21(DE3) pAzide cells were transformed with plasmid pET21a rpoC-H6 and amber derivatives or pET21d rpoB-H6 and amber derivatives, plated onto LB plates containing 100ug/mL ampicillin and 25ug/ml tetracycline and grown overnight at 37 °C.

A single colony was inoculated into 5ml of LB medium containing 100ug/mL ampicillin and 25ug/ml tetracycline and grown at 37 °C for 10h. The cells were collected by centrifugation at 4000rpm for 10 min and the LB medium was discarded. The cell pellet was suspended in 1ml of minimal medium and inoculated into 50mL of M9 minimal medium containing 100ug/mL ampicillin and 25ug/ml tetracycline and incubated overnight at 37 °C. 25ml of the overnight culture was inoculated into 500ml of M9 minimal medium supplemented with 100ug/mL of ampicillin, 25ug/ml tetracycline and 1mM p-azido-L-phenylalanine (Chem-Impex International, 103mg) and incubated at 37 °C until $OD_{600} = 0.8$ (5 hours). Protein expression was induced with 1mM IPTG (isopropyl-beta-D-thiogalactopyranoside) and cells were harvested after four hours by centrifugation.

Preparation of C-terminal Hexahistidine-tagged RNA polymerase β' and β subunits and derivatives containing p-azido-L-phenylalanine

Cell pellet from 500ml culture was suspended in 25ml of lysis buffer (40mM Tris HCl pH 7.9, 300mM KCl, 10mM EDTA, 1mM phenyl methyl sulfonyl fluoride) plus 0.2% (w/v) sodium desoxycholate. Cells were lysed using an Avestin EmulsiFlex-C5 (Avestin Inc.). Sample was centrifuged at 15,000g for 30 min and the pellet containing the inclusion bodies was collected. The pellet was suspended in 10ml lysis buffer plus 0.2% n-octyl- β -D-glucopyranoside and sonicated with three 45-s sonication pulses at 40% maximum sonication output and centrifuged for 20 min at 15,000g at 4 °C. The pellet was washed again with the lysis buffer plus 0.2% n-octyl- β -D-glucopyranoside. The

pellet was suspended in 5ml lysis buffer containing 10% glycerol and divided into 1-ml aliquots and stored at $-80\text{ }^{\circ}\text{C}$. Yield: $\sim 50\text{mg}$ ($10\text{mg}/\text{aliquot}$).

The inclusion body of $\sim 15\text{mg}$ protein was dissolved in buffer A (6M GuHCl, 100mM sodium phosphate, 10 mM Tris HCl, pH 7.5) and centrifuge for 2min at 13,000 rpm.

The supernatant was loaded onto a 1.5-ml Ni Sepharose high performance (GE Healthcare) column pre-equilibrated with 10ml buffer A. The flowthrough was reloaded onto column. The column was washed with 10ml buffer A containing 10mM imidazole, 10ml buffer A containing 20mM imidazole and eluted with 5ml buffer A containing 300mM imidazole. The fractions containing full-length protein were stored at $-80\text{ }^{\circ}\text{C}$.

Labeling of β' and β derivatives through Staudinger ligation

To 100 μl of β' or β derivatives eluted from Ni-column (1.5 mg/ml, $10\mu\text{M}$) in buffer A (6M GuHCl, 100mM sodium phosphate, 10 mM Tris HCl, pH 7.5) plus 300mM imidazole was added 12.5 μl of Alexa 488 phosphine or Cy3B phosphine in DMF (1.6mM). The reaction was carried out at $37\text{ }^{\circ}\text{C}$ with shaking for 16h. The reaction mixture was then loaded onto 1 ml column packed with Bio-Gel P30 Gel (Bio-rad) and preequilibrated in 50mM Tris HCl, pH 7.9, 6M GuHCl. The labeled protein was eluted in 50mM Tris HCl, pH 7.9, 6M GuHCl and stored at $-80\text{ }^{\circ}\text{C}$.

Purification of NFLAG α^I NTD- α^{II} NTD

BL21 (DE3) cells transformed with plasmid pET28aNF α^I NTD- α^{II} NTD were incubated at 37 °C in 1 liter of LB medium containing 40ug/ml kanamycin to an OD600 of 0.6. Expression of NFLAG α^I NTD- α^{II} NTD was then induced by addition of 1 mM isopropylthio- β -D-galactosidase (IPTG). After an additional 2 hr induction at 37 °C, cultures were harvested, and cells were lysed in 25ml of lysis buffer (20mM Tris HCl pH 7.9, 500mM NaCl, 10mM EDTA,) plus protease inhibitor (Sigma P8849). Cells were lysed using an Avestin EmulsiFlex-C5 (Avestin Inc.). Lysate was cleared by centrifugation at 13,000 rpm for 20min. NFLAG α^I NTD- α^{II} NTD was precipitated with ammonium sulfate (35g per 100ml supernatant) and recovered by centrifugation 10min at 8,000 rpm. The pellet was dissolved in 10ml of TBS buffer buffer (50mM Tris HCl pH 7.4, 150mM NaCl, 5% glycerol) and loaded onto the two 5ml columns packed with ANTI-FLAG M2 affinity gel (Sigma) pre-equilibrated in TBS buffer. The column was washed with 50ml TBS buffer and protein was eluted in TBS + 0.1mg/ml FLAG peptide. Fractions containing NFLAG α^I NTD- α^{II} NTD fusion protein were pooled and concentrated (yield: 13mg) and stored in α storage buffer (50 mM Tris-HCl pH 7.9, 200 mM KCl, 10mM MgCl₂, 1 mM EDTA, 5 mM β -me, 50% glycerol) at -80°C. The NFLAG α^I NTD- α^{II} NTD in the supernatant was precipitated with ammonium sulfate and stored at -80 °C.

Purification of recombinant no His-tag RNA polymerase β' and β subunits

The RNA polymerase β' subunit without His-tag was purified from BL21(DE3) cells transformed with plasmid pET21a rpoC and β subunits without His-tag was purified from XL1-Blue cells transformed with plasmid pMKSe2 (Naryshkin et al.).

Purification of ω subunit

BL21(DE3) cells transformed with plasmid pT7 ω were incubated at 37 °C in LB medium containing 200 μ g/ml ampicillin to an OD₆₀₀ of 0.6. Expression of ω was then induced by addition of 1 mM isopropyl-thio- β -D-galactosidase (IPTG). After an additional 3 hr induction at 37 °C, cultures were harvested, and cells were lysed in lysis buffer (50mM Tris HCl pH 7.9, 100mM NaCl, 2mM EDTA, 1mM phenyl methyl sulfonyl fluoride) (Gentry & Burgess, 1990). Ω was purified by ammonium sulfate precipitation (40g ammonium sulfate per 100ml solution). The typical yield was 30 mg/liter of culture, and the purity was >85%. The ω subunit was stored at -80 °C.

Purification of σ^{70}

BL21 (DE3) cells transformed with plasmid pGEMD σ^{70} were plated on ampicillin containing LB plates and grown overnight at 37 °C. A single colony was inoculated into 5ml of LB with ampicillin and grown overnight at 37 °C. The overnight culture was inoculated into 1L of LB media supplemented with ampicillin and grown to OD₆₀₀=0.6. Protein expression was induced with 1mM IPTG (isopropyl-beta-D-thiogalactopyranoside) and cells were harvested after three hours by centrifugation. Cell

pellet was suspended in 150ml of lysis buffer (40mM Tris HCl pH 7.9, 300mM KCl, 10mM EDTA, 1mM phenyl methyl sulfonyl fluoride) plus 0.2% (w/v) sodium desoxycholate. Cells were lysed using an Avestin EmulsiFlex-C5 (Avestin Inc.). Sample was centrifuged at 9,000 rpm for 30 min and the pellet containing the inclusion bodies of sigma 70 was collected. The pellet was washed twice with the lysis buffer plus 0.5% of Triton X-100 (Sigma) for the first wash and the lysis buffer plus 0.5% Triton X-100 plus 10mM DTT (dithiothreitol, Sigma) for the second wash. The pellet was dissolved in 50ml of denaturation buffer (50mM Tris HCl pH 7.9, 6M Guanidine HCl, 10mM MgCl₂, 10uM ZnCl₂, 1mM EDTA, 10mM DTT, 10% glycerol) and dialyzed against 2 L of the TGEB buffer (20mM Tris HCl pH7.9, 0.1mM EDTA, 10mM 2-mercaptoethanol, 5% glycerol) plus 0.2M NaCl for 36 hours with three changes of the refolding buffer. Dialyzed sample was centrifuged at 15,000g for 30min and the supernatant was loaded onto MonoQ HR 10/10 (GE Healthcare) anion exchange column equilibrated in TGEB buffer plus 0.3 MNaCl. Protein was eluted with a linear gradient of NaCl (from 0.3M to 0.5M). Fraction containing sigma 70 were pooled, concentrated and stored in storage buffer (25mM Tris HCl pH 7.9, 50% glycerol, 0.1M NaCl, 0.1mM EDTA, 1mM β -mercaptoethanol) at -80 °C. The yield was ~ 30mg per liter culture.

In vitro reconstitution of RNAP labeled with Alexa488 and Cy3B

Alexa488, Cy3B-RNAP was reconstituted from NFLAG α^I NTD- α^{II} NTD, Cy3B labeled β subunit, Alexa488 labeled β' subunit, and σ^{70} subunit using a modified procedure based on Tang et al (1996). The reconstitution mixture (61ml) contained 4.16 mg (80 nmol)N-

terminally FLAG-tagged $\alpha^{\text{I}}\text{NTD}-\alpha^{\text{II}}\text{NTD}$, 3.0 mg (20nmol) Cy3B labeled β , 7.75 mg (50nmol) Alexa488 labeled β' , and 2.0 mg (200nmol) ω in denaturation buffer (6 M guanidine-HCl, 50 mM Tris-HCl pH 7.9, 10 mM MgCl₂, 10 μ M ZnCl₂, 1 mM EDTA, 10 mM DTT, 10% glycerol). The reconstitution mixture was dialyzed without stirring overnight at 4 °C against 2 liters of reconstitution buffer (50 mM Tris-HCl pH 7.9, 200 mM KCl, 10 mM MgCl₂, 10 μ M ZnCl₂, 1mM EDTA, 5 mM β -ME, 20% glycerol). Then the mixture was dialyzed against 2 liters of reconstitution buffer for 8hr and another 2 liters of reconstitution buffer without β -ME overnight. After dialysis, insoluble residue was removed by centrifugation. The reconstitution mixture was supplemented with 0.7 mg (10nmol) of σ 70 and incubated for 45 min at 30 °C, and cleared by centrifugation at 15,000rpm for 20 min at 4 °C. The sample was adsorbed onto 3ml of ANTI-FLAG M2 affinity gel (Sigma) column pre-equilibrated in TBS buffer (50mM Tris HCl pH 7.4, 150mM NaCl, 5% glycerol). The column was washed with 30ml of TBS buffer and eluted with TBS + 0.1mg/ml FLAG peptide. Then the reconstituted labeled RNAP holoenzyme was further purified by anion-exchange chromatography on Mono-Q column. Under this condition, the typical yield was ~200 μ g RNAP holoenzyme, and the purity was >90%. The reconstituted RNAP holoenzymes were stored in RNAP storage buffer (25mM Tris HCl pH 7.9, 50% glycerol, 0.1M NaCl, 0.1mM EDTA, 1mM β -mercaptoethanol) at -20 °C.

4.1.4. Analysis of labeled RNAP activity

Fluorescence-detected abortive initiation assay

Fluorescence-detected abortive initiation assay was performed as described in Mukhopadhyay et al (2004). Reaction mixtures contained (46.5 μ l) 100 nM RNAP holoenzyme, 20 nM DNA fragment lac cons UV5 in TB (50mM Tris-HCl [pH 8.0], 100mM KCl, 10mM MgCl₂, 1mM dithiothreitol, 10 μ g/ml bovine serum albumin, and 5% glycerol). Following 15 min at 37°C, 1 μ l 0.5 mg/ml heparin was added, following a further 2min at 37°C, 1 μ l of 5 mM (γ -AmNS)UTP (Molecular Probes) was added, and reaction mixtures were transferred to submicro fluorometer cuvettes (Starna Cells). Following 5 min at 37°C, RNA synthesis was initiated by addition of 2.5 μ l of 10 mM ApA, and fluorescence emission intensity was monitored for 10 min at 37 °C (excitation wavelength, 360 nm, and emission wavelength; excitation and emission slit widths, 5 nm; QuantaMaster QM1 spectrofluorometer [PTI]). The quantity of UMP incorporated into RNA was determined from the quantity of (γ -AmNS)UTP consumed, which, in turn, was calculated as follows (Schlageck et al. 1979):

$$(\gamma\text{-AmNS})\text{UTP}_{\text{consumed}} = [(\gamma\text{-AmNS})\text{UTP}_0](F_t - F_0)/(12.4 \times F_0)$$

Where (γ -AmNS)UTP₀ is the quantity of (γ -AmNS)UTP at time 0, F₀ is the fluorescence emission intensity at time 0, and F_t is the fluorescence emission intensity at time t.

Immediately after the mixing, the accumulation of the abortive transcription initiation products (ApApU and ApApUpU for *lac* promoter and derivatives) were detected by monitoring the increase of the intensity of fluorescence emission with the excitation

wavelength at 360 nm and the emission wavelength at 500 nm. The intensity of fluorescence emission was measured continuously for 30-60 min in 37 °C until the transcription reaction well reached the steady state.

DNA templates

The sequences of DNA template used in this study are shown in Figure 3.6. The DNA templates were prepared by PCR amplification from PAGE purified oligonucleotides *lac* CONS (-107/-13) (5' - TCC CGA CTG GAA AGC GGG CAG TGA GCG CAA CGC AAT AAA TGT GAT CTA GAT CAC ATT TTA GGC ACC CCA GGC TTG ACA CTT TAT GCT TCG GCT CG - 3'), *lac* CONS (-46/+54-11C) (5' - CGT AAT CAT GGT CAT AGC TGT TTC CTG TGT GAA ATT GTT ATC CGT CTC ACA ATT CCA CAC ATT ATA CGA GCC GAA GCA TAA AGT GTC AAG CCT GGG GTG C - 3'), *lac* CONS (-42/+60-15C) (5' - CGT AAT CAT GGT CAT AGC TGT TTC CTG TGT GAA ATT GTT ATC CGT CCT CCT CAC AAT TCC ACA CAT TAT ACG AGC CGA AGC ATA AAG TGT CAA GCC TGG G - 3'), *lac* CONS (-107/-83) (5' - TCC CGA CTG GAA AGC GGG CAG TGA G - 3'), *lac* CONS (+19/+53) (5' - CGT AAT CAT GGT CAT AGC TGT TTC C - 3').

Electrophoretic mobility shift assays

Reaction mixtures contained (20 μ l) 100 nM RNAP holoenzyme, 20 nM DNA fragment laccons UV5 in TB (50mM Tris-HCl [pH 8.0], 100mM KCl, 10mM MgCl₂, 1mM dithiothreitol, 10 μ g/ml bovine serum albumin, and 5% glycerol). Following 15 min at 37°C, 1 μ l of 0.5 mg/ml heparin was added (to disrupt nonspecific complexes), and, following a further 2min at 37 °C, reaction mixtures were applied to 5% polyacrylamide slab gels (30:1 acrylamide/bisacrylamide; 6 x 9 x 0.1 cm), electrophoresed in 90 mM Tris-borate (pH8.0) and 0.2 mM EDTA (20v/cm; 1.5h at 37 °C), and analyzed using a fluorescence scanner (Typhoon).

4.2. Results and discussion

4.2.1. Preparation of *E. coli* RNAP β' and β derivatives with azido-phenylalanine residue at desired positions

E. coli RNAP β' subunit is encoded by the *rpoC* gene and is 1407 amino acids in length (Matzura et al., 1971; Ovchinnikov et al., 1982). *E. coli* RNAP β subunit is encoded by the *rpoB* gene and is 1342 amino acids in length (Ovchinnikov, 1981). Plasmids encoding β' or β subunit with a C-terminal hexahistidine tag under control of the bacteriophage T7 gene 10 promoter were constructed. Site-directed mutagenesis experiments were performed on the plasmids containing *rpoC* or *rpoB* genes to introduce an amber stop codon substituting residues 150 and 284 of β' subunit and residues 106 and 222 of β subunit. Using these amber derivatives, β' and β subunits containing p-azido-phenylalanine at desired positions ([AzPhe150] β' , [AzPhe284] β' , [AzPhe106] β , and [AzPhe222] β) were overproduced in *E. coli* strain BL21(DE3)(pAzide) cells in the presence of 1mM p-azido-L-phenylalanine (pAzPhe) (Figure 4.1). BL21DE3(pAzide) contain cells contain a plasmid (pAmberAzide, Figure 4.2) that constitutively expresses a *Methanococcus jannaschii* mutant amber suppressor tRNA^{Tyr}_{CUA} (mutRNA^{Tyr}_{CUA}) and a mutant *M. jannaschii* tyrosyl-tRNA synthetase (MjTyrRS) which specifically charges tRNA^{Tyr}_{CUA} with pAzPhe. The full length AzPhe containing β' and β derivatives and truncated β' and β fragments were produced at a high level and were found in the insoluble fraction after cell lysis and centrifugation. The isolated and washed inclusion body pellets were dissolved in 6 M guanidine hydrochloride and the full length

derivatives were purified from the truncated fragments via the C-terminal His6 tag using metal-ion-affinity chromatography.

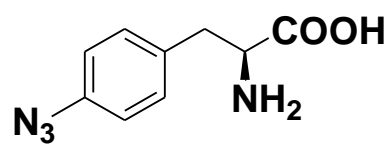


Figure 4.1. The chemical structure of p-azido-L-phenylalanine

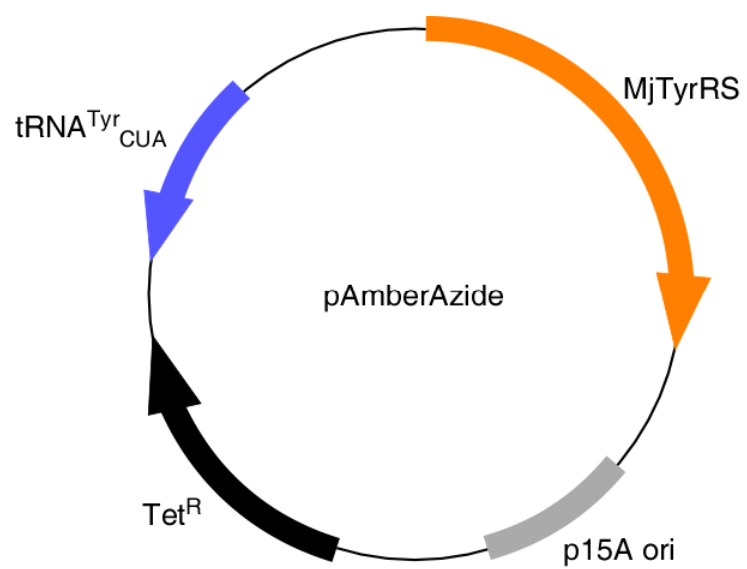


Figure 4.2. Plasmid pAmberAzide

Selectivity and efficiency of the incorporation of pAzPhe into proteins

To determine the incorporation selectivity, protein expressions in BL21(DE3) cells transformed with plasmids listed in Table 4.2 were carried out in the presence and absence of 1mM pAzPhe. As a negative control, wild-type β' and β were expressed and purified using the same procedure. The isolated inclusion body pellets and Ni-affinity column fractions were analyzed by SDS-PAGE (Figure 4.3-4.9). In the absence of pAzPhe, no produce of full-length β' and β subunits were detected from plasmids with amber mutations even after enrichment by Ni-affinity chromatography, indicating that MjTyrRS does not utilize tyrosine or other endogenous amino acids to any significant degree (Figure 4.4-4.9). The band intensities of full-length β' and β derivatives and truncated fragments were analyzed. The incorporation efficiency was ~30% for β' derivatives and was ~60% for β derivatives (Table 4.2 and Figure 4.3).

Table 4.2. Parallel expression series for each protein studied

Expression trial	Expression vector	pAmberAzide vector	p-azido-L-phenylalanine
1.	pET21a rpoC-H6	pAmberAzide	none
2.	pET21a rpoC-H6	pAmberAzide	1 mM
3.	pET21a rpoC-H6 150 TAG	pAmberAzide	none
4.	pET21a rpoC-H6 150 TAG	pAmberAzide	1 mM
5.	pET21a rpoC-H6 284 TAG	pAmberAzide	none
6.	pET21a rpoC-H6 284 TAG	pAmberAzide	1 mM
7.	pET21d rpoB-H6 106 TAG	pAmberAzide	none
8.	pET21d rpoB-H6 106 TAG	pAmberAzide	1 mM
9.	pET21d rpoB-H6 222 TAG	pAmberAzide	none
10.	pET21d rpoB-H6 222 TAG	pAmberAzide	1 mM
11.	pET21d rpoB-H6	pAmberAzide	none
12.	pET21d rpoB-H6	pAmberAzide	1 mM

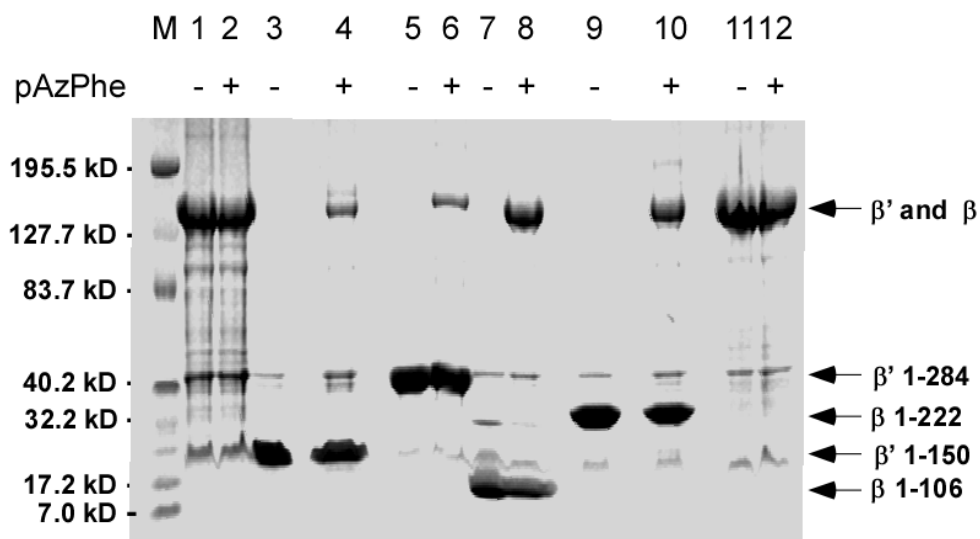


Figure 4.3. SDS-PAGE (4-20% gradient) of purified inclusion bodies produced from expression trials indicated in Table 2. The gel was stained with Coomassie Blue. Lane M shows the molecular weight standards. Lane 1-12: expression trials 1-12 in table 2.

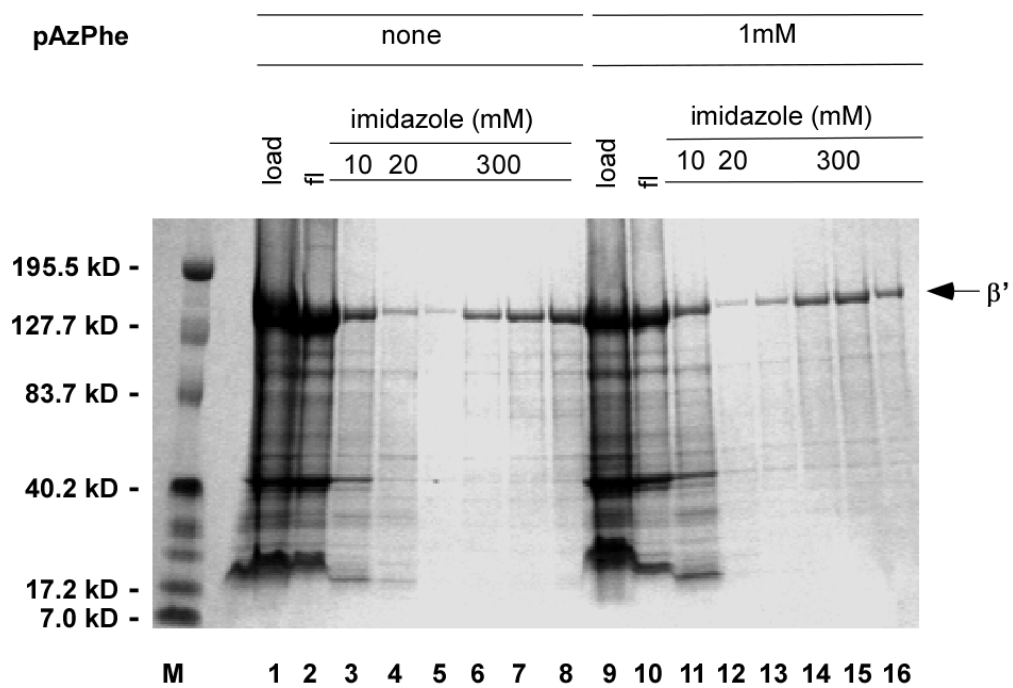


Figure 4.4. SDS-PAGE (4-20% gradient) of fractions from Ni-affinity chromatography

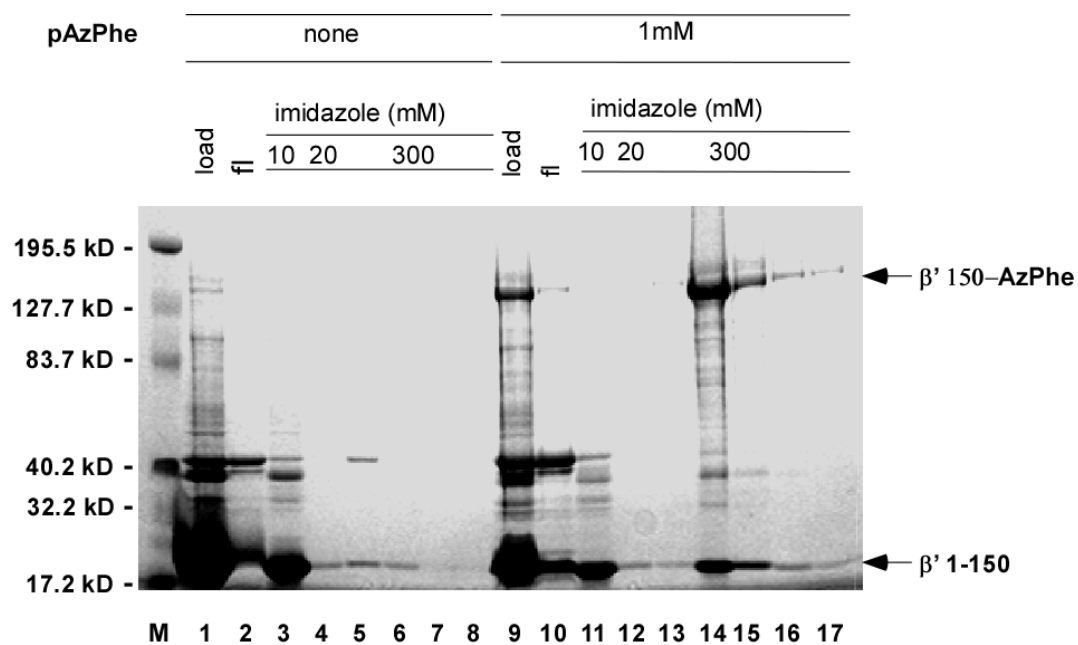


Figure 4.5. SDS-PAGE (4-20% gradient) of fractions from Ni-affinity chromatography

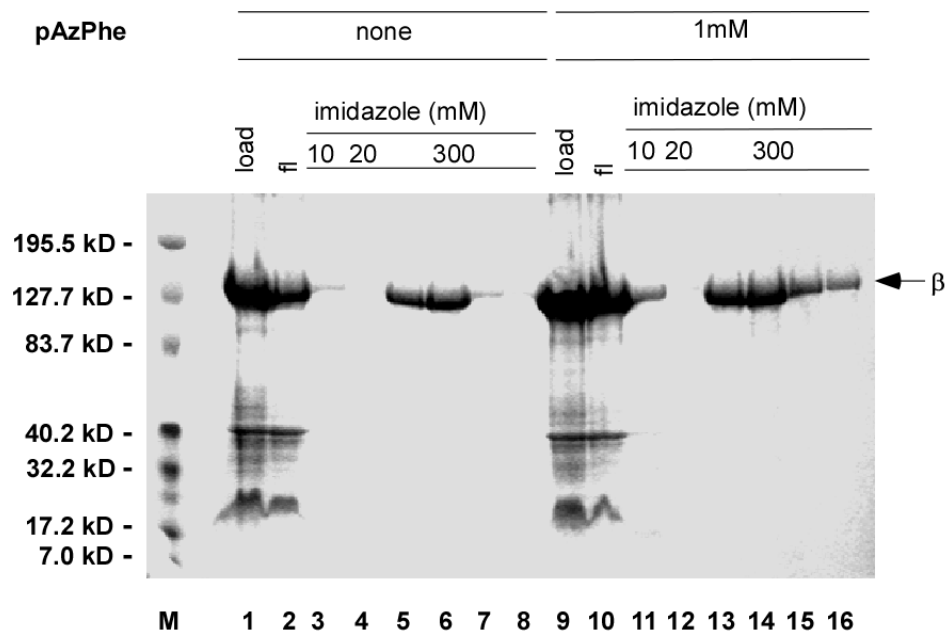


Figure 4.7. SDS-PAGE (4-20% gradient) of fractions from Ni-affinity chromatography

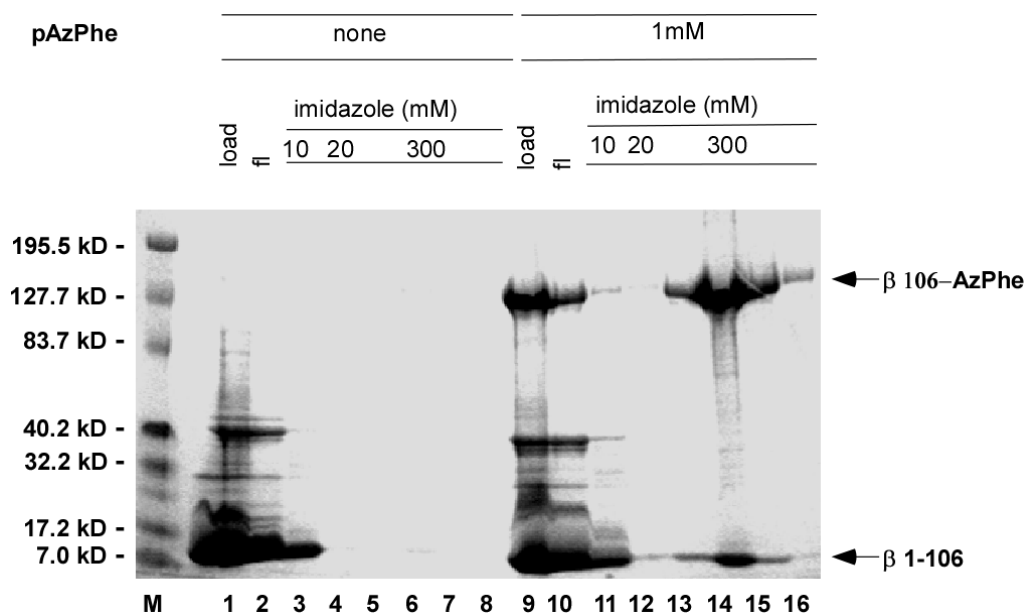


Figure 4.8. SDS-PAGE (4-20% gradient) of fractions from Ni-affinity chromatography

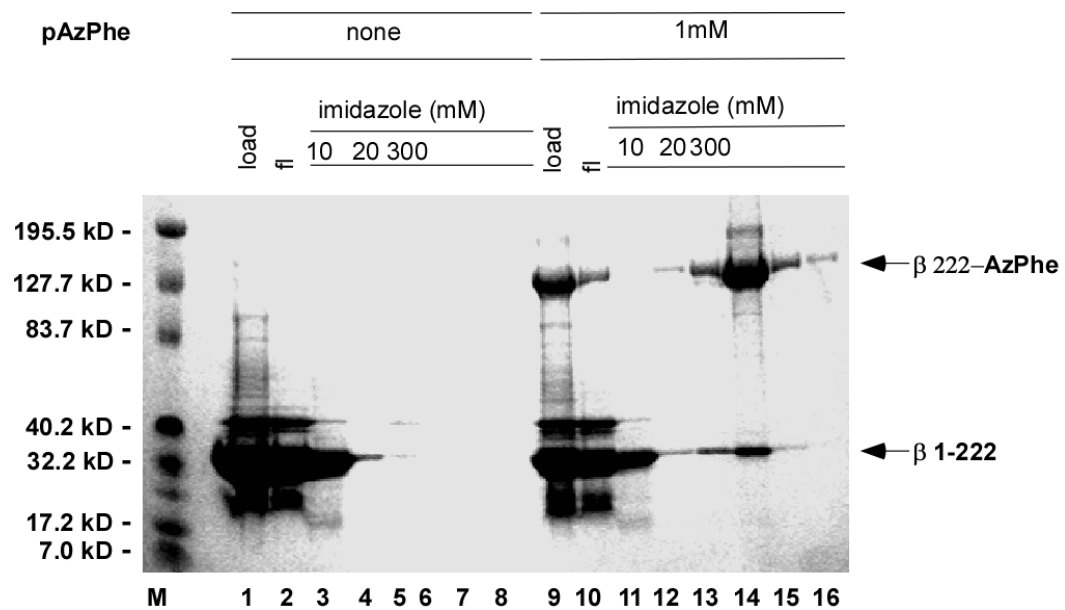


Figure 4.9. SDS-PAGE (4-20% gradient) of fractions from Ni-affinity chromatography

4.2.2. Labeling of RNA polymerase β and β' derivatives through Staudinger ligation

Synthesis of Alexa488 and Cy3B phosphine derivatives

The synthesis of the Alexa 488 and Cy3B triphenylphosphine derivative began with the Sandmeyer reaction of commercially available 1-methyl-2-aminoterephthalate to form the aryl-iodide **1**. This compound was reacted with diphenylphosphine by means of a palladium-mediated cross-coupling reaction to provide 1-Methyl-2-Diphenylphosphinoterephthalate (compound **2**) (Figure 4.10). The Alexa 488 phosphine derivative was produced by the coupling reaction of compound **2** with commercially available Alexa Fluor 488 cadaverine in the presence of dicyclohexylcarbodiimide (DCC) at ambient temperature for 3h and purified by reversed-phase HPLC (Figure 4.11). The Cy3B phosphine derivative was produced by the coupling reaction of compound **2** with N-(2-Amino-ethyl)-Cy3B which was prepared from commercial available Cy3B NHS ester in the presence of dicyclohexylcarbodiimide for 3h and purified by reversed-phase HPLC (Figure 4.13). The Alexa 488 and Cy3B phosphine derivatives were characterized by mass spectroscopy (Figure 4.12).

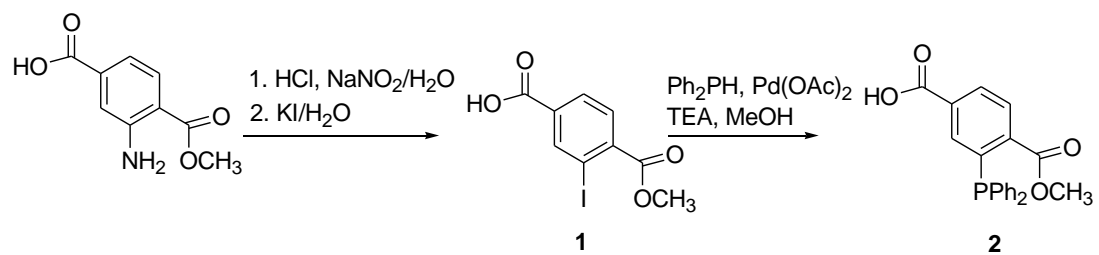


Figure 4.10. Synthesis of 1-Methyl-2-Diphenylphosphinoterephthalate (compound **2**)

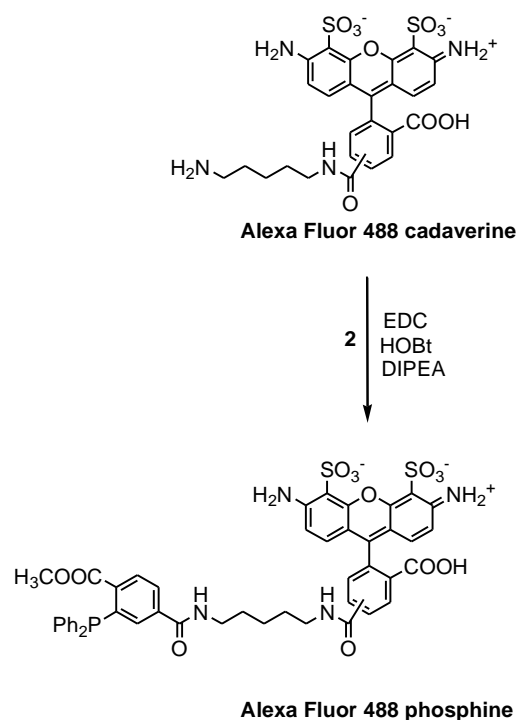
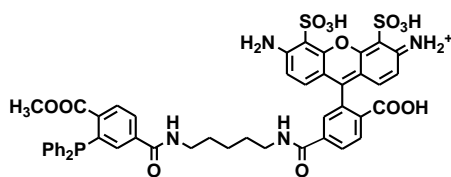


Figure 4.11. Synthesis Alexa Fluor 488 phosphine derivative



$C_{47}H_{42}N_4O_{13}PS_2^+$
Exact Mass: 965.19
Mol. Wt.: 965.96

Alexa Fluor 488 phosphine

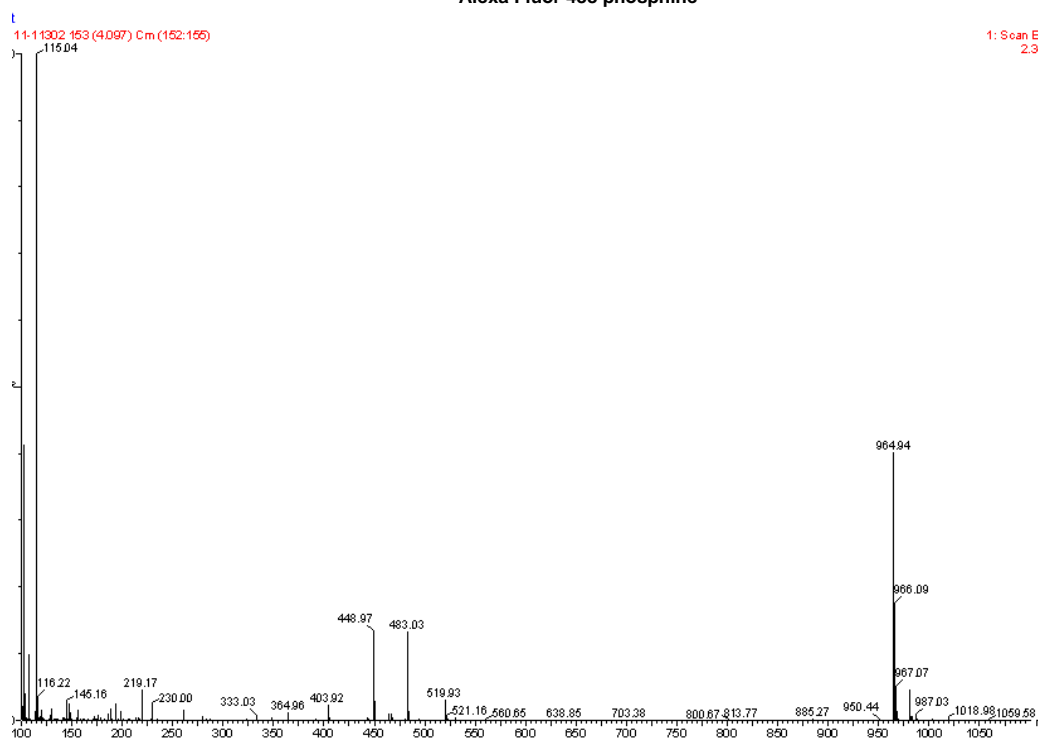


Figure 4.12. Mass spectra (ESI) of Alexa 488 phosphine

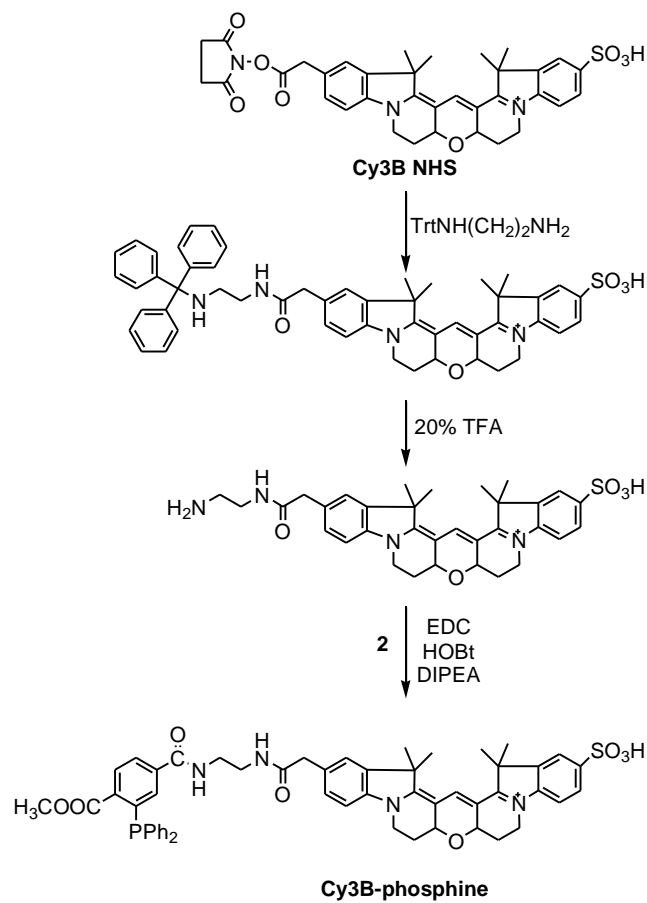


Figure 4.13. Synthesis of Cy3B phosphine derivatives. EDC 1-(3-dimethylaminopropyl)-3-ethyl carbodiimide hydrochloride, HOBt N-hydroxy benzotriazole, TFA trifluoroacetic acid, DIPEA N,N-diisopropylethylamide

Labeling of β' and β derivatives through Staudinger ligation

The Ni-affinity column purified [AzPhe150] β' and [AzPhe284] β' derivatives were reacted with Alexa488 phosphine and [AzPhe106] β and [AzPhe222] β derivatives were reacted with Cy3B phosphine. The Alexa488 and Cy3B phosphine derivatives reacted with β' and β azido-containing derivatives to form an aza-ylide intermediate, followed by intramolecular cyclization to yield a fluorescent labeled product. As a control, wild-type RNA polymerase β' and β subunits were subjected to the same reaction conditions. The ligation reactions were carried out at 37 °C in 6M Gu HCl at pH 7.5 for 16 hours, and the mixture were then purified through size exclusion column and subjected to SDS-PAGE analysis. The fluorescent signals from the gel were detected using a Typhoon imaging system. The gel was then stained with Coomassie blue. The results showed a high degree of selectivity (>95%, Figure 4.14) between phosphine and the azide-containing β' and β subunits. The efficiency of labeling was determined from UV/Vis absorption spectra as follows: $\text{eff}_{\text{Alexa 488}} = (\text{OD}_{496}/\epsilon_{\text{Alex488}, 496})/[\beta']$; $\text{eff}_{\text{Cy3B}} = (\text{OD}_{562}/\epsilon_{\text{Cy3B}, 562})/[\beta]$; where $\epsilon_{\text{Alex488}}$ is the molar extinction coefficient for Alexa 488 at 496 nm ($71,000 \text{ M}^{-1} \text{ cm}^{-1}$), where ϵ_{Cy3B} is the molar extinction coefficient for Cy3B at 563 nm ($130,000 \text{ M}^{-1} \text{ cm}^{-1}$) and where $[\beta']$ and $[\beta]$ are the concentrations of β' and β determined by Bradford assay. Efficiencies of labeling typically were ~ 90%.

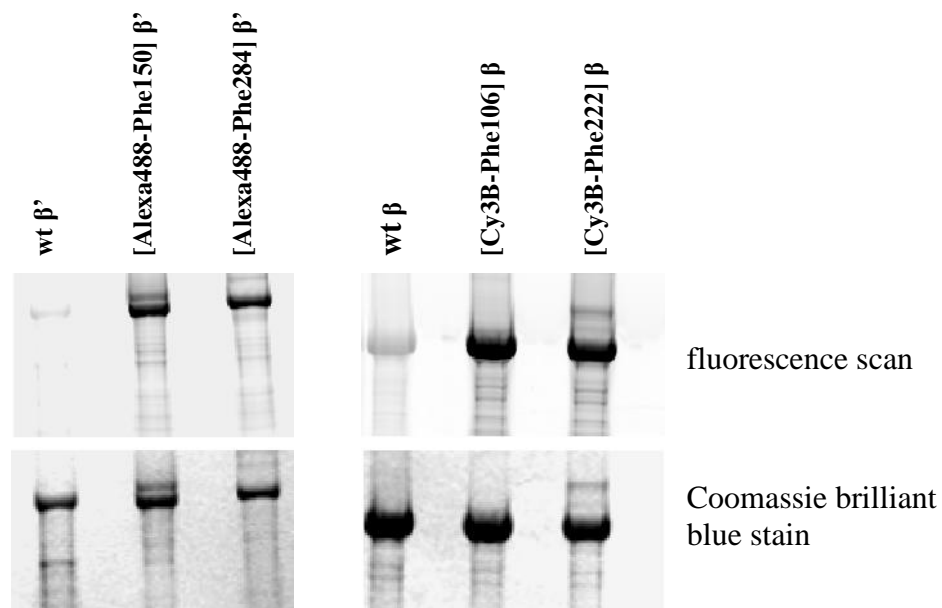
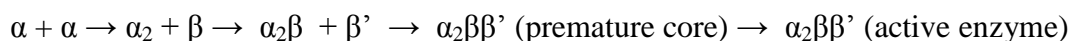


Figure 4.14. Fluorescence scan and Coomassie-stained SDS-PAGE of proteins labeled with Alexa 488 and Cy3B phosphine derivatives

4.2.3. In vitro reconstitution of RNAP with the fluorescent donor Alexa 488 at the distal tip of the β' pincer and the fluorescent acceptor Cy3B at the distal tip of the β pincer

Escherichia coli RNA polymerase can be reconstituted in fully functional form starting from individually overexpressed and purified subunits (Tang et al., 1995; Borukhov et al., 1993; Fujita et al., 1996). Reconstitution of RNA polymerase from its individual subunits proceeds according to the following pathway (Ishihama, 1981):



Following conventional RNAP reconstitution procedures (Tang et al., 1995; Borukhov et al., 1993), the donor-only, acceptor-only and donor-acceptor fluorescent labeled RNAP derivatives were prepared using the Alex488 labeled β' derivatives and Cy3B labeled β derivatives and RNAP recombinant subunits. After thermoactivation the reconstitution mixtures were purified through ANTI-FLAG M2 affinity column to remove free β , β' , ω and σ subunits. Then, subassembly intermediates α_2 , $\alpha_2\beta$ were separated from the core $\alpha_2\beta\beta'\omega$ or holoenzyme $\alpha_2\beta\beta'\omega\sigma$ by anion exchange chromatography on a Mono Q column. During reconstitution, a large amount of RNAP subunits would precipitate. The recovery of purified RNAP after Mono Q column was very low (~ 1%) and the recovered RNAP displayed significant heterogeneity. When analyzed by nondenaturing PAGE, a large portion of the RNAP was seen on the top of the gel and only a small portion of RNAP could enter into the gel, indicating the presence of aggregated forms in the purified RNAP from Mono Q column (Figure 4.15). When the activities of the

reconstituted RNAPs were measured by fluorescence detected abortive initiation assay, they displayed low or no activities compared to wild-type RNAP. Nondenaturing PAGE analysis of RNAP was shown to be powerful and convenient in resolving properly folded form of RNAP from aggregates and in estimation of the fraction of aggregated RNAP. It was therefore used throughout this study to estimate the fraction of aggregated RNAP in the total recovered protein.

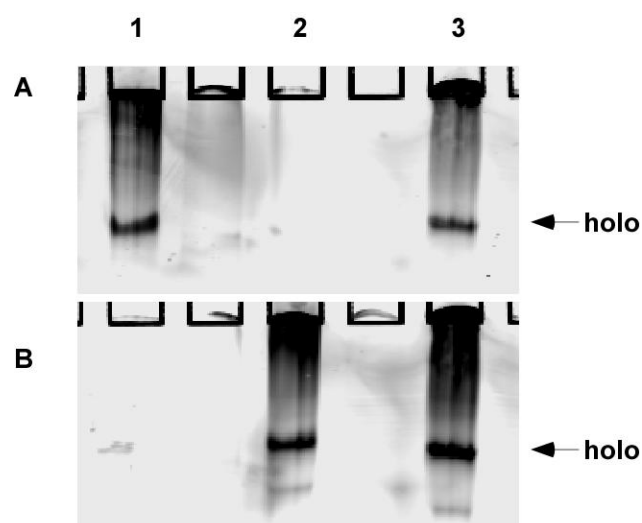


Figure 4.15. Nondenaturing PAGE analysis of reconstituted RNAP holoenzyme derivatives. Lane 1, holo β' 284Alexa488; Lane 2, holo β 106Cy3B; Lane 3, holo β' 284A488 β 106 Cy3B. Fluorescence scanning for Alexa488 (A: excitation 488 nm; emission 526 nm) and for Cy3B (B: excitation 532 nm; emission 580 ± 15 nm)

The reconstitution of fluorescent labeled RNAP suffers from two limitations: the low yield of reconstitution and the high fraction of aggregated RNAP in the total recovered RNAP. The labeled RNAP containing high fraction of aggregates is suitable for in-gel FRET experiments but not useful for in solution ensemble and single-molecule FRET. To reduce the amount of aggregated RNAP and increase the activity of reconstituted RNAP, we therefore focused on the optimization of reconstitution conditions.

Optimization of RNAP reconstitution

In the attempt to prepare highly active reconstituted RNAP, the following optimized conditions for the reconstitution of fluorescent labeled RNAP were developed: (1) using excess amount of α subunit; (2) using $\alpha^{\text{I}}\text{NTD}-\alpha^{\text{II}}\text{NTD}$ fusion protein instead of full-length α ; (3) addition of σ subunit during the thermoactivation step

(1) using excess amount of α subunit

The molar $\alpha:\beta:\beta':\omega:\sigma$ ratio was optimized to 4:1:2:8:1. Excess amount of α subunit was used in the reconstitution reaction due to the difficulty of preparing fluorescent labeled β' and β derivatives. Excess amount of α could largely prevent the appearance of free β and β' subunits.

(2) using $\alpha^{\text{I}}\text{NTD}-\alpha^{\text{II}}\text{NTD}$ fusion protein instead of full-length α

Dimerization of α subunit is the first step in the assembly pathway and thus α plays a key role in RNA polymerase formation. It has been shown that a C-terminal deleted α mutant consisting of the amino-terminal 235 amino acid residues (the wild-type α subunit contains 329 residues) is competent for dimerization, RNAP assembly, and basal transcription (Igarashi et al., 1991; Igarashi & Ishihama, 1991; Tang et al., 1995). The crystal structures of RNAP core and α NTD dimer (Zhang et al., 1998) demonstrate that the C-terminal of α^I -NTD can be connected to the N-terminal of α^{II} -NTD by a short linker. Connecting of the two α NTD would not affect the two α NTD interaction and their interactions with β' and β subunits but stabilize the assembled core complex.

The results (Table 4.3) showed that using a α^I -NTD- α^{II} -NTD fusion protein in reconstitution yielded RNAP with higher activity than using full-length α subunit. The activity of recombinant RNAP was determined in the fluorescent-detected abortive initiation assay by measuring the consumption of γ -AmNS-UTP using DNA *lac*CONS as template. 100% of activity corresponds to the activity of native RNAP.

Table 4.3. Increase of activity using α^I NTD- α^{II} NTD instead of α

RNAP	Activity (%)
Native RNAP holoenzyme	100
RNAP(α^I NTD- α^{II} NTD β '284 Alex488 $\beta\omega\sigma$)	48
RNAP($\alpha\beta$ '284Alex488 $\beta\omega\sigma$)	12

(3) addition of σ subunit at the thermoactivation step:

The core RNAP reconstituted at low temperature (4 °C) is known to exist as an inactive premature form (Ishihama et al., 1973). It can be activated by heating at 30 °C for 30-60 min. Activation to the mature form involves the correct rearrangement of the subunits, primarily the β' subunit, for the RNA polymerase activity to be revealed. The addition of σ subunit is known to facilitate the maturation process of the inactive complex (Ishihama et al., 1973; Fukuda et al., 1974).

Our results demonstrated that the addition of σ subunit during the thermoactivation step highly increase the fraction of active RNAP (the RNAP that can enter into the native gel and form promoter open complex) to the aggregated RNAP (the RNAP that cannot enter into the native gel and cannot form promoter open complex) (Table 4.5 and Figure 4.16). The activities of formation of promoter open complex (RP_o) and elongation complex (RDe) by reconstituted RNAPs were assessed by electrophoretic mobility shift experiments using a 165-bp DNA template containing *lacUV5* consensus promoter. Figure 4.15 shows that ~ 85% core enzyme purified from MonoQ column is aggregated and not active and ~ 65% of holoenzyme reconstituted by adding a fourfold molar excess of $\sigma 70$ subunit to the purified core enzyme is aggregated. However, while addition of $\sigma 70$ during thermoactivation less than 15% of purified holoenzyme form aggregation.

Table 4.4. The effect of σ on reconstitution of active RNAP

Thermoactivation (30 °C, 45 min)	Addition before assay	Activity (%)	Fraction of active RNAP
+ σ	no	100	80%
- σ	yes	33	35%

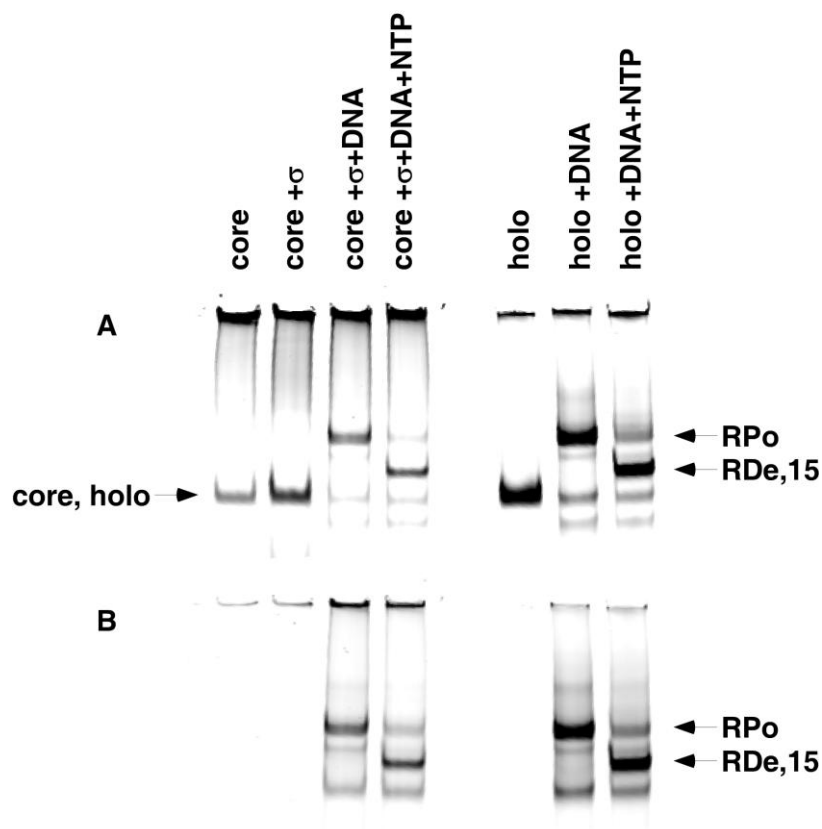


Figure 4.16. Nondenaturing PAGE of Alexa488-Cy3B labeled core, holo, RPo and RDe,15 (Alexa488 at β '284, Cy3B at β 222, DNA template was labeled with Cy5). Lane 1, 2 pmol of core; lane 2, 2 pmol of core + 10 pmol σ ; lane 3, 2 pmol of core + 10 pmol σ + 10 pmol DNA template; lane 4, 2 pmol of core + 10 pmol σ + 10 pmol DNA template + ApA, UTP, GTP, ATP and 3'-OMe CTP; lane 5, 2 pmol of holo; lane 6, 2 pmol of holo + 10 pmol DNA template; lane 7, 2 pmol of holo + 10 pmol DNA template + ApA, UTP, GTP, ATP and 3'-OMe CTP. Fluorescence scanning for Cy3B (A: excitation 532 nm; emission 580 ± 15 nm) and for Cy5 (B: excitation 633 nm; emission 670 ± 15 nm)

Preparation of fluorescent labeled RNAP derivatives

Using optimized conditions, fluorescent labeled RNAP holoenzyme derivatives suitable for ensemble in solution FRET experiments were prepared. To prepare the donor-only singly labeled RNA polymerase, the FLAG-tagged α NTD fusion protein (40 nmol), wild-type β subunit (10 nmol), Alexa488 labeled β' derivative (26nmol) and ω subunit (104 nmol) dissolved separately in 6M GuHCl were mixed together. The mixture was diluted with 6M GuHCl denaturation buffer to final protein concentration of 0.45 mg/ml for the reconstitution.

To prepare the acceptor-only singly labeled RNA polymerase, the FLAG-tagged α NTD fusion protein (40 nmol), Cy3B labeled β derivative (10 nmol), wild-type β' subunit (20 nmol), and ω subunit (80 nmol) dissolved separately in 6M GuHCl were mixed together. The mixture was diluted with 6M GuHCl denaturation buffer to final protein concentration of 0.45 mg/ml for the reconstitution.

To prepare donor-acceptor doubly labeled RNAP, the FLAF-tagged α NTD fusion protein (80 nmol), Cy3B labeled β derivative (20 nmol), Alexa488 labeled β' derivative (50 nmol) and ω subunit (200 nmol) dissolved in 6M GuHCl were mixed. The mixture was diluted with 6M GuHCl denaturation buffer to final protein concentration of 0.45 mg/ml for the reconstitution.

After dialysis 20 nmol $\sigma 70$ was added during thermoactivation at 30°C. Then the reconstitution mixtures were purified through ANTI-FLAG M2 affinity column and Mono Q column. The recovery for singly-labeled RNAP is ~10 fold higher than doubly-labeled RNAP.

The reconstituted labeled RNAP derivatives were subjected to abortive initiation assay and promoter open complex and elongation complex formed from the labeled RNAP were subjected to nondenaturing PAGE analysis. The results (Figure 4.17) showed that these labeled RNAP derivatives are highly active. The fractions of aggregated RNAP in recovered total RNAP were very low.

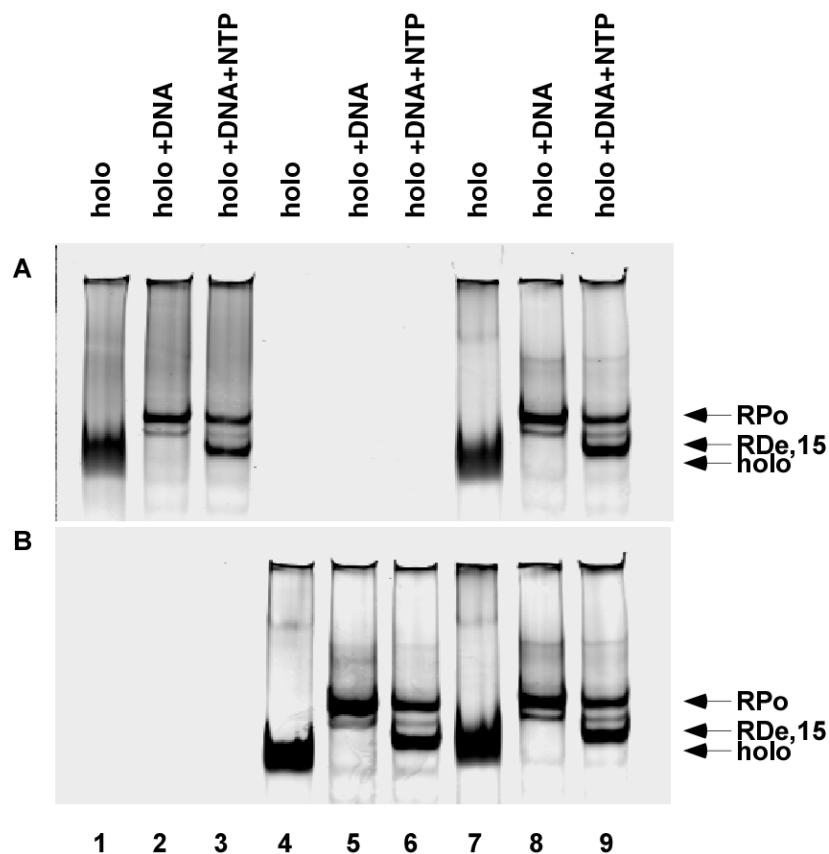


Figure 4.17. Nondenaturing PAGE of Alexa488-Cy3B labeled RNAP derivatives, and RPo and RDe,15. Lane 1, 2 pmol of holo β' 284Alexa488; lane 2, 2 pmol of holo β' 284Alexa488 + 10 pmol DNA template; lane 3, 2 pmol of holo β' 284Alexa488 + 10 pmol DNA template + ApA, UTP, GTP, ATP and 3'-OMe CTP; Lane 4, 2 pmol of holo β 222Cy3B; lane 5, 2 pmol of holo β 222Cy3B + 10 pmol DNA template; lane 6, 2 pmol of holo β 222Cy3B + 10 pmol DNA template + ApA, UTP, GTP, ATP and 3'-OMe CTP; lane 7, 2 pmol of holo β' 284Alexa488 β 106Cy3B; lane 8, 2 pmol of holo β' 284Alexa488 β 106Cy3B + 10 pmol DNA template; lane 9, 2 pmol of holo β' 284Alexa488 β 106Cy3B + 10 pmol DNA template + ApA, UTP, GTP, ATP and 3'-OMe CTP. Fluorescence scanning for Alexa488 (A: excitation 488 nm; emission 526 nm) and for Cy3B (B: excitation 532 nm; emission 580 ± 15 nm)

5. RNAP clamp conformational states

5.1. Objectives

In chapter 4, we have described procedures that allow the preparation of fluorescent labeled RNAP derivatives with the fluorescent donor (Alexa 488) at the distal tip of the RNAP clamp and the acceptor (Cy3B) at the distal tip of the RNAP β pincer.

The objective of this chapter was to define the mean clamp conformations in the context of RNAP holoenzyme (composition $\beta'/\beta/\alpha^I/\alpha^{II}/\omega/\sigma^{70}$), in the context of the RNAP-promoter open complex (RP_o ; composition $\beta'/\beta/\alpha^I/\alpha^{II}/\omega/\sigma^{70}/DNA$), in the context of initial transcribing complex (RP_{itc} ; composition $\beta'/\beta/\alpha^I/\alpha^{II}/\omega/\sigma^{70}/DNA/NTP$), and in transcription elongation complex (RDe ; composition $\beta'/\beta/\alpha^I/\alpha^{II}/\omega/\sigma^{70}/DNA/NTP$) and to define the effect of switch-region-target inhibitors (Myx, Cor, Rip, and Lpm) and ppGpp/DksA on opening and closing of the RNAP active-center cleft using fluorescence energy transfer assay.

5.2. Materials and methods

5.2.1. Fluorescent labeled RNAP derivatives

The fluorescent labeled RNAP holoenzyme derivatives: [Alexa488-Phe284] β' -RNAP labeled with donor only, [Cy3B-Phe106] β -RNAP and [Cy3B-Phe222] β -RNAP labeled with acceptor only, [Alexa488-Phe284] β' ; [Cy3B-Phe106] β -RNAP and [Alexa488-Phe284] β' ; [Cy3B-Phe222] β -RNAP labeled with donor and acceptor were prepared as described in chapter 4.

5.2.2. Fluorescence Resonance Energy Transfer (FRET)

The theory of FRET has been developed in the late 1940s (Förster, 1948; Lilley and Wilson, 2000; Selvin 2000). FRET occurs in a system having a fluorescent probe serving as a donor (D) and a second fluorescent probe serving as an acceptor (A), where the emission wavelength of the donor overlaps the excitation wavelength of the acceptor. In such a system, upon excitation of the donor with light of its excitation wavelength, energy can be transferred from the donor to the acceptor, resulting in excitation of the acceptor and emission at the acceptor's emission wavelength. The efficiency of energy transfer, E , is a function of the Förster parameter, R_0 , and of the distance between the donor and the acceptor, R :

$$E = [1 + (R/R_0)^6]^{-1} \quad (\text{Eq. 1})$$

Thus, the average distances R between D and A can be calculated directly from the efficiency of energy transfer from D to A and R_0 using equation 1. With commonly used fluorescent probes, FRET permits accurate determination of distances in the range of ~ 20 to ~ 100 Å.

R_0 is the distance between donor and acceptor at which 50% energy transfer occurs. R_0 is determined by experiments independent of energy transfer and its value depends on the spectral properties of the donor and acceptor, the relative orientation of their transition dipoles and the physical properties of the solution:

$$R_0 = 8.79 \times 10^{-25} (n^{-4} Q_D \kappa^2 J)^{1/6} \quad (\text{Eq. 2})$$

Where n is the refractive index of the medium through which the transfer process occurs.

Q_D is the fluorescent quantum yield of the donor in the absence of acceptor, κ^2 is the orientation factor between the donor emission and acceptor excitation dipoles and J is the integral of the spectral overlap between donor emission and acceptor absorbance spectra.

J is defined by the following equation:

$$J = \frac{\int F_D(\lambda) \varepsilon_A(\lambda) \lambda^4 d\lambda}{\int F_D(\lambda) d\lambda} \quad (\text{Eq. 3})$$

Where λ is the wavelength in cm, $F_D(\lambda)$ is the peak-normalized fluorescence of the donor at wavelength λ , and $\varepsilon_A(\lambda)$ is the molar extinction coefficient of the acceptor at wavelength λ .

5.2.3. Fluorescence anisotropy

Fluorescence anisotropy is a measure of rotational freedom of a fluorophore in the solution. In general, a small fluorophore is depolarized in solution due to random Brownian motion and gives rise to a low fluorescence anisotropy value. When it is bound to a macromolecule, its rotational motion is restricted and it becomes more polarized, resulting in higher fluorescence anisotropy value. The extent of the polarization or the orientation of the dipole moment associated with the fluorophore depends on the local environment of the binding site of the macromolecule.

Steady-state fluorescence anisotropies were measured for [Alexa488-Phe284] β' -RNAP, [Cy3B-Phe106] β -RNAP, and [Cy3B-Phe222] β -RNAP holoenzyme derivatives. Anisotropies were measured using a QuantaMaster QM1 spectrofluorometer equipped T-format Glan-Thompson polarizers (PTI, Inc.). Excitation and emission wavelengths were 490 nm and 518 nm for the donor, and 535 nm and 575 nm for the acceptor. All measurements were performed in transcription buffer (TB: 50mM Tris-HCl [pH 8.0], 100 mM KCl, 10 mM MgCl₂, 1 mM DTT, 10 ug/ml bovine serum albumin, and 5% glycerol) at 37 °C. Anisotropy (A) was calculated as (Chen and Bowman, 1965):

$$A = (I_{VV} - GI_{VH}) / (I_{VV} + 2GI_{VH})$$

where I_{VV} and I_{VH} are fluorescence intensities with the excitation polarizer at the vertical position and the emission polarizer at, respectively, the vertical position and the

horizontal position; G is the grating correction factor that accounts for bias in the detection of polarized light. The G factor was measured as the ratio I_{HV}/I_{HH} , where I_{HV} and I_{HH} are fluorescence intensities with the excitation polarizer at a horizontal position and the emission polarizer at vertical and horizontal positions respectively.

5.2.4. Fluorescence Spectroscopy

Steady-state fluorescence emission spectra were collected with a QuantaMaster QM1 fluorescence spectrophotometer (Photon Technology International). Experimental samples were excited by a 75-W Xenon arc-lamp through a single-grating monochromator at 490 nm (Alexa 488) or 535 nm (Cy3B). The emitted fluorescence was collected using a single-grating monochromator interfaced to a photomultiplier tube. Slit-widths were set at 5 nm.

Steady-state measurements of mean clamp conformations

Fluorescence measurements were taken for donor-acceptor labeled RNAP (DA), for donor-only labeled RNAP (D), and for acceptor-only labeled RNAP (A) at 37 °C. Reaction mixtures contained 2 pmol of labeled holoenzyme derivative in 50 μ l of transcription buffer (TB: 50mM Tris-HCl [pH 8.0], 100 mM KCl, 10 mM MgCl₂, 1 mM DTT, 10 μ g/ml bovine serum albumin, and 5% glycerol) were transferred to submicro fluorometer cuvettes (Starna Inc.). After incubation for 5 min at 37 °C, fluorescence emission intensities were measured (data for holoenzyme). 1 μ l of 10 μ M (10 pmol)

DNA template (*lac* CONS-11 or *lac* CONS-15) was added to the reaction mixture, and fluorescence emission intensities were measured after incubation for 15 min at 37 °C (data for RP₀). 1 µl of 10 mM ApA was added to the reaction mixture, and fluorescence emission intensities were measured after incubation for 5 min at 37 °C (data for RP_{itc,≤2}). 1 µl of 5 mM UTP was added to the reaction mixture, and fluorescence emission intensities were measured after incubation for 5 min at 37 °C (data for RP_{itc,≤4}). 1 µl of 5 mM GTP was added to the reaction mixture, and fluorescence emission intensities were measured after incubation for 5 min at 37 °C (data for RP_{itc,≤7}). 1 µl of 5 mM ATP and 1 µl of 5 mM 3'-OMe CTP were added to the reaction mixture, and fluorescence emission intensities were measured after incubation for 5 min at 37 °C (data for RD_{e,11} or RD_{e,15}). Two emission spectra were taken for each measurement by exciting at 490 nm (emission 505-600 nm) and 535 nm (emission 555-600 nm). The slit widths for both excitation and emission monochromators were set to 5 nm. All experiments were done at least three times.

The efficiency (E) of FRET between the donor and acceptor probes was calculated from the enhanced fluorescence of acceptor (Clegg, 1992). Fluorescence intensities (F) were corrected for background by subtraction of fluorescence intensities for transcription buffer. The fluorescence intensity attributable to FRET ($F_{575,490}^{\text{FRET}}$), the efficiency of FRET

(E), were calculated as follows (Clegg, 1992; Mukhopadhyay et al., 2001):

$$F_{575,490}^{\text{FRET}} = F_{575,490}^{\text{DA}} - \frac{F_{518,490}^{\text{DA}} \times F_{575,490}^{\text{D}}}{F_{518,490}^{\text{D}}} - \frac{F_{575,535}^{\text{DA}} \times F_{575,490}^{\text{A}}}{F_{575,535}^{\text{A}}}$$

$$E = \frac{F_{575,490}^{\text{FRET}} \times \epsilon_{535}^{\text{A}}}{F_{575,535}^{\text{DA}} \times \epsilon_{490}^{\text{D}} \times d}$$

where d is the fraction of the RNAP holoenzyme derivatives that contain a donor label (0.31, determined by use of alternating-laser excitation (ALEX)-confocal single molecule measurement (Kapanidis et al 2004, 2005) to directly assess quantities of acceptor-only and donor+acceptor species (Figure 5.1)), $\epsilon_{490}^{\text{D}}$ is the extinction coefficient of the donor at 490 nm ($59,000 \text{ M}^{-1} \text{ cm}^{-1}$) calculated from the excitation spectrum of the donor using $\epsilon_{496}^{\text{D}}$ ($71,000 \text{ M}^{-1} \text{ cm}^{-1}$), $\epsilon_{535}^{\text{A}}$ is the extinction coefficient of the acceptor at 535 nm ($71,000 \text{ M}^{-1} \text{ cm}^{-1}$) calculated from the excitation spectrum of the acceptor using $\epsilon_{563}^{\text{A}}$ ($130,000 \text{ M}^{-1} \text{ cm}^{-1}$).

The Förster distance (R_0) was calculated from Eq. 2

$$R_0 = 8.79 \times 10^{-25} (n^{-4} Q_D \kappa^2 J)^{1/6} \quad (\text{Eq. 2})$$

A value of 1.4 was used for n , the refractive index of the medium (Clegg, 1992). Q_D is the quantum yield of Alexa488 in RNAP complexes in the absence of the acceptor, measured as 0.60 using fluorescein in 0.1 M NaOH as a standard ($Q_{\text{fluorescein}} = 0.92$) (Lakowicz, 1999). κ^2 is the orientation factor relating the donor emission dipole and the acceptor excitation dipole (approximated as 2/3-justified by fluorescence anisotropy measurements indicating donor and acceptor reorient on the time scale of the donor

excited-state life time). J is the spectral overlap integral of the donor emission spectrum and the acceptor excitation spectrum. It was calculated by Eq. 3 ($5.2 \times 10^{-13} \text{ cm}^3 \text{ M}^{-1}$; determined using corrected spectra for donor-only and acceptor-only controls). Using the calculated efficiency of transfer (E) and the Förster distance (R_o), the average proximal distance (R) between donor and acceptor was calculated by the equation.

$$R = R_o [(1-E)/E]^{1/6} \quad (\text{Eq. 4})$$

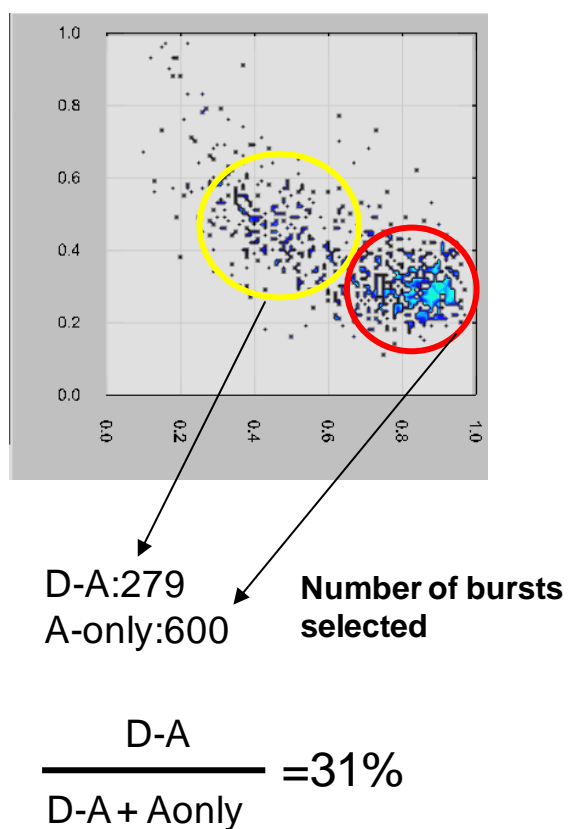


Figure 5.1. Determination of donor labeling efficiency (d) in reconstituted donor-acceptor labeled RNAP derivative by use of alternating-laser excitation (ALEX)-confocal single molecule measurement

5.3. Results and discussions

5.3.1. Anisotropy results

Steady-state anisotropy measurements were used to reduce the uncertainty associated with the orientation factor κ^2 (Dale et al., 1979). The most significant uncertainty introduced in distance measurements by energy transfer arises from the orientation factor κ^2 . Depending upon the relative orientation of the emission dipole of the donor and the absorption dipole of the acceptor, κ^2 can range from 0 to 4. For collinear and parallel transition dipoles, $\kappa^2 = 4$, and for perpendicular dipoles, $\kappa^2 = 1$. Since the sixth root of κ^2 is taken in calculating the distance, variation of κ^2 from 1 to 4 results no more than 30% no more than a 30% error in the calculated value of the distance between donor and acceptor (Stryer, 1978). In most cases, the isotropic assumption ($\kappa^2 = 2/3$) due to dynamic averaging of the dipole orientations during the life time of the excited state is used. However, if the dipoles are oriented perpendicular to one another, $\kappa^2 = 0$, which would result in serious errors in the calculated distance (Wu and Brand, 1994). By measurements of the fluorescence anisotropy of the donor and the acceptor, one can obtain the limits of the orientation factor and thereby minimize uncertainties in the calculated distance.

Measured anisotropy for Alexa488 in [Alexa488-Phe284] β' -RNAP was 0.26 in holoenzyme and 0.28 in RP_o . Measured anisotropy for Cy3B in [Cy3B-Phe106] β -RNAP was 0.22 in holoenzyme and 0.27 in RP_o . Measured anisotropy for Cy3B [Cy3B-Phe222] β -RNAP was 0.22 in holoenzyme and 0.23 in RP_o . The measured fluorescence

anisotropies for both donor and acceptor were low compared to fundamental anisotropy (0.4). This indicates considerable depolarization due to the local rotational motion during the fluorescence lifetimes of both the dyes, resulting in dynamic averaging of dipole orientations, and validates use of $\kappa^2 = 2/3$ in R_o calculation.

5.3.2. R_o calculation

The spectral properties of Alexa488 and Cy3B were measured to calculate the R_o of the pair. Normalized donor emission and acceptor absorbance spectra are presented in Figure 5.1. The major assumption made in calculating R_o is that the orientation factor $\kappa^2 = 2/3$, meaning that the donor and acceptor probes are isotropically distributed within the fluorescence lifetime of the donor probe (i.e., ~4.1 nanoseconds). Using the spectral overlap of the pair (calculated using Eq.3), the spectral properties of the dyes in context of complex and the κ^2 value for dynamic averaging ($\kappa^2 = 2/3$), the R_o for the Alexa488-Cy3B pair was calculated to be 60.2 Å for Alexa488 at β' residue 284 and Cy3B at β residue 106 and β residue 222.

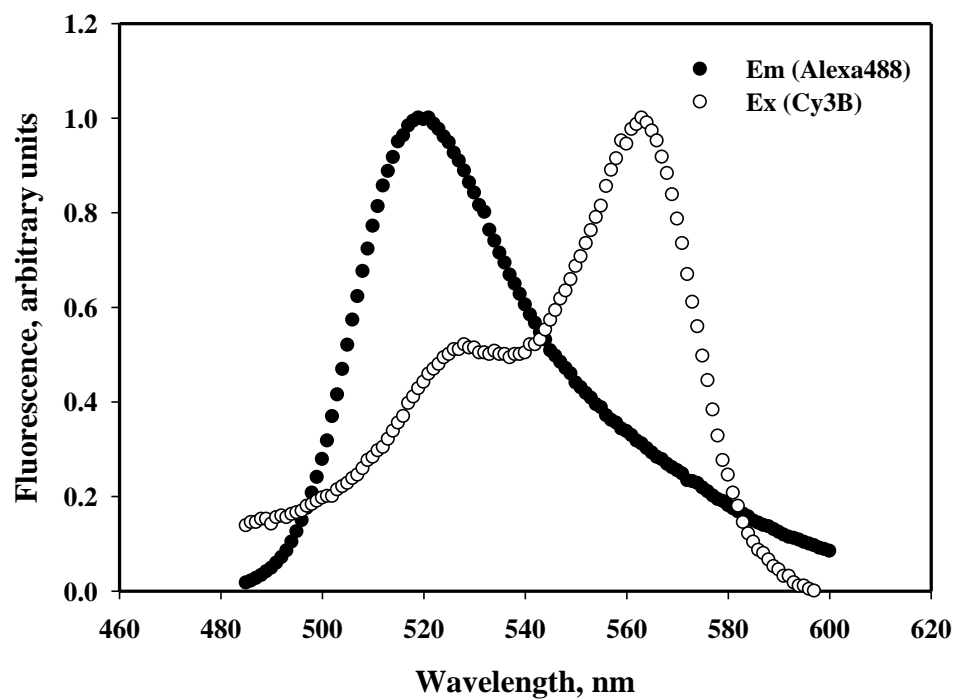


Figure 5.2. Spectral overlap between Alexa488 and Cy3B. A normalized fluorescence emission spectrum of Alexa488-labeled RNAP and an absorption spectrum of Cy3B-labeled RNAP are plotted together to show the overlap region. The fluorescence emission spectrum of Alexa488-labeled RNAP was recorded with excitation at 470 nm.

5.3.3. Ensemble FRET measurements of mean clamp conformational states

To determine RNAP clamp conformations in RNAP holoenzyme, RNAP-promoter open complexes, RNAP-promoter initial transcribing complexes, and transcription elongation complexes, we performed ensemble FRET experiments in solution using [Alexa488-Phe284] β' ; [Cy3B-Phe106] β -RNAP which has a fluorescent donor incorporated at the tip of the β' pincer (the “clamp”; residue 284 of β') and a fluorescent acceptor incorporated at the tip of the β pincer (residue 106 of β) and [Alexa488-Phe284] β' ; [Cy3B-Phe222] β -RNAP which has a fluorescent donor incorporated at the tip of the β' pincer (the “clamp”; residue 284 of β') and a fluorescent acceptor incorporated at the tip of the β lobe (residue 222 of β).

Upon addition of the DNA fragment that permits formation of RP_o to RNAP holoenzyme in transcription buffer and incubation for 15min, there is a increase in FRET from 0.46 to 0.52 for [Alexa488-Phe284] β' ; [Cy3B-Phe106] β -RNAP and a increase in FRET from 0.35 to 0.44 for [Alexa488-Phe284] β' ; [Cy3B-Phe222] β -RNAP. There is no further change in FRET upon addition of limited sets NTPs that permit formation of initial transcribing complexes and elongation complexes (Figure 5.3).

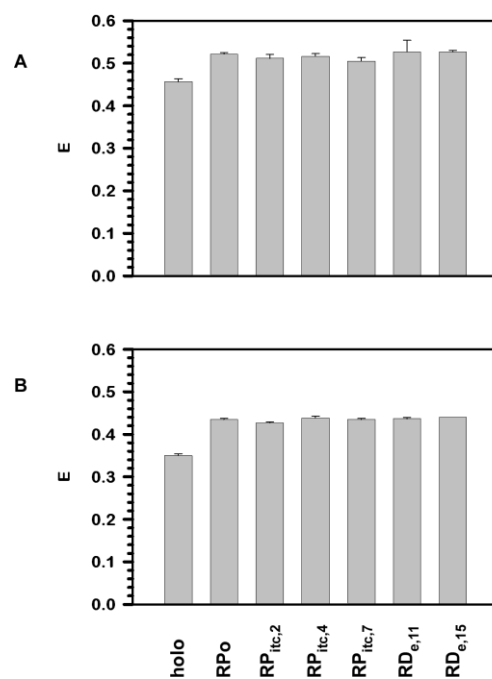


Figure 5.3. FRET results for holoenzyme, RP_o, RP_{itc, ≤2}, RP_{itc, ≤4}, RP_{itc, ≤7}, RD_{e,11} and RD_{e,15} formed by (A) [Alexa488-Phe284]β'; [Cy3B-Phe106]β-RNAP with *lac* CONS-11 and *lac* CONS-15; (B) [Alexa488-Phe284]β'; [Cy3B-Phe222]β-RNAP with *lac* CONS-11 and *lac* CONS-15.

The donor-acceptor distances were calculated from the measured FRET efficiencies through the use of the Förster equation. For probes at β' residue 284 and β residue 106, the donor-acceptor distance is 61.9 ± 0.1 Å in RNAP holoenzyme, 59.3 ± 0.2 Å in open complex, 59.7 ± 0.4 Å in initial transcribing complex and 59.1 ± 0.1 Å in elongation complex (Table 5.1). For probes at β' residue 284 and β residue 222, the donor-acceptor distance is 66.6 ± 0.1 Å in RNAP holoenzyme, 62.9 ± 0.1 Å in open complex, 63.0 ± 0.1 Å in initial transcribing complex and 62.8 ± 0.1 Å in open complex (Table 5.2). The results indicate that the RNAP clamp closes ($\sim 2\text{-}3$ Å) upon formation of the RNAP-promoter open complex and remains closed exhibiting no further change in mean clamp conformation upon formation RNAP-promoter initial transcribing complexes and transcription elongation complexes.

The distance changes ($\sim 2\text{-}3$ Å) are smaller than the distance changes observed in crystal structures (PDB 1I3Q, PDB 1HQM, PDB 1L9Z) that the donor-acceptor distances for donor at β' residue 284 and acceptor at β residue 106 are ~ 80 Å in an open clamp conformational state, ~ 65 Å in partly closed clamp conformational state, and ~ 50 Å in a fully closed clamp conformational state; and the donor-acceptor distances for probes at β' residue 284 and β residue 222 are ~ 95 Å in an open clamp conformational state, ~ 85 Å in partly closed clamp conformational state, and ~ 70 Å in a fully closed clamp conformational state. Our FRET measurements are likely to give an underestimate of the magnitude of the clamp movement, due to the fact that our measurements are done under equilibrium conditions in solution, where signals from different conformational states are averaged.

The results indicate that: (1) RNAP holoenzyme in solution exists predominantly in a partly closed clamp conformational state [a state similar or identical to that in crystal structures of RNAP holoenzyme (Vassylyev et al., 2002; Murakami et al., 2002); (2) the RNAP clamp closes upon formation of the RNAP-promoter open complex, yielding a fully closed clamp conformational state [a state similar or identical to that in crystal structures of transcription elongation complexes] (Vassylyev et al., 2007); (3) the RNAP clamp remains closed—and exhibits no further change in mean clamp conformation—upon formation of RNAP-promoter initial transcribing complexes and transcription elongation complexes. The results support proposals that clamp closure occurs upon formation of open complex (Ebright 2000) and argue against proposals that clamp closure occurs only upon formation of initial transcribing complexes or transcription elongation complexes (Cramer et al., 2001; Gnatt et al., 2001; Vassylyev et al., 2007).

Table 5.1. In-solution FRET results for holoenzyme, RP_o , $RP_{itc, \leq 2}$, $RP_{itc, \leq 4}$, $RP_{itc, \leq 7}$, $RD_{e,11}$, and $RD_{e,15}$ formed by [Alexa488-Phe284] β' ; [Cy3B-Phe106] β -RNAP with *lac* CONS-11 and *lac* CONS-15

complex	E (%)	R (Å)
holoenzyme	46 \pm 0.2	61.9 \pm 0.1
RP_o	52 \pm 0.3	59.3 \pm 0.1
$RP_{itc, \leq 2}$	51 \pm 0.9	59.7 \pm 0.4
$RP_{itc, \leq 4}$	52 \pm 0.6	59.5 \pm 0.2
$RP_{itc, \leq 7}$	51 \pm 0.8	60.0 \pm 0.3
$RD_{e,11}$	53 \pm 2.7	59.1 \pm 1.1
$RD_{e,15}$	53 \pm 0.3	59.1 \pm 0.1

Table 5.2. In-solution FRET results for holoenzyme, RP_o , $RP_{itc, \leq 2}$, $RP_{itc, \leq 4}$, $RP_{itc, \leq 7}$, $RD_{e,11}$, and $RD_{e,15}$ formed by [Alexa488-Phe284] β' ; [Cy3B-Phe222] β -RNAP with *lac* CONS-11 and *lac* CONS-15

complex	E (%)	R (Å)
holoenzyme	35 ± 0.2	66.6 ± 0.1
RP_o	44 ± 0.2	62.9 ± 0.1
$RP_{itc, \leq 2}$	43 ± 0.2	63.2 ± 0.1
$RP_{itc, \leq 4}$	44 ± 0.3	62.6 ± 0.1
$RP_{itc, \leq 7}$	43 ± 0.2	63.0 ± 0.1
$RD_{e,11}$	44 ± 0.3	62.8 ± 0.1
$RD_{e,15}$	44 ± 0.0	62.7 ± 0.0

5.3.4. Detection of effects on RNAP clamp conformation of switch-region-target inhibitors

It has been hypothesized that the transition between the open clamp conformational state and the closed clamp conformational state is accompanied by and possibly requires the conformational changes in switch-region and switch-region-target inhibitors, Myx, Cor, Rip, and Lpm, inhibit transcription by interfering the RNAP clamp conformational changes.

To determine the effects on RNAP clamp conformation of switch-region-target inhibitors. Our hypothesis is that switch-region-target inhibitors interfere with switch-region-conformational cycling, thereby preventing opening of the RNAP clamp required to permit entry of DNA into the RNAP active-center cleft, preventing closing of the RNAP clamp required to permit retention of DNA within the RNAP-active-center cleft, or both. The fundamental testable prediction of this working hypothesis is that switch-region-target inhibitors affect clamp conformation in solution and/or affect clamp dynamics in solution. We tested this prediction by determining directly the effects of switch-region-target inhibitors on clamp conformation in solution.

The effects of switch-region-target inhibitors on clamp conformation were determined by comparing the FRET in holoenzyme and in RNAP-inhibitor complexes. An increase in FRET efficiency upon addition of Myx, Rip or Cor to holoenzyme was observed and a decrease in FRET upon addition of Lpm to holoenzyme (Figure 5.4 and Figure 5.5) was

observed. Binding of Myx, Rip, Cor and Lpm to [Alexa488-Phe284] β' ; [Cy3B-Phe106] β -RNAP caused an increase in FRET from 0.46 to 0.54, an increase in FRET from 0.46 to 0.51, an increase in FRET from 0.46 to 0.53, and a decrease in FRET from 0.46 to 0.39, respectively. Binding of Myx, Rip, Cor and Lpm to [Alexa488-Phe284] β' ; [Cy3B-Phe222] β -RNAP, caused an increase in FRET from 0.35 to 0.39, an increase in FRET from 0.35 to 0.39, an increase in FRET from 0.35 to 0.40, and a decrease in FRET from 0.35 to 0.32, respectively. The corresponding distance changes showed that the binding of Myx, Rip and Cor to RNAP closes the active-center-cleft $\sim 2\text{\AA}$ while the binding of Lpm to RNAP opens the active-center-cleft $\sim 2\text{\AA}$ (Table 5.3 and Table 5.4).

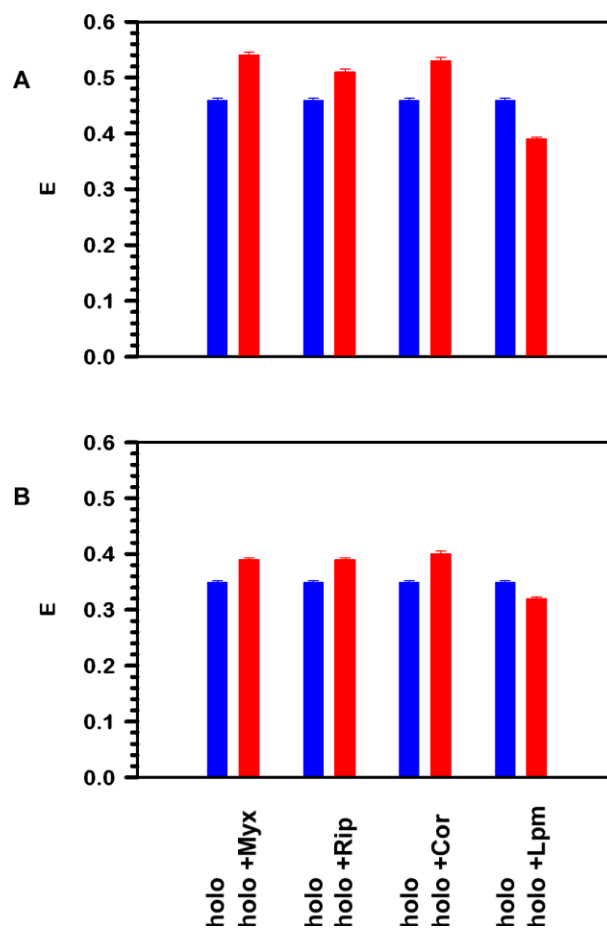


Figure 5.4. Effects of Myx, cor, Rip and Lpm on RNAP holoenzyme clamp conformation (A) [Alexa488-Phe284] β' ; [Cy3B-Phe106] β -RNAP; (B) [Alexa488-Phe284] β' ; [Cy3B-Phe222] β -RNAP

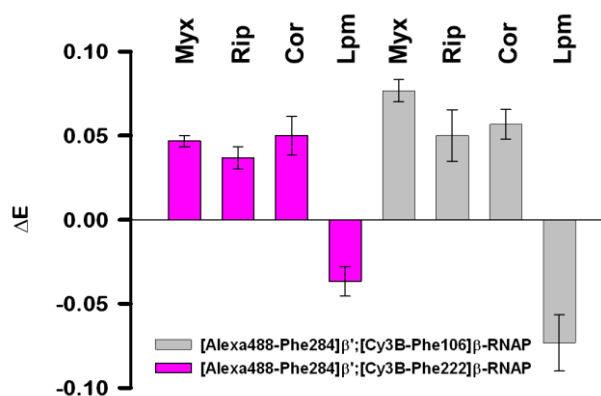


Figure 5.5. Changes in FRET efficiency induced by Myx, Cor, Rip and Lpm binding to RNAP holoenzyme. Increases or decreases in FRET efficiency are shown relative to that of RNAP holoenzyme (Gray) [Alexa488-Phe284]β'; [Cy3B-Phe106]β-RNAP; (Red) [Alexa488-Phe284]β'; [Cy3B-Phe222]β-RNAP. Error bars show standard errors for changes in FRET efficiency calculated from triplicate measurements.

Table 5.3. Effects of Myx, Cor, Rip and Lpm on RNAP holoenzyme [Alexa488-Phe284] β' [Cy3B-Phe106] β -RNAP clamp conformation

complex	E	ΔE	R (\AA)	ΔR (\AA)
holo	0.46 ± 0.003		61.9 ± 0.1	
holo + Myx	0.54 ± 0.006	0.08 ± 0.007	58.6 ± 0.2	-3.1 ± 0.3
holo + Rip	0.51 ± 0.006	0.05 ± 0.01	59.8 ± 0.2	-2.0 ± 0.6
holo + Cor	0.53 ± 0.007	0.06 ± 0.009	59.1 ± 0.3	-2.3 ± 0.4
holo + Lpm	0.39 ± 0.007	-0.07 ± 0.01	65.0 ± 0.3	3.2 ± 0.7

Table 5.4. Effects of Myx, Cor, Rip and Lpm on RNAP holoenzyme [Alexa488-Phe284] β' [Cy3B-Phe222] β -RNAP clamp conformation

complex	E	ΔE	R (\AA)	ΔR (\AA)
holo	0.35 ± 0.002		66.6 ± 0.1	
holo + Myx	0.39 ± 0.003	0.05 ± 0.003	64.7 ± 0.1	-2.2 ± 0.2
holo + Rip	0.39 ± 0.003	0.04 ± 0.007	64.7 ± 0.2	-1.7 ± 0.3
holo + Cor	0.40 ± 0.006	0.05 ± 0.01	64.4 ± 0.3	-2.3 ± 0.5
holo + Lpm	0.32 ± 0.003	-0.04 ± 0.009	68.4 ± 0.2	1.9 ± 0.4

The antibiotics CBR703, FPET (Artsimovitch et al 2003), CTC-ME, CTC-EE (Arhin et al 2006; Ebright unpublished results) (Figure 5.6) have been identified inhibiting bacterial RNAP through interactions with RNAP β lobe. The effects of these compounds on RNAP clamp conformation were also assessed. No change in clamp conformation was observed upon addition of these compounds to the holoenzyme (Table 5.5, 5.6).

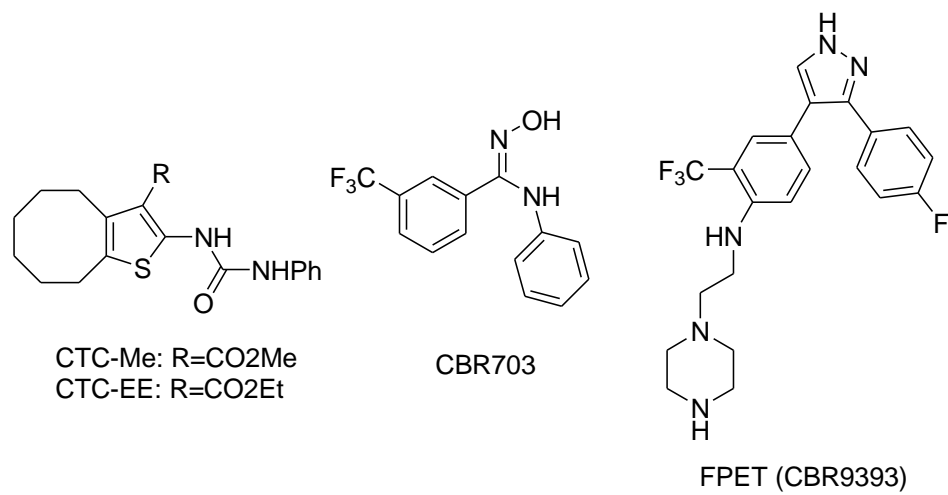


Figure 5.6. RNAP inhibitors: CTC-ME, CTC-EE, CBR703, and FPET

Table 5.5. Effects of CBR703, FPET, CTC-ME and CTC-EE on RNAP holoenzyme [Alexa488-Phe284] β' [Cy3B-Phe106] β -RNAP clamp conformation

complex	E	R (Å)
holo	0.46 \pm 0.003	61.9 \pm 0.1
holo + CBR703	0.46 \pm 0.003	61.7 \pm 0.1
holo + FPET	0.43 \pm 0.01	63.2 \pm 0.5
holo + CTC-ME	0.44 \pm 0.01	62.5 \pm 0.4
holo + CTC-EE	0.46 \pm 0.01	61.8 \pm 0.6

Table 5.6. Effects of CBR703, FPET, CTC-ME and CTC-EE on RNAP holoenzyme [Alexa488-Phe284] β' [Cy3B-Phe222] β -RNAP clamp conformation

complex	E	R (Å)
holo	0.36 \pm 0.003	66.3 \pm 0.1
holo + CBR703	0.36 \pm 0.003	66.1 \pm 0.2
holo + FPET	0.37 \pm 0.003	65.6 \pm 0.2
holo + CTC-ME	0.37 \pm 0.003	65.9 \pm 0.2
holo + CTC-EE	0.36 \pm 0.003	66.4 \pm 0.2

The observations indicate that the binding of Myx, Cor, Rip and Lpm to RNAP results in changing in RNAP clamp conformational state. The results support the proposal that Myx, Cor, Rip and Lpm bind to an RNAP- switch-region conformational state and Myx. Cor, Rip and Lpm inhibit RNAP function by trapping the RNAP switch region in this conformational state, thereby interfering with conformational cycling of RNAP clamp important for RNAP function. Myx, Cor, and Rip interact with an RNAP conformational state in which the RNAP clamp is in a partly closed to fully closed conformational state; Lpm interacts with an RNAP conformational state in which the RNAP clamp is in an open to partly closed conformational state. The results suggest that Myx, Cor, and Rip function by preventing RNAP clamp opening required for the entry of DNA into the RNAP active-center cleft, and Lpm functions by preventing clamp closure required for DNA retention.

6. Conclusions and perspectives

We have extended the two approaches of nonsense suspension and Staudinger-Bertozzi ligation for protein labeling to the incorporation of fluorescent probes into RNAP. We have developed a procedure that permits incorporation of a fluorescent probe at any position of interest within a protein. We have used this procedure to incorporate one fluorescent probe, serving as a donor, at the tip of the β' pincer and another fluorescent probe, serving as an acceptor, at the tip of the β pincer. Using fluorescence resonance energy transfer, we have shown that RNAP clamp closes from partly closed state to fully closed state upon transition from holoenzyme to RNAP-promoter open complex and remains in the fully closed state in initial transcribing complexes and elongation complexes. The results argue against the presumption that there is a closure of RNAP clamp upon transition from initiation to elongation. The results support the proposal that Myx, Cor, Rip and Lpm interact with RNAP- switch-region interfering with conformational cycling of RNAP clamp important for RNAP function.

In this thesis, FRET measurements were performed in ensemble conditions. However, the samples containing RNAP and transcription complexes are not homogeneous. In the ensemble measurements of RP_o , a heterogeneous mixture of complexes containing holoenzyme, open complex were formed; in the ensemble measurements of RP_{itc} , a heterogeneous mixture of complexes containing holoenzyme, open complex, initial transcribing complexes were formed; and in the ensemble measurements of RD_e , a

heterogeneous mixture of complexes containing holoenzyme, open complex, initial transcribing complexes and elongation complexes were formed. Ensemble FRET measurement provides only population-averaged results. The resulting mean FRET efficiencies are averages of all these complexes. Using this method we obtained only the mean donor-acceptor distance and defined only the mean clamp conformation in each stage of transcription.

Further experiments will be performed within single molecules of RNAP and transcription complexes in solution using confocal optical microscopy with two-color or three-color alternating-laser excitation (ALEX) to monitor fluorescence. FRET detected at single molecule level can provide accurate descriptions of heterogeneous and asynchronous populations. FRET values can be determined from individual biomolecules and their histogram can directly give information on FRET value distribution. Single-molecule FRET also provides the opportunity to study the dynamics of transitions between different conformational states.

References:

- Agard, N., Prescher, J. and Bertozzi, C. (2004) A strain-promoted [3+2] azide-alkyne cycloaddition for covalent modification of biomolecules in living systems. *J. Am. Chem. Soc.* **126**, 15046-15047.
- Aiyar, S., Gourse, R. and Ross, W. (1998) Upstream A-tracts increase bacterial promoter activity through interactions with the RNA polymerase alpha subunit. *Proc. Natl. Acad. Sci. USA* **95**, 14652-14657.
- Arhin, F., Bédanger, O., Ciblat, S., Dehbi, M., Delorme, D., Dietrich, E., Dixit, D., Lafontaine, Y., Lehoux, D., Liu, J., McKay, G., Moeck, G., Reddy, R., Rose, Y., Srikumar, R., Tanaka, K., Williams, D., Gros, P., Pelletier, J., Parr, T and Fara, A. (2006) A new class of small molecule RNA polymerase inhibitors with activity against Rifampicin-resistant *Staphylococcus aureus*. *Bioorg. Med. Chem.* **14**, 5812-5832.
- Armache, K., Kettenberger, H. and Cramer, P. (2003) Architecture of initiation-competent 12-subunit RNA polymerase II. *Proc. Natl. Acad. Sci. USA* **100**, 6964-6968.
- Artsimovitch, I., Chu, C., Lynch, S. and Landick, R. (2003) A new class of bacterial RNA polymerase inhibitor affects nucleotide addition. *Science* **302**, 650-654.
- Augustiniak, H., Irschik, H., Reichenbach, H. and Hofle, G. (1996) Antibiotics from gliding bacteria. Part LXXVIII. Ripostatin A, B, and C. Isolation and structure elucidation of novel metabolites from *Sorangium cellulosum*. *Liebigs Ann.* **10**, 1657-1663.
- Ayers, B.; Blaschke, U.; Camarero, J.; Cotton, G.; Holford, M. and Muir, T. (2000) Introduction of unnatural amino acids into proteins using expressed protein ligation. *Biopolymers* **51**, 343-354.
- Barne, K., Bown, J., Busby, S. and Minchin, S. (1997) Region 2.5 of the *Escherichia coli* RNA polymerase σ^{70} subunit is responsible for the recognition of the "extended -10" motif at promoters. *EMBO J.* **16**, 4034-4044.
- Baskin, J., Prescher, J., Laughlin, S., Agard, N., Chang, P., Miller, I., Lo, A., Codelli, J. and Bertozzi, C. (2007) Copper-free click chemistry for dynamic in vivo imaging. *Proc. Natl. Acad. Sci. USA* **104**, 16793-16797.
- Borukhov, S. and Goldfarb, A. (1993) Recombinant *Escherichia coli* RNA polymerase: Purification of individually overexpressed subunits and *in Vitro* assembly. *Protein expression and purification* **4**, 503-511.

- Bown, J. Owens, J., Meares, C., Fujita, N., Ishihama, A., Busby, S., and Minchin, S. (1999) Organization of open complexes at *Escherichia coli* promoters. Location of promoter DNA sites close to region 2.5 of the σ^{70} subunit of RNA polymerase. *J. Biol. Chem.* **274**, 2263-2270.
- Buc, H., McClure, W. R. (1985). Kinetics of open complex formation between *Escherichia coli* RNA polymerase and the lac UV5 promoter. Evidence for a sequential mechanism involving three steps. *Biochemistry.* **24**, 2712-23.
- Buck, M., Gallegos, M., Studholme, D., Gou, Y., and Gralla, J. (2000) The bacterial enhancer-dependent sigma (54) (sigma(N))transcription factor. *J. Bacteriol* **182**, 4129-4136.
- Busby, S. and Ebright, R. (1994) Promoter structure, promoter recognition, and transcription activation in prokaryotes. *Cell* **79**, 743-746.
- Bushnell, D., Westover, K., Davis R. & Kornberg, R. (2004) Structural basis of transcription: an RNA polymerase II-TFIIB cocrystal at 4.5 angstroms. *Science* **303**, 983-988.
- Bushnell, D. & Kornberg, R. (2003) Complete, 12-subunit RNA polymerase II at 4.1-A resolution: implications for the initiation of transcription. *Proc. Natl. Acad. Sci. USA* **100**, 6969-6973.
- Campbell, E., Muzzin, O., Chlenov, M., Sun, J., Olson, C., Weinman, O., Trester-Zedlitz, M. & Darst, S. (2002) Structure of the bacterial RNA polymerase promoter specificity sigma subunit. *Mol. Cell* **9**, 527-539.
- Chamberlin, M. (1976). RNA polymerase – an overview. In *RNA polymerase* (Losic, R. and Chamberlin, M., eds),pp.17-67, Cold Spring Harbor, New York.
- Chen, R. and Bowman, R. (1965) Fluorescence polarization: measurement with ultraviolet-polarizing filters in a spectrophotofluorometer. *Science* **147**, 729-732.
- Chin, J. W., Santoro, S. W., Martin, A. B., King, D. S., Wang, L. and Schultz, P. G. (2003) Addition of p-Azido-L-phenylalanine to the genetic code of *Escherichia coli*. *J. Am. Chem. Soc.* **124**, 9026-9027.
- Clegg, R. (1992) Fluorescence resonance energy transfer and nucleic acids. *Methods Enzymol.* **211**, 353-388.
- Cooper, M., Ebner, A., Briggs, M., Burrows, M., Gardner, N., Richardson, R. and West, R. (2004) Cy3B: improving the performance of cyanine dyes. *J. Fluoresc.* **14**, 145-150.

- Cramer, P., Bushnell, D. & Kornberg, R. (2001) Structural basis of transcription: RNA polymerase II at 2.8 angstrom resolution. *Science* **292**, 1863-1876.
- Darst, S., Opalka, N., Chacon, P., Polyakov, A., Richter, C., Zhang, G. and Wriggers, W. (2002) Conformational flexibility of bacterial RNA polymerase. *Proc. Natl. Acad. Sci. USA* **99**, 4296-4301.
- deHaseth, P., Zupancic, M. & Record, M.T.J. (1998) RNA polymerase-promoter interactions: the comings and goings of RNA polymerase. *J. Bacteriol.* **180**, 3019-3025.
- Deiters, A., Cropp, T. A., Mukherji, M., Chin, J. W., Anderson, J. C., and Schultz, P. G. (2003) Adding amino acids with novel reactivity to the genetic code of *Saccharomyces Cereviviae*. *J. Am. Chem. Soc.* **125**, 11782-11783.
- Dale, R. E., Eisinger, J. and Blumberg, W. E. (1979). The orientational freedom of molecular probes. The orientation factor in intramolecular energy transfer. *Biophys J* **26**, 161-193.
- Dove, S., Darst, S. & Hochschild, A. (2003) Region 4 of σ as a target for transcription regulation. *Mol. Microbiol.* **48**, 863-874.
- Durfee, T., Hansen, A., Zhi, H., Blattner, F. & Jin, D. (2008) Transcription profiling of the stringent response in *Escherichia coli*. *J. Bacteriol.* **190**, 1084-1096.
- Ebright, R. H. (2000). RNA polymerase: structural similarities between bacterial RNA polymerase and eukaryotic RNA polymerase II. *J Mol Biol.* **304**, 687-98.
- Ebright, R. H. and Busby, S. (1995) *Escherichia coli* RNA polymerase α subunit: structure and function. *Curr. Opin. Genet. Dev.* **5**, 197-203.
- Ebright, R. (2007) Switch region target and method for inhibition of bacterial RNA polymerase. WO2007/094799.
- Föster, T. (1948). Zwischenmolekulare Energiewanderung und Fluoreszenz. *Ann. Phys.* **2**, 55-75.
- Fujita, N. and Ishihama, A. (1996) Reconstitution of RNA polymerase. *Methods in enzymology* **273**, 121-130.
- Fukuda, R. and Ishihama, A. (1974) Subunits of RNA polymerase in function and structure: V. Maturation in vitro of core enzyme from *Escherichia coli*. *J. Mol. Biol.* **87**, 523-540.
- Fujita, N. and Ishihama, A. (1996) Reconstitution of RNA polymerase. *Methods in enzymology* **273**, 121-130.

- Gentry, D.R. and Burgess, R.R. (1990) Overproduction and purification of the ω subunit of *Escherichia coli* RNA polymerase. *Protein Expr. Purif.* **1**, 81-86.
- Geoghegan, K. and Stroh, J. (1992) Site-directed conjugation of nonpeptide groups to peptides and proteins via periodate oxidation of a 2-amino alcohol. Application to modification at N-terminal serine. *Bioconjug. Chem.* **3**, 138-146.
- Ghosh, P., Ishihama, A. and Chatterji, D. (2001) *Escherichia coli* RNA polymerase subunit ω and its N-terminal domain bind full-length β' to facilitate incorporation into the $\alpha_2\beta$ subassembly. *Eur. J. Biochem.* **268**, 4621-4627.
- Gnatt, A., Cramer, P., Fu, J., Bushnell, D. and Kornberg, R. (2001) Structural basis of transcription: RNA polymerase II elongation complex at 3.3 Å resolution. *Science* **292**, 1876-1882.
- Griffin, B., Adams, S., and Tsien, R. (1998) Specific covalent labeling of recombinant protein molecules inside live cells. *Science* **281**, 269-272.
- Griffin, B., Adams, S., Jones, J., and Tsien, R. (2000) Fluorescent labeling of recombinant proteins in living cells with FLaSH. *Methods Enzymol.* **327**, 565-578.
- Gross, C., Chan, C., Dombroski, A., Gruber, T., Sharp, M., Tupy, J. & Yoctung, B. (1998) The functional and regulatory roles of sigma factors in transcription. *Cold Spring Harbor Symp. Quant. Biol.* **63**, 141-155.
- Gross, C., Lonetto, M. and Losick, R. (1992) Bacterial sigma factors. In transcriptional Regulation, eds. McKnight, S. & Yamamoto, K. (Cold Spring Harbor Laboratory, Cold Spring Harbor, New York), Vol. 1, pp. 129-176.
- Hager, D.A. Jin, D., and Burgess, R.R. (1990) Use of Mono Q high-resolution ion-exchange chromatography to obtain highly pure and active *Escherichia coli* RNA polymerase. *Biochemistry* **29**, 7890-7894.
- Harley, C. B., Reynolds, R. P. (1987), Analysis of *E. coli* promoter sequences. *Nucleic Acids Res.* **15**, 2343-61.
- Hawley, D. and McClure, W. (1983) Composition and analysis of *Escherichia coli* promoter DNA sequences. *Nucl. Acids Res.* **11**, 2237-2255.
- Helmann, J. and Chamberlin, M. (1988) Structure and function of bacterial sigma factors. *Annu. Rev. Biochem.* **57**, 839-872.
- Hochlowski, J.E., Swanson, S.J., Ranfranz, L.M., Whittern, D.N., Buko, A.M. and McAlpine J.B. (1987) Tiacumicins, a novel complex of 18-membered macrolides II. Isolation and structure determination. *J. Antibiot.* **40**, 575-588.

- Hu, T., Schaus, J., Lam, K., Palfreyman, M., Wuonola, M., Gustafson, G. and Panek, J. (1998) total synthesis and preliminary antibacterial evaluation of RNA polymerase inhibitors (+/-)-Myxopyronin A and B. *J. Org. Chem.* **63**, 2401-2406.
- Igarashi, K. and Ishihama, A. (1991) Bipartite functional map of the E. coli RNA polymerase α subunit: involvement of the C-terminal region in transcription activation by cAMP-CRP. *Cell*, **65**, 1015-1022.
- Igarashi, K., Fujita, N. and Ishihama, A. (1991) Identification of a subunit assembly domain in the alpha subunit of *Escherichia coli* RNA polymerase. *J. Mol. Biol.* **218**, 1-6.
- Irschik, H., Gerth, K., Hofle, G. Kohl, W. and Reichenbach, H. (1983) The myxopyronins, new inhibitors of bacterial RNA synthesis from *Myxococcus fulvus* (Myxobacterales). *J. Antibiot.* **36**, 1651-1658.
- Irschik, H., Jansen, R., Hofle, G., Gerth, K. and Reichenbach, H. (1985) The coralopyronins, new inhibitors of bacterial RNA synthesis from Myxobacteria. *J. Antibiot.* **38**, 145-152.
- Irschik, H., Augustiniak, H., Gerth, K., Hofle, G. and Reichenbach, H. (1995) The ripostatins, novel inhibitors of eubacterial RNA polymerase isolated from myxobacteria. *J. Antibiot.* **48**, 787-792.
- Ishihama, A. (1981) Subunit assembly of *Escherichia coli* RNA polymerase. *Advan. Biophys.* **14**, 1-35.
- Ishihama, A., Fukuda, R. and Ito, K. (1973) Subunits of RNA polymerase in function and structure: IV. Enhancing role of sigma in the subunit assembly of *Escherichia coli* RNA polymerase. *J. Mol. Biol.* **79**, 127-136.
- Kapanidis, A., Lee, N., Laurence, T., Doose, S., Margeat, E. & Weiss, S. (2004) Fluorescence-aided molecular sorting: Analysis of structure and interactions by alternating-laser excitation of single molecules. *Proc. Natl. Acad. Sci. USA* **101**, 8936-8941.
- Kapanidis, A., Laurence, T., Lee, N., Margeat, E., Kong, X. & Weiss, S. (2005) Alternating-laser excitation of single molecules. *Accts. Chem. Res.* **38**, 523-533.
- Kapanidis, A., Ebright, Y. and Ebright, R. (2001) Site-specific incorporation of fluorescent probes into protein: Hexahistidine-tag-mediated fluorescent labeling with $(\text{Ni}^{2+}$: Nitrilotriacetic acid)_n- fluorochrome conjugates. *J. Am. Chem. Soc.* **123**, 12123-12125.

- Kapanidis, A., Margeat, E., Laurence, T., Doose, S., Ho, S., Mukhopadhyay, J., Kortkhonjia, E., Mekler, V., Ebright, R. & Weiss, S. (2005) Retention of transcription initiation factor σ^{70} in transcription elongation: single molecule analysis. *Mol. Cell* **20**, 347-356.
- Keilty, S. and Rosenberg, M. (1987) Constitutive function of a positively regulated promoter reveals new sequences essential for activity. *J. Biol. Chem.* **262**, 6389-6395.
- Kettenberger, H., Armache, K. & Cramer, P. (2003) Architecture of the RNA polymerase II-TFIIS complex and implications for mRNA cleavage. *Cell* **114**, 347-357.
- Kiick, K. L., Saxon, E., Tirrell, D.A. and Bertozzi, C. R. (2002) Incorporation of azides into recombinant proteins for chemoselective modification by the Staudinger ligation. *Proc. Natl. Acad. Sci. USA* **99**, 19-24.
- Köhn, M. & Breinbauer, R. (2004) The Staudinger ligation--a gift to chemical biology. *Angew. Chem. Int. Ed.* **43**, 3106-3116.
- Korzheva, N., Mustaev, A., Kozlov, M., Malhotra, A., Nikiforov, V., Goldfarb, A. and Darst, S. (2000) A structural model of transcription elongation. *Science* **289**, 619-625.
- Landick, R. (2001) RNA polymerase clamps down. *Cell* **105**, 567-570.
- Lakowicz, J. (1999) Principles of Fluorescence Spectroscopy, Vol. 27 (New York: Kluwer).
- Lee, N., Kapanidis, A., Wang, Y., Michalet, X., Mukhopadhyay, J., Ebright, R. & Weiss, S. (2005) Accurate FRET measurements within single diffusing biomolecules using alternating-laser excitation. *Biophys. J.* **88**, 2939-2953.
- Lee, J., Kashlev, M., Borokhov, S. and Goldfarb, A. (1991) *Proc. Natl. Acad. Sci. U.S.A.* **88**, 6018.
- Lilley, D., and Wilson, T. (2000). Fluorescence resonance energy transfer as a structural tool for nucleic acids. *Curr. Opin. Chem. Biol.* **4**, 507-517.
- Lonetto, M., Gribskov, M. and Gross, C. (1992) The σ^{70} family: sequence conservation and evolutionary relationships. *J. Bacteriol.* **174**, 3843-3849.
- Malhotra, A., Severinov, E. and Darst, S. (1996) Crystal structure of a σ^{70} subunit fragment from E. Coli RNA polymerase. *Cell* **87**, 127-136.

- Matzura, H., Molin, S. and Maaloe, O. (1971) Sequential biosynthesis of the β and β' subunits of the DNA-dependent RNA polymerase from *E. coli*. *J. Mol. Biol.* **59**, 17-25.
- Mekler, V., Kortkhonjia, E., Mukhopadhyay, J., Knight, J., Rvyakin, A., Kapanidis, A. N., Niu, W., Ebright, Y. W., Levy, R. and Ebright, R. H. (2002). Structural organization of bacterial RNA polymerase holoenzyme and the RNA polymerase-promoter open complex. *Cell* **108**, 599-614.
- Minakhin, L., Bhagat, S., Brunning, A., Campbell, E. A., Darst, S. A., Ebright, R. H., and Severinov, K. (2001). Bacterial RNA polymerase subunit omega and eukaryotic RNA polymerase subunit RPB6 are sequence, structural, and functional homologs and promote RNA polymerase assembly. *Proc Natl Acad Sci.* **98**, 892-7.
- Muir, T., Sondhi, D. and Cole, P. (1998) Expressed protein ligation: A general method for protein engineering. *Proc. Natl. Acad. Sci. U.S.A.* **95**, 6705-6710.
- Mukhopadhyay J, Kapanidis AN, Mekler V, Kortkhonjia E, Ebright YW, Ebright RH, transcription: fluorescence resonance energy transfer assay for movement relative to DNA. *Cell* 106(4):453-63.
- Murakami, K., Darst, S. A. (2003). Bacterial RNA polymerase. *Curr. Opin. Structl. Biol.* **13**, 31-39.
- Murakami, K. S., Masuda, S., Darst, S. A. (2002). Structural basis of transcription initiation: RNA polymerase holoenzyme at 4Å resolution. *Science* **296**, 1280-4.
- Murakami, K. S., Masuda, S., Campbell, E. A., Muzzin, O. and Darst, S. A. (2002). Structural basis of transcription initiation: RNA polymerase holoenzyme-DNA complex. *Science* **296**, 1285-90
- Naryshkin, N., Kim, Y., Dong, Q., and Ebright, R.H. (2001) Site-specific protein-DNA photocrosslinking. Analysis of bacterial transcription initiation complexes. *Methods Mol Biol.* **148**, 337-361.
- Naryshkin, N., Revyakin, A., Kim, Y., Mekler, V., Ebright, R. H. (2000). Structural organization of the RNA polymerase-promoter open complex. *Cell* **101**, 601-11.
- Niu, W., Kim, Y., Tau, G., Heyduk, T. and Ebright, R. (1996) Transcription activation at Class II CAP-dependent promoters: two interactions between CAP and RNA polymerase. *Cell* **87**, 1123-1134.
- Ovchinnikov, Y., Monastyrskaya, G., Gubanov, V., Guryev, S., Chcertov, O., Modyanov, N., Ginkevich, U., Marakova, I., Marchenko, T., Polovnikova, I., Lipkin, V. and Sverdlov, E. (1981) The primary structure of *E. coli* RNA polymerase: nucleotide

- sequence of the rpoB gene and the amino acid sequence of the β subunit. *Eur. J. Biochem.* **116**, 621-629.
- Ovchinnikov, Y., Monastyrskaya, G., Gubanov, V., Guryev, S., Salomatina, I., Shuvaeta, T., Lipkin, V. and Sverdlov, E. (1982) The primary structure of *E. coli* RNA polymerase: nucleotide sequence of the rpoC gene and the amino acid sequence of the β' subunit. *Nucl. Acids Res.* **10**, 4035-4044.
- Paget, M. and Helmann, J. (2003) The sigma 70 family of sigma factors. *Genome Biol.* **4**, 687-698.
- Panchuk-Voloshina, N., Haugland, R., Bishop-Stewart, J., Bhalgat, M., Millard, P., Mao, F., Leung, W. and Haugland, R. (1999) Alexa dyes, a series of new fluorescent dyes that yield exceptionally bright, photostable conjugates. *J. Histochem. Cytochem.* **47**, 1179-1188.
- Ponnambalam, S., Webster, C., Bingham, A., and Busby, S. (1986) Transcription initiation at the *Escherichia coli* galactose operon promoters in the absence of the normal -35 region sequences. *J. Biol. Chem.* **261**, 16043-16048.
- Rao, L., Ross, W., Appleman, J., Gaal, T., Leirmo, S., Schlax, P. and Gourse, R. (1994) Factor independent activity of rrnB P1. An "extended" promoter with an upstream element that dramatically increase promoter strength. *J. Mol. Biol.* **235**, 1421-1435.
- Record, M.T.J., Reznikoff, W., Craig, M., McQuade, K. & Schlax, P. (1996) *Escherichia coli* RNA polymerase ($E\sigma^{70}$), promoters, and the kinetics of the steps of transcription initiation. In *Escherichia coli and Salmonella*, Vol. 1, ed. Neidhart, F.C. (ASM Press, Washington, D.C.), pp.792-820.
- Ring, B., Yarnell, W. and Roberts, J. (1996) Function of *E. coli* RNA polymerase σ factor σ^{70} in promoter-proximal pausing. *Cell* **86**, 485-493.
- Roberts, C. and Roberts, J. (1996) Base-specific recognition of the nontemplate strand of promoter DNA by *E. coli* RNA polymerase. *Cell* **86**, 495-501.
- Ross, W., Gosink, K., Salomon, J., Igarashi, K., Zou, C., Ishihama, A., Severinov, K., and Gourse, R. (1993) A third recognition element in bacterial promoters: DNA binding by the alpha subunit of RNA polymerase. *Science* **262**, 1407-1413.
- Rostovtsev, V., Green, L., Fokin, V. and Sharpless, K. (2002) A stepwise Huisgen cycloaddition process: Copper(I)-catalyzed regioselective "ligation" of azides and terminal alkynes. *Angew. Chem. Int. Ed.* **41**, 2596-2599.
- Saxon, E., and Bertozzi, C. R. (2000) Cell surface engineering by a modified Staudinger reaction. *Science* **287**, 2007-2010.

- Selvin, P. (2000) The renaissance of fluorescence resonance energy transfer. *Nat. Struct. Biol.* **7**, 730-734.
- Severinova, E., Severinov, K., Fenyo, D., Marr, M., Brody, E., Roberts, J., Chait, B. & Darst, S. (1996) domain organization of the Escherichia coli RNA polymerase sigma 70 subunit. *J. Mol. Biol.* **263**, 637-647.
- Severinov, K., Mooney, R., Darst, S.A. and Landick, R. (1997) Tethering of the large subunits of *Escherichia coli* RNA polymerase. *J. Biol. Chem.* **272**, 24137-24140.
- Sharp, M., Chan, C., Lu, C., Marr, M., Nechaev, S., Merritt, E., Severinov, K., Roberts, J. and Gross, C. (1999) The interface of σ with core RNA polymerase is extensive, conserved, and functionally specialized. *Genes Dev.* **13**, 3015-3026.
- Staudinger, H., and Meyer, J. (1919) Uber neue organische phosphorverbindungen III. Phosphinmethylen-derivate und phosphinimine *Helv. Chim. Acta* **2**, 635-646.
- Stryer, L. (1978) Fluorescence energy transfer as a spectroscopic ruler. *Annu. Rev. Biochem.* **47**, 819-846.
- Tang, H., Severinov, K., Goldfarb, A., and Ebright, R.H. (1995) Rapid RNA polymerase genetics: One-day, no-column preparation of reconstituted recombinant *Escherichia coli* RNA polymerase. *Proc. Natl. Acad. Sci. USA* **92**, 4902-4906.
- Tang, H., Kim, Y., Severinov, K., Goldfarb, A., and Ebright, R.H. (1996) Escherichia coli RNA polymerase holoenzyme: Rapid reconstitution from recombinant α , β , β' , and σ subunits. *Methods in enzymology* **273**, 131-134.
- Tolbert, T.; Wong, C.-H. (2000) Intein-mediated synthesis of proteins containing carbohydrates and other molecular probes. *J. Am. Chem. Soc.* **122**, 5421-5428.
- Tsao, M.-L., Tian, F. and Schultz, P. (2005) Selective Staudinger modification of proteins containing *p*-Azidophenylalanine. *ChemBiochem* **6**, 2147-2149.
- Vassilyev, D., Sekine, S., Laptenko, O., Lee, J., Vassilyeva, M., Borukhov, S. and Yokoyama, S. (2002) Crystal structure of bacterial RNA polymerase holoenzyme at 2.6 Å resolution. *Nature* **417**, 712-719.
- von Hippel, P. H. (1998) an integrated model of the transcription complex in elongation, termination, and editing. *Science* **281**, 660-5.
- Wang, C., Seo, T. S., Li, Z., Ruparel, H., and Ju, J. (2003) Site-specific fluorescent labeling of DNA using Staudinger ligation. *Bioconjugate Chem.* **14**, 697-701.

- Wang, D., Meier, T., Chan, C., Feng, G., Lee, D. and Landick, R. (1995) Discontinuous movements of DNA and RNA in RNA polymerase accompany formation of a paused transcription complex. *Cell* **81**, 341-350.
- Wang, L., and Schultz, P. G. (2005) Expanding the genetic code. *Angew. Chem. Int. Ed.* **44**, 34-66.
- Wang, L., Brock, A., Herberich, B., and Schultz, P. G. (2001) Expanding the genetic code of *Escherichia coli*. *Science* **292**, 498-500.
- Wang, L., Zhang, Z., Brock, A., Schultz, P. G. (2003) Addition of the keto functional group to the genetic code of *Escherichia coli*. *Proc. Natl. Acad. Sci. USA* **100**, 56-61.
- Westover, K., Bushnell, D. & Kornberg, R. (2004) Structural basis of transcription: separation of RNA from DNA by RNA polymerase II. *Science* **303**, 1014-1016.
- Wheeler, A., Woody, A., Woody, R. (1987). Salt-dependent binding of *Escherichia coli* RNA polymerase to DNA and specific transcription by the core enzyme and holoenzyme. *Biochemistry*. 26:3322-33
- Wu, P. and Brand, L. (1994). Resonance energy transfer: methods and applications. *Anal. Biochem.* **218**, 1-13.
- Young, B., Gruber, T., Gross, C. (2002). Views of transcription initiation. *Cell* **109**, 417-420.
- Zhang, G., Campbell, E. A., Minakhin, L., Richeter, C., Severinov, K., Darst, S. A. (1999). Crystal structure of *Thermus aquaticus* core RNA polymerase at 3.3 Å resolution. *Cell*. **98**, 811-24.
- Zhang, G. and Darst, S.A. (1998) Structure of the *Escherichia coli* RNA polymerase α subunit amino-terminal domain. *Science*, **281**, 262-266.

CURRICULUM VITA

Dongye Wang

EDUCATION:

- 9/1992 --- 6/1996 Nanjing University, Nanjing, Jiangsu, China
Chemistry, B.S.
- 9/1996--6/1999 Shanghai Institute of Organic Chemistry, Chinese Academy of
Sciences, Shanghai, China
Organic Chemistry, M.S.
- 1/2001--5/2002 Colorado State University, Fort Collins, Colorado
Biochemistry, M.S.
Advisor: Dr. Olve B. Peersen
- 08/2002—10/2008 Rutgers, The State University of New Jersey, New Brunswick,
New Jersey
Chemistry and Chemical Biology, Ph.D.
Advisor: Dr. Richard H. Ebright

PUBLICATIONS:

- Ebright, R. and Wang, D. Bipartite inhibitors of bacterial RNA polymerase. US Provisional Patent 60/630,200 (filed 11/24/2004).
- Wang, D.-Y., Wu, Y., Wu, Y.-L., Li, Y., and Shan, F. (1999) Synthesis, ion(II)-induced cleavage and in vivo antimalarial efficacy of 10-(2-hydroxy-1-naphyl)-deoxoqinghaosu (deoxoartemisinin). *J. Chem. Soc. Perkin Trans. I* 1999, 1827.
- Wu, Y.-L., Chen, H.-B., Jing, K., Li, Y., Shan, F., Wang D.-Y., Wang, Y.-F., Wu, W.-M., Wu, Y., Yao, Z.-J., Yue, Z.-Y., and Zhou, C.-M. (1999) Interaction of biomolecules with qinghaosu (artemisinin) and its derivatives in the presence of ferrous ion--an exploration of antimalarial mechanism. *Pure Appl. Chem.* 71, 1139.
- Wang, D.-Y. and Wu, Y.-L. (2000) A possible antimalarial action mode of qianghaosu (artemisinin) series compounds. Alkylation of reduced glutathione by C-centered primary radicals produced from antimalarial compound qinghaosu and 12-(2,4-dimethoxy-1-phenyl)-deoxoqinghaosu. *Chem. Comm.* 2000, 2193.
- Wang, D.-Y., Wu, Y., Wu, Y.-L., Li, Y., and Shan, F. (2001) Further evidence for the participation of primary carbon-centered free radicals in the antimalarial action of qinghaosu (artemisinin) series of compounds. *J. Chem. Soc. Perkin Trans. I* 2001, 605.